INVESTIGATION OF WASTEWATER TREATMENT USING WASTE MATERIALS AND ALGAE THROUGH CARBONIZATION AND ACTIVATION PROCESSES

A Thesis by

Rakib Mustafa

Bachelor of Science, Bangladesh University of Engineering and Technology, Bangladesh, 2015

Submitted to the Department of Mechanical Engineering
and the faculty of the Graduate School of
Wichita State University
in partial fulfillment of
the requirements for the degree of
Master of Science

December 2018

INVESTIGATION OF WASTEWATER TREATMENT USING WASTE MATERIALS AND ALGAE THROUGH CARBONIZATION AND ACTIVATION PROCESSES

The following faculty members have examined the final copy of this thesis for form and content and recommend that it be accepted in partial fulfillment of the requirements for the degree of Master of Science, with a major in Mechanical Engineering.

_____
Eylem Asmatulu, Committee Chair

_____
Wei Wei, Committee Member

_____
M. Bayram Yildirim, Committee Member

DEDICATION

To my old lad and lady

From childhood, I was never really a sharp student. Many people doubted that I would be able to complete higher studies. But two persons always helped me. They always supported me when I was down. They taught me that if there is a will, there is a way. They taught me that failure is a part of life, but do not give up soon. These two persons are my parents: my old lad and lady.

ACKNOWLEDGEMENTS

I express my heartfelt gratitude to my supervisor Dr. Eylem Asmatulu, Assistant Professor, Department of Mechanical Engineering, Wichita State University (WSU), for sharing her profound knowledge with me. Her advice, ideas, support, proper guidance, motivation, encouragement, and valuable suggestions helped me to complete this research work. I also express gratitude to my other committee members, Dr. Wei Wei, Assistant Professor, Department of Mechanical Engineering, WSU, and Dr. Mehmet Bayram Yildirim, Professor, Department of Industrial and Manufacturing Engineering, WSU, for their suggestions and guidance. I very much appreciate Dr. Ramazan Asmatulu, Professor, Department of Mechanical Engineering, WSU, for letting me use his horizontal tube furnace and vortex mixer. I also thank Dr. Muhammad Rahman, Chair, Department of Mechanical Engineering, WSU. He has been like a guardian to me. My special thanks and appreciation go to Kriti Tamrakar, Emaad Malik, and Mr. Stephen Copeland for their help during the experiments. I am very grateful to Mahmood Al Bashir, Farshad Houtaham and Tharun R. Chillakuru for assisting me in the formatting of this thesis and preparing my presentation.

Finally, I am very thankful to my parents, my family members, and one other person for their mental support and inspiration, which helped me complete my work successfully.

ABSTRACT

Clean drinking water is one of the most important issues in the world and will be one of the most studied subjects together with food in the near future. Some freshwater sources are contaminated with sulfur, nitrogen, phosphorous, and other organic and inorganic contaminants. Desalination, a solution to this wastewater problem, is a costly and time-consuming process. The objective of this study was to develop a cheaper and sustainable process for cleaning lakes and other drinking water sources using waste materials. In this study, algae, clothes, waste paper, and fruit waste, such as date and olive seeds, were used to produce activated carbons (ACs). These materials were briquetted under high pressure using different amounts of molasses as a binder. Date and olive seeds were crushed, sieved, and dried prior to the briquetting process. Chemical activation of the seed briquettes was performed using zinc chloride ($ZnCl_2$) and calcium chloride ($CaCl_2$). Following chemical activation, carbonization in an inert atmosphere was performed to prepare the proper samples. The pH adjustments were applied after the chemical activation and carbonization processes. Additionally, Brunauer-Emmett-Teller (BET) and scanning electron microscopy (SEM) tests were performed to determine the surface area, morphology, and porosity of the produced ACs. This is a promising technique to clean wastewater; activated carbons are expected to remove nitrogen, phosphorus, sulfur, and other contaminants from wastewater. The produced ACs were used to build a water column filter. Water quality was investigated before and after filtration. It was observed that after filtering using AC, the water became suitable for drinking.

TABLE OF CONTENTS

TABLE OF CONTENTS (continued)

Chapter Page

TABLE OF CONTENTS (continued)

Chapter Page

LIST OF TABLES

LIST OF FIGURES

LIST OF FIGURES (continued)

LIST OF FIGURES (continued)

LIST OF FIGURES (continued)

LIST OF FIGURES (continued)

Figure Page

LIST OF ABBREVIATIONS

A	Angstrom
AC	Activated Carbon
BET	Brunauer-Emmett-Teller
BJH	Barrett-Joyner-Halenda
C	Carbon
$CaCl_2$	Calcium Chloride
CO	Carbon Monoxide
CO_2	Carbon Dioxide
COD	Chemical Oxygen Demand
CV	*Chlorella vulgaris*
DI	Deionized
DSC	Date Seed Carbon
EC	Electrical Conductivity
FNU	Formazine Nephelometric Unit
FO	Forward Osmosis
FTIR	Fourier Transform Infrared Spectroscopy
GAC	Granular Activated Carbon
H_2	Hydrogen
H_2O	Water
H_3PO_4	Phosphoric Acid
H_2SO_4	Sulfuric Acid
HCl	Hydrochloric Acid

Hg	Mercury
HTC	Hydrothermal Carbonization
JTU	Jackson Turbidity Units
$K_2Cr_2O_7$	Potassium Dichromate
KOH	Potassium Hydroxide
MSD	Multi-Stage Distillation
N_2	Nitrogen
$NaHCO_3$	Sodium Bicarbonate
NaOH	Sodium Hydroxide
NO_2	Nitrogen Dioxide
NTU	Nephelometric Turbidity Unit
OPC	Olive Pit Carbon
PBR	Photobioreactor
PDS	Palm Date Seed
ppm	Parts Per Millions
PSD	Pore Size Distribution
PVC	Polyvinyl Chloride
RO	Reverse Osmosis
rpm	Revolutions per Minute
SBE	Spent Bleaching Earth
SEM	Scanning Electron Microscopy
SM	*Spirulina maxima*

SO_2	Sulfur Dioxide
TDS	Total Dissolved Solids
TN	Total Nitrogen
TP	Total Phosphorous
VCD	Vapor Compression Distillation
VMD	Vacuum Membrane Distillation
WHO	World Health Organization
$ZnCl_2$	Zinc Chloride

CHAPTER 1

INTRODUCTION

1.1 Background

Whether it is an overpopulated city or a rural area with limited resources, the demand for clean drinking water has been increasing around the world for the past few decades. According to Schwarzenbach et al. [1] and The World Wildlife Fund [2], around 1.1 billion people worldwide do not have access to water. In addition, the other half of the population has access to water but lacks the quality resource. Pollution is the major cause of scarcity of pure or usable water. Air, water, or chemical pollution could be connected to water resources. The industrial revolution along with improper waste disposal have contaminated natural resources for decades, resulting in poor water quality. Many aquatic species have been endangered due to the poor quality of water. For example, the contamination of water resources in the city of Rio de Janeiro in Brazil left international athletes in disgust at the 2016 Olympics [3]. Guanabara Bay in Rio de Janeiro has a dense population of approximately 16 million as well as a scarcity of sanitation and quality water. Such water bodies carry a high percentage of waterborne diseases, raw sewage, and litter. The aquatic wildlife here has decreased dramatically [2]. Another place that faces such extreme water pollution is Indonesia, which holds six percent of the world's freshwater resources but due to urbanization, industrialization, and negligence, the water is highly contaminated [4]. Almost every city in Indonesia has at least one river flowing through it. The capital of the country, Jakarta, alone has 15 rivers. The overpopulated area in the capital is believed to be turning the region near the river banks into a slum area. There is no clean water, and the existing resources have ended up being a huge disposal area causing water scarcity, loss of aquatic life, and many waterborne diseases. Figure 1.1 shows a couple of examples of severe water pollution activities in recent times.

(a) (b)

Figure 1.1: Water pollution: (a) due to oil spilling [5], and (b) due to industrial waste [6]

Research in water scarcity and water quality treatment has been the most in demand. The lack of safe drinking water will be one of the world's leading problem in future decades. This has affected more than 1.1 billion people globally, which means that one in every six people does not have access to safe drinking water. This lack of water is due not only to climate change or a regional variance but also to physical scarcity and economic issues. Economic issues are most common in African continents. The amount of money being invested in water resources and the relevant human capacity in a certain region or area is not quite enough to meet the water demands in the area. Also, most individuals do not have the money to make use of an acceptable water source on its own [7]. The United Nations Economic Commission for Africa estimated in 2006 that 300 million out of 800 million who live on the African continent live in a water-scarce environment.

The human body is 60% water, thus the importance of water quality and finding methods to consistently improve it is imperative. The amount of water on earth is the same as when the earth was first formed; it simply gets recycled countless times—not just drinking water but also water for recreation, crops, industrial processes, and the production of edible fish and sea creatures.

Water quality is not only important to protect human health, but it provides ecosystem habitats for farming, fishing, and areas devoted to tourism and divertissement. If the earth's water quality is not maintained, then its recreational and environmental value will be drained dramatically.

The Middle East has been suffering from the spilling or leakage of oil from factories and boats into the water. Tons of sea creatures die of polluted water due to hypothermia and other diseases. Birds that feed on sea creatures may also get poisoned and die. Fishermen catch fish that have been exposed to oil and sell them with other fish, which has led to various food poisoning incidents across the Middle East.

Over the decades, different measures have been taken to clean water resources or to treat water. Denitrification is a way to remove ammonium waste or nitrogen from sewage and urbanization waste for water treatment [8]. This will prevent polluting groundwater from excessive use of fertilizers. Wastewater can also be treated on land by distributing effluent over slightly inclined grassland with adequate impermeable soil. The area for treatment is broken down into small parts, and the water flows evenly down slopes forming ditches. In such treatment, water-tolerant grass and the cover crops play an important role in this method preventing soil erosion, providing nutrients and a medium for biological treatment. This overland flow method removes pathogens from sewage effluent at levels comparable with other treatments without any chlorination. Thus, this program should be monitored and further tested for the wastewater treatment process and the quality of the effluent for different day-to-day applications.

Recently, activated carbon (AC) has been used in many purification and adsorption procedures. Water is no exception here. Activated carbon is a carbonaceous, highly porous substance that can attract and retain organic chemicals. It is meant to have small and low-volume pores that would increase the existing surface area for adsorption or chemical reactions [9].

Activated carbon is formed by burning the carbonaceous substance from any of a variety of sources in the absence of oxygen, thereby resulting in the formation of carbon char. Some of the common sources used are coal, rye starch, wood pulp with low ash content, any agricultural byproducts, nutshells, seeds, or any materials that are rich in carbon content. The AC char is then treated chemically, or sometimes physically, to develop a consistent sequence of pores inside the carbon. This step increases the surface area of its internal pore network, thereby resulting in a tremendous surface area that takes part in chemical reactions for attracting and retaining organic chemicals. Due to its adsorption property, activated carbon is used in the purification or cleaning process. It can be any type of purification, such as air and gold purification, poison removal treatment, or gastric lavage. Adsorption can easily occur in order to capture chemical organic compounds that are smaller or similar to the pore size but not those compounds with a size greater than the pores. This creates a new platform of challenge in the application of ACs. During the adsorption process, bond attraction forces, such as van der Waals forces, trap the unwanted molecules within the carbon's internal pore structure and accumulate it onto a solid surface. Activated carbon has several different applications including metal extraction, sewage treatment and purification, medicinal, clothing, automobile, and others [10].

Filtration is one of the simple and most common treatments to purify water and make it acceptable for human consumption. During filtration, liquid is passed through a filtering material or screen through which only water can pass but not impurities. Large visible particles can be easily filtered out from the filtering screen, but small impurities on the ionic level need deeper treatment. Such treatment can involve one experiment or a series of experiments with different chemical compounds. In some filtration processes, the filtration material with different porous

structures is changed, but some material may need to be purified chemically. This is where activated carbon comes into play.

1.2 Motivation

Finding a source of clean water is becoming a challenge in many parts of the world. There is a huge scarcity of clean drinking water in many developing countries. However, few water-purification processes are really effective. The nutrient film technique is one of these. This technique is a modern water purification process involving a hydroponic plant growth system in which plants grow on an impermeable surface and wastewater is added to it continuously [11]. The dense root growth on the surface will act as a filter and accumulate the large impurities. The upper part of the plant grows, taking in nutrients and water and removing impurities by transpiration. This prevents algae growth, and the purified water is collected at one end of an apparatus. Furthermore, this method promotes nutrient conversion due to biomass production and water cycling in the environment via the plants [12].

According to the water treatment information given out by the Greater Vancouver Regional District, the primary water treatment process involves six steps [13]. First, the incoming untreated wastewater is screened to remove visible materials such as rock, wood, branches, and even dead creatures. The presence of such large impurities can disrupt the treatment process later on. The treatment process needs to be mounted at a height above ground level or at a level where the treated water can be dumped so that the water flows down the treatment plan setup by means of gravity. Therefore, the water is pumped to a higher level after screening and is then prepared for aerating. The water is exposed to air so that any existing dissolved gas is released. Any sludge or scum present is removed by sedimentation and pumping, and then filtered by carbon for removing organic particles. This is the part of the process where activated carbon can play a useful role.

Eventually the water is treated with an adequate amount of chlorine, sufficient enough to kill bacteria but not harmful to health. The treated water is referred to as the effluent, which is then passed on to the local water resources.

Desalination is one of the most effective ways to remove salt and minerals from a liquid. This multi-stage process uses sedimentation, separation, filtration, and reverses osmosis (RO) to obtain clean drinkable water.

The processes discussed above are effective for filtering water, but they are very expensive. Underdeveloped and developing countries cannot afford these methods. A low-cost and sustainable filtration process is required to solve this problem. If the main materials for producing activated carbon for adsorption and filtration is available and inexpensive, then this that would be extremely beneficial. This is the motivation behind this research.

1.3 Objectives

The main objective of this research was to clean various types of wastewater using waste materials. Activated carbon was used to filter the water and to attain the main objective. The following tasks were performed in this research:

- Activated carbon was prepared using low-cost materials, i.e., waste materials such as fruit waste, and chemical activation involving $ZnCl_2$ and $CaCl_2$ as the chemical agents.
- To investigate the Brunauer-Emmett-Teller (BET) surface area, pore volume, and porosity, scanning electron microscopy (SEM) images and adsorption isotherms of the produced activated carbon were determined in order to find the best one for the filtration process.
- A water column filter using the produced activated carbon was prepared.

- After filtration using the water column filter, the quality of the water was investigated based on a selected set of parameters: total dissolved solids (TDS), electrical conductivity (EC), pH, and turbidity.

CHAPTER 2

LITERATURE REVIEW

2.1 Water Treatment Processes

Water treatment involves the removal of impurities and contaminants such as bacteria, minerals, sulfur, nitrogen, manganese, and other organic and inorganic substances. Due to the diversity of the contaminants, there is no one specific way or mechanism to clean or remove the impurities. The water treatment process is selected based on the type and concentration of the contaminants. Some of the most common water treatment processes used worldwide are the following:

- **Desalination:** In this process, which is usually used for sea water, minerals are extracted.
- **Filtration:** In this physical treatment process, solid particles and slurries are separated from the liquid by passing the liquid through a passage of filters or membranes.
- **Sedimentation:** This very basic process uses gravity to suspend solid particles from the liquid.
- **Coagulation-Flocculation**: This chemical treatment process involves colloids that are extracted as a form of flake by using a chemical or clarifying agent.
- **Chlorination**: This mechanism is used to kill bacteria and microbes from the water with the use of chlorine or hypochlorite.
- **Aeration**: This secondary treatment process is an activated sludge process, whereby air is pumped through the water and forms flocs of organic and inorganic microbes that feed on the bacteria.

When only physical particles need to be removed from water, sedimentation, filtration, and coagulation-flocculation are frequently used. For removing dissolved organic and inorganic

materials, aeration, desalination, adsorption, and chemically activated membranes are recommended.

Industrial water is very difficult to clean. Due to the high amount of dissolved chemicals and dyes, filtration requires special and multiple-cycle treatments. There are two main water treatment processes involving boiler water and cooling water. With the proper recycling and treatment, industrial water can also be reusable.

2.2 Desalination Process

Desalination basically refers to the removal of salt and other minerals from water. This process is popular with Gulf Corporation Countries, the Middle East, and the North America region [14]. Some of the common desalination processes are vacuum membrane distillation (VMD), vapor compression distillation (VCD), multi-stage distillation (MSD), reverse osmosis, and forward osmosis (FO) desalination. Among these, RO and FO are frequently applied. The VMD, VCD, MSD processes are driven by a thermal membrane, while both osmosis processes are driven by a pressure membrane. Semi-permeable membranes, which are pressure sensitive, are used in RO desalination. Due to the pressure difference, the membrane allows water or liquid to enter while rejecting the salt [15]. Figure 2.1 shows the basic mechanism of osmosis and reverse osmosis. From Figure 2.2, it can be seen that RO desalination is a multistage refining process for removing minerals and salt [16]. Forward osmosis is a relatively new desalting process in which the salt concentration gradient is the driving force through a synthetic membrane. In FO, the feed solution extracts water due to the high osmotic pressure of the concentrated draw solution.

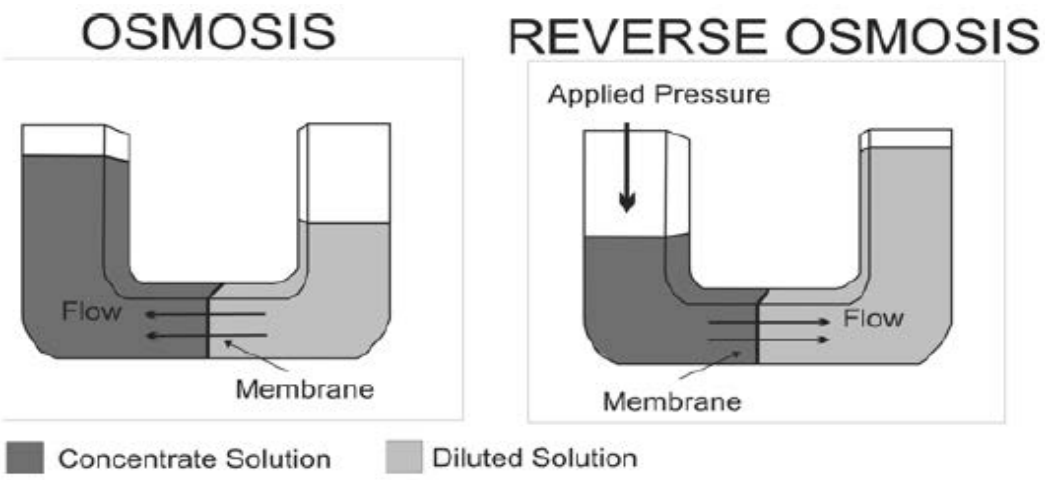

Figure 2.1: Basic mechanism of osmosis and reverse osmosis [15]

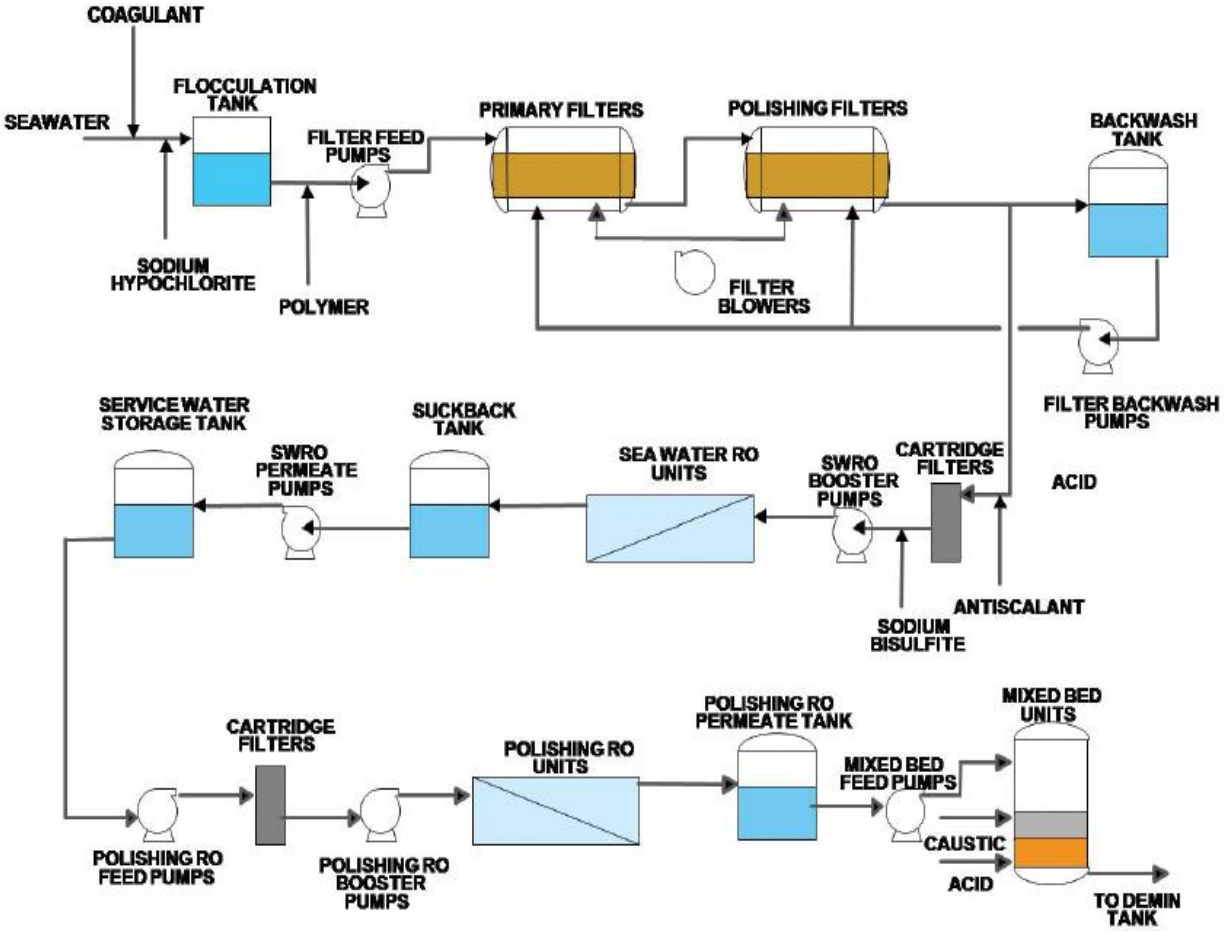

Figure 2.2: RO desalination process of Philippine's largest power plant [16]

One of the advantages of FO is that it requires very low hydraulic pressure [17]. It also ensures the rejection of a broad range of contaminants and lower membrane fouling propensity. The RO process is shown in Figure 2.3. Recently, the FO approach has been combined with the RO desalination process to determine if there are improvements. This includes the performance observation of water flux and membrane fouling rates. With all the benefits of the desalination process, there is one major drawback. It is extremely expensive and time-consuming.

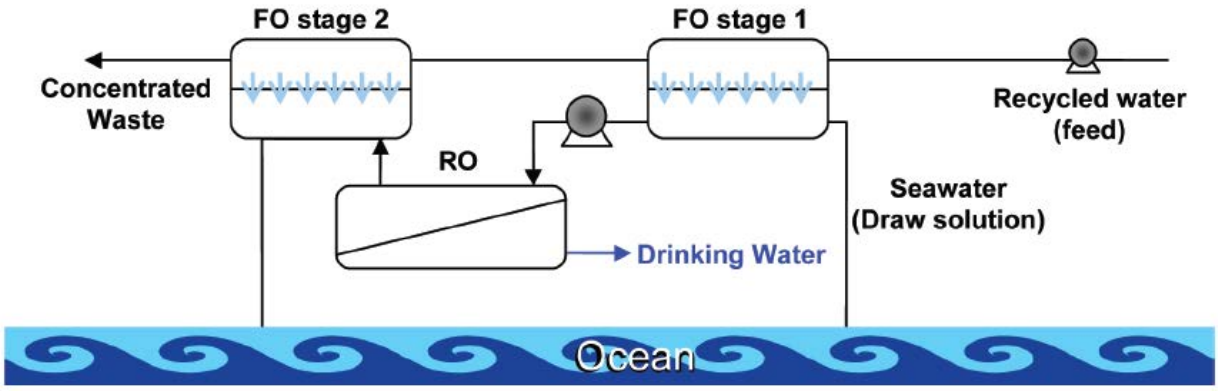

Figure 2.3: Schematic drawing of novel hybrid FO/RO process [17]

2.3 Carbonization

Carbonization is the process of converting organic materials into carbon and carbon-embedded residue, among other by-products. Carbonization is generally performed by a thermochemical decomposition process called pyrolysis. Pyrolysis is the chemical and physical decomposition of organic precursor materials into carbon-rich compounds at an elevated temperature. Effective pyrolysis requires an inert environment, typically, helium, argon, or nitrogen gas [18]. Carbonization is a very complex process with many steps. The efficiency of carbonization depends on oxygen removal from the system. With the presence of oxygen, instead of carbonization, combustion or oxidation process occur very quickly, which lessens the quality of the carbon residue. But it is very difficult to remove all oxygen from the process. Therefore,

due to the presence of oxygen, several stages of a chemical reaction occur before carbonization is complete.

The first stage in carbonization is the combustion stage, where the existing oxygen oxidizes carbon (C), nitrogen (N_2), hydrogen (H_2), and sulfur (S) and produces carbon dioxide (CO_2), nitrogen dioxide (NO_2), water (H_2O), sulfur dioxide (SO_2), and some carbon monoxide (CO) are also produced. The following combustion or oxidation reactions occur:

$$C + O_2 \Rightarrow CO_2 \quad \text{(Exothermic)}$$
$$2H_2O + O_2 \Rightarrow 2H_2O \quad \text{(Exothermic)}$$
$$N_2 + 2O_2 \Rightarrow 2NO_2 \quad \text{(Exothermic)}$$
$$S + O_2 \Rightarrow SO_2 \quad \text{(Exothermic)}$$
$$C + CO_2 \Rightarrow 2CO \quad \text{(Endothermic)}$$

The second stage is known as the gasification stage. Here, almost no oxygen remains, but the generated gases from the oxidation process start to react. A little amount of remaining oxide is converted into carbon monoxide CO. The following gasification reactions have been noticed:

$$C + O \Rightarrow CO \quad \text{(Endothermic)}$$
$$C + H_2O \Rightarrow CO + H_2 \quad \text{(Endothermic)}$$
$$C + CO_2 \Rightarrow 2CO \quad \text{(Endothermic)}$$
$$C + 2H_2 \Rightarrow CH_4 \quad \text{(Exothermic)}$$
$$CO + H_2O \Rightarrow CO_2 + H_2 \quad \text{(Exothermic)}$$

Following gasification, only the organic part of the materials is heated without any oxygen at a very high temperature. To avoid combustion with oxygen, it is recommended to use an inert environment from the beginning. For pyrolysis, 500°C–900°C is considered the temperature range. The temperature setup depends highly on the materials used as well as the activation process. For example, Amaya et al. used rice husk for carbonization at 500°C for 2 hrss [19]. Johns et al. used granular activated carbon (GAC) for absorbing dissolved metals and organics, setting the temperature to 750°C [20]. The rate of heating also plays a vital role in carbonization. During slow

pyrolysis (heating rate 10°C/min), more solid fractions are expected to be extracted, while during fast pyrolysis (heating rate 50°C/min), higher liquid fractions are expected.

2.4 Activated Carbon

Activated carbon can be defined as processed carbon that has small and low-volume pores in its structure. This small and low-volume structure provides a higher surface area [21]. A quality AC ensures high adsorption capacity. Activated carbon was first used during World War I in gas masks to adsorb poisonous gases [22]. Since then, AC has been used in many fields. It is used in the medical field to treat poisonings [23]. AC slows down the enterohepatic circulation of toxins or drugs. It is also used to remove oil vapors, odors, and hydrocarbons from gas [24]. AC with iodine and sulfur is used to trap mercury (Hg) emissions [25–27]. The most popular application of AC is the removal of pollutants from air and water. It is widely used in groundwater and drinking water filtration. Carbon can be activated in two ways:

- Physical Activation
- Chemical Activation

In physical activation, the raw material is pyrolyzed at a higher temperature (i.e., 600°C–900°C) in an inert atmosphere. Then the carbonized material is exposed to the oxidizing atmosphere (oxygen or steam) at a higher temperature. This temperature can vary according to the requirement (ranges from 600°C–1200°C).

In chemical activation, before or after carbonization, the raw material is impregnated with certain chemicals. Generally, an acid, strong base, or salt is used: hydrochloric acid (HCl), phosphoric acid (H_3PO_4), sodium hydroxide (NaOH), potassium hydroxide (KOH), zinc chloride ($ZnCl_2$), calcium chloride ($CaCl_2$), etc. Chemical activation can be done as either a two-step activation method or a single-step activation method. In the two-step activation method, the raw

material is carbonized first and then impregnated with chemicals for activation. In the single-step activation method, materials are first impregnated with chemical agents and then carbonized in an inert environment. Generally, chemical activation is preferred over physical activation due to the lower temperature and shorter time requirement involved; however, this depends on the conditions and requirements.

Many raw materials are used for producing activated carbon with chemical agents. Coffee waste has been used to produce AC to adsorb mercury, cadmium, and zinc from aqueous solutions. $ZnCl_2$ and KOH have been used as chemical agents, and 700°C was applied during the activation process [28]. One investigation of chromium removal from wastewater was done using AC, where tamarind wood was the raw material. The pre-heated temperature was kept at around 250°C–300°C, and a temperature of almost 450°C was applied during carbonization [29]. Granular activated carbon was used in sorption cycles to remove nitrates [30, 31], where $CaCl_2$ was used as the activation agent in that process [32]. The adsorption of cadmium in AC was investigated using coconut coir pith as the raw material for the AC and dilute HCl as the chemical agent [33]. Waste dog rose (rosa canina) seeds were used to produce GAC to adsorb dye. An activation treatment was performed at different temperatures—350°C, 500°C, 600°C, 700°C—and $ZnCl_2$ was the activating agent [34]. Calcium chloride-treated beech sawdust was used as AC to inspect the dye adsorption rate in batch and fluid-bed systems [35]. Activated carbon from agricultural waste bagasse was used for the adsorption of an acid dye, using $ZnCl_2$ as the activating agent. Here, the pyrolysis temperature was increased at a ramp rate of 10°C/min with nitrogen gas flow, and the temperature was held at 500°C for half an hour [36].

The efficiency of activated carbon from macadamia nut shells was analyzed for phenol removal using physical activation. The heating rate was 5K/min, and the temperature was raised

to 1123K [37]. The removal rate of methylene blue was inspected by using AC prepared from cola nut shell with $ZnCl_2$ as the activating agent, and the carbonization temperature was kept at 500°C for 1 hr [38]. The adsorption of copper ion from textile industrial water using AC was analyzed using coconut shell as the raw material [39]. The presence and removal of salt in tap water were also investigated using coconut shell as the raw material for the AC. Here, NaCl, $CaCl_2$, and $ZnCl_2$ were used individually as the chemical agents to observe the rate of removal rate. The coconut hell was carbonized at 350°C for 3 hrs and then activated at 100°C for 2 hrs [40, 41]. Nitrate removal from water using coconut shell-AC was also investigated. In this case, the slurry was kept in the oven for 110°C for 24 hrs and the carbonization temperature was 400°C–600°C [42]. Carbon was synthesized from areca nutshell to observe the effect of activation. Here, some carbons were left non-activated and some were activated using KOH and steam [43]. Then electric potentials, SEM images, and porosity were compared. An activated carbon filtration process was used in the treatment of drinking water to observe the removal of lead, odor, and dissolved radon [44]. Hazelnut shells and wood sawdust were separately used to produce AC. That AC was used as adsorbents to compare the rate of methylene blue dye removal [45]. Agricultural by-products, such as rice straw, pecan shell, peanut shell, walnut, molasses (as a binder), etc., were used as raw materials to produce granular activated carbon. That GAC was used to adsorb dissolved metals and organics [18, 20]. Palm kernel shell was also applied for water treatment, and the resulting X-ray diffraction, X-ray photo spectrum, and SEM images of the palm kernel shell showed higher porosity and surface area, which are ideal characteristics for an adsorbent [46]. Potassium hydroxide was used for the impregnation and activation of palm kernel shell. The shells were carbonized at 400°C for 1 hour, and during activation, the temperature was kept at 800°C–1000°C

[47]. A proper carbonization and activation process that is not expensive but efficient needs to be developed.

2.5 Briquetting

2.5.1 Background on Briquetting

The process in which waste materials and residues are compacted into greater density is referred to as briquetting or densification. Briquetting has recently attracted a great deal of interest from all over the world because of its ability to recycle energy sources. The densification process can be classified into closed die or open die. Closed die densification is also known as "tableting or roll-press briquetting," which is very popular for producing charcoal briquettes and pharmaceutical tablets [48]. Open die densification, or extrusion method, is used to produce biomass pellets, cubes, and briquettes. In this process, the feedstock is continuously forced through the die [48]. A heated die screw press, roller press, and piston press are commonly used for biomass briquetting. The heated screw press technology was developed in Japan in the mid-1940s to produce biomass briquettes as a fuel source [49]. Now, this technology is popular in many countries, including China, Korea, Bangladesh, Malaysia, Philippines, and Vietnam. The piston press technology is used in Brazil, India, and Africa. Based on the piston pressure, briquettes can be classified into three groups [50]

- Low-Pressure Briquettes (<5 MPa)
- Intermediate-Pressure Briquettes (5 MPa–100 MPa)
- High-Pressure Briquettes (>100 MPa)

The bulk density of biomass can be increased by approximately 10–20 times its original bulk density by briquetting or the palletization process. Briquetting improves the handling properties, dimensional stability, and strength of the precursor feedstock.

Amaya et al. studied rice husk and eucalyptus wood as raw materials and concentrated grape must as a binder to prepare briquettes. These briquettes were carbonized and activated to study the porosity, i.e., microsurface area and (BET surface area [19]. Nasrin et al. investigated the briquetting of fruit bunch fiber and palm shell for use as a renewable energy fuel. The ash content, moisture content, and calorific value of the briquettes were studied [51]. Inomata et al. studied the gas storage capacity of activated carbon briquettes without a binder. Anhydrous microcrystal powder was used as the raw material, and the operating pressure ranged from 0 to 98.1 MPa. Pellets were carbonized at a high temperature with the flow of nitrogen and activated by the flow of carbon dioxide. After activation, bulk density, SEM images, BET surface area, and total pore volume were studied to observe the gas storage capability [52]. Hassan et al. experimented with briquettes of palm oil mill effluent and palm oil frond waste as an alternative biomass fuel. Calorific value, gas content, ignition time, and crack analysis of the briquettes were studied [53]. Wilson et al. used peanut shell briquettes to produce AC that was used to observe the adsorption of metal ions such as cadmium (Cd^{2+}), copper (Cu^{2+}), lead (Pb^{2+}), nickel (Ni^{2+}), and zinc (Zn^{2+}). Surface area and adsorption capacity were also studied [54]. Withatanang et al. used waste materials, such as wastewater sludge and banana peel waste, to produce briquettes in order to use them as recycled fuel. Compressive strength, volatile matter, ash content, carbon content, and heating value were analyzed [55]. Sotannde et al. prepared charcoal briquettes from neem wood residues, using cassava starch and gum Arabic as individual binders. Compressed density and durability testing were conducted [56]. Suhartini et al. used spent bleaching earth (SBE) to prepare fuel briquettes. SBE is actually the solid waste produced from cooking oil industries. The calorific value, moisture content, and ash content were analyzed [57]. Ward et al. studied fecal char as the raw material for briquettes. The human wastes were carbonized at 300°C, 450°C, and

750°C, and molasses, lime, and starch were used as binders. The calorific value and strength of the briquettes were tested [58]. Arvanitoyannis et al. studied the use of thermally treated olive oil waste as a raw material of biodiesel, activated carbon, and briquette production [59].

2.5.2 Agglomeration Mechanism

Agglomeration or densification is one of the measuring qualities of briquette production. The quality of briquettes depends on properties such as bulk density, void volume, thermal properties, and moisture content. Most of these properties are linked with densification. In some cases, higher pressure will provide better densification because of the compaction strength due to Vander Walls forces, valence forces, or interlocking. Raw materials may need binders even under high operating pressure, which forms an adhesive bond between the two. A few of the several densification mechanisms are as follows:

- Solid bridge between particles
- Interfacial forces and capillary pressure
- Adhesive and cohesive forces in bonding
- Attraction between solid particles
- Interlocking

2.5.2.1 Solid Bridges

Solid bridges can be formed by many different methods, including sintering, chemical reactions, melting, binder hardening, and crystallization. Sintering is the process by which adjacent atoms are pressed at a high pressure, resulting in the adjacent boundaries merging together. Eventually the merged boundary vanishes with time and becomes a single cell. The oxidation reaction may form a solid bridge during the melting of the materials. During melting, the point of contact between the particles may merge together. This usually occurs when thermoplastic

materials are used at a higher pressure. If the materials are mixed with inorganic binders, solid bridges can be formed by the hardening process, whereby a mortar bridge would be formed. When the materials are moist and solid, they can dissolve into the liquid by the process of crystallization. In this process, solid bridges are formed in the vicinity of the contact point. The best way to increase the strength of a briquette is to create solid bridges in its structure.

2.5.2.2 Interfacial Forces and Capillary Pressure

On the basis of the interaction of the fluid surface, materials with moisture will create granulation in three stages. The fluid solid-to-gas interface will experience surface tension along the liquid surface when the space between particles is partially filled. Here, a negative capillary pressure will be generated. When the solids are filled with moisture, they will create an attraction towards the granules. This is known as the "pendular state" [60, 61].

As the densification process progresses, the voids will be filled with liquid, resulting in the bonding forces gradually starting to rise between the granules. However, the liquid does not completely surround the granules; rather, only a part of the liquid concave surface is in contact with the outer gas boundary, a condition that will create a negative capillary pressure towards the liquid. An increase in tensile strength in granules will be observed. This is referred to as the "funicular state."

When the solid is completely immersed in liquid, concave surfaces from the previous stage will be changed on the convex surfaces. This convex surface formation will remove all intergranular capillary bonding forces. However, the grains are still connected by the surface tension of the liquid droplets. This state is known as the "capillary state." The different steps of the granulation effect are shown in Figure 2.4 [62].

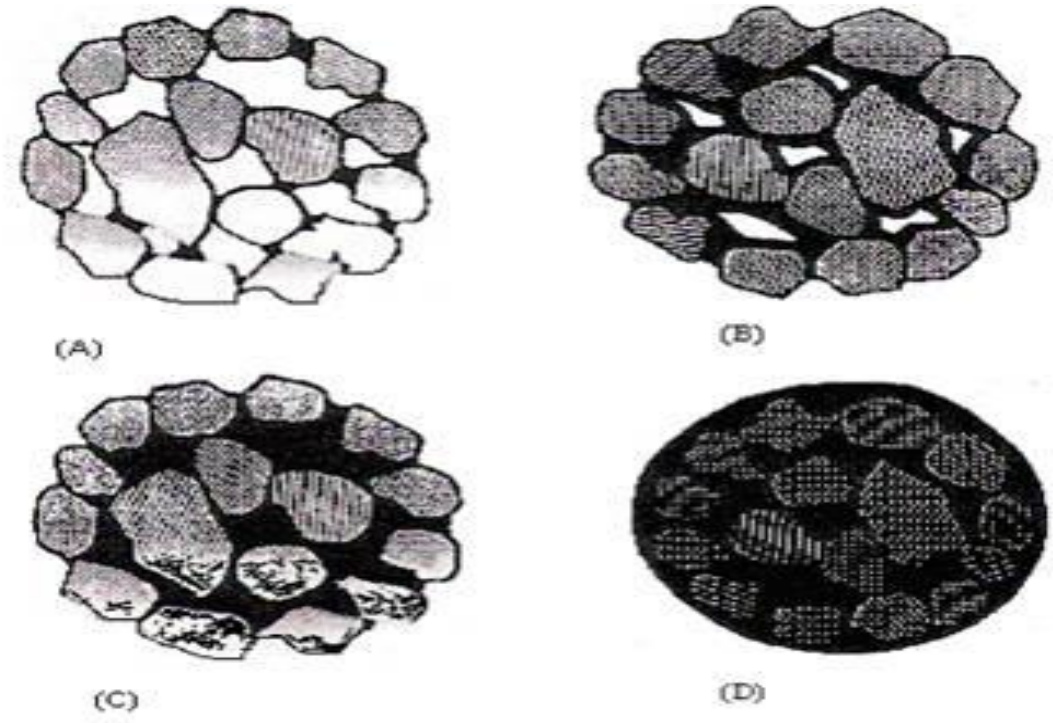

Figure 2.4: Moisture and granulation effect: (A) pendular state, (B) funicular state, (C) capillary state, and (D) droplet state [62]

2.5.2.3 Adhesive and Cohesive Forces

The above discussion has explained the bonding forces based on interfacial force and capillary pressure. However, this is only valid for less viscous fluids and solid materials with high moisture content. In the case of immovable liquids, such as viscous binders and adsorption layers, no significant capillary pressure is generated. In this case, adhesive and cohesive forces help to create strong bonds. For viscous binders, interfacial forces discharged on liquid would be reduced by the formation of a thin layer. This may result in reduced mobility and reduced liquid pressure. As a result, plastic material tends to hold its shape, and a large amount of energy would be required to deform the surface. In the solid-liquid interface, adhesive forces develop, and cohesive forces on a viscous binder would continue to strengthen until the stronger of the two prevails and make one of the bonds several magnitudes over the initial interaction. This scenario is shown in Figure 2.5. These binders tend to harden after certain periods of time and make solid bridges [63].

A thin adsorption layer, one that is less than 30 angstrom (A), can freely move. The capillary condensation will be negligible, and the full force of the molecular attraction will prevail. This condition frequently occurs at the roughness peaks of two particles without a large liquid layer preventing the interaction. Figure 2.5 shows the adhesive and cohesive bonding in a solid structure.

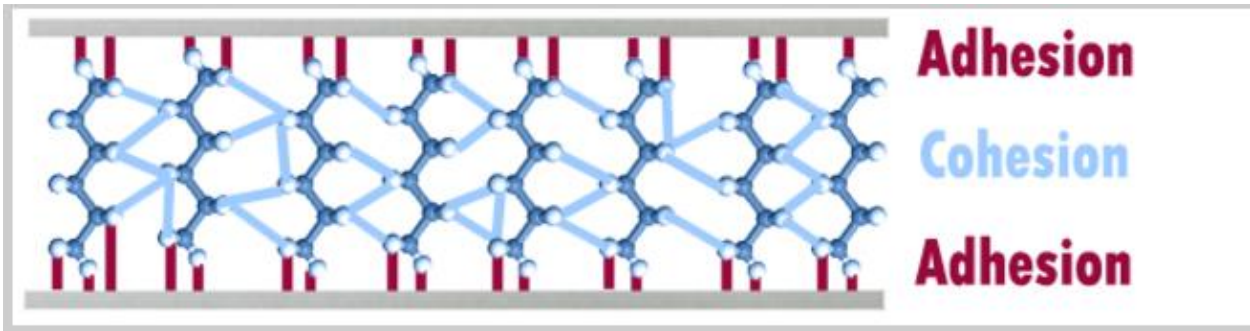

Figure 2.5: Adhesive forces with solid-liquid interface, and cohesive forces with viscous binder [64]

2.5.2.4 Attraction between Solid Particles

In some briquetting processes or material composites, solid or liquid bridges cannot be formed. However, molecular or electrostatic attraction forces can provide tensile loads between the constituents. With the decrease in distance between adjacent molecules, molecular attraction generally increases. When the molecular distance reaches approximately 100 A°, van der Waals forces could act as a significant bonding force.

Electrostatic attraction forces can be generated during the briquette compaction and enhance the size reduction. Based on the material type and motion during this phase, the amount of the charge absorbed by the particles may differ. Therefore, in a bonding mechanism, negatively and positively charged particles are very important when solid and liquid bridges are slow to impart [63]. Figures 2.6 and 2.7 show electrostatic forces and van der Waals forces, respectively, in a structure.

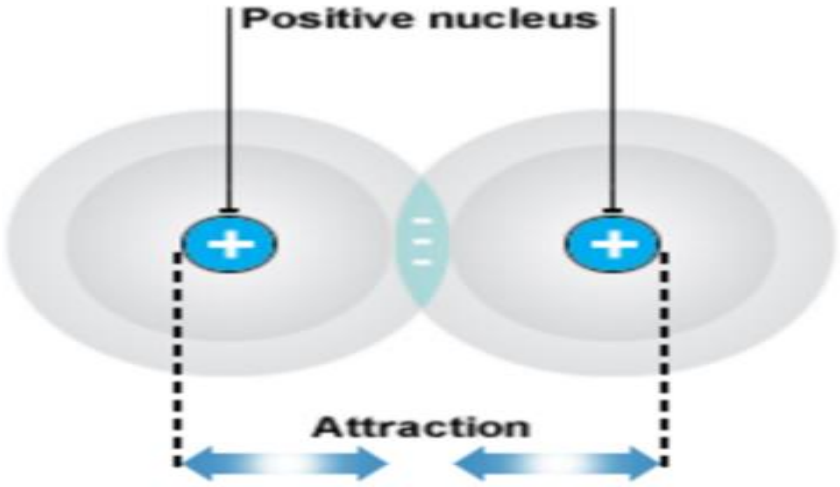

Figure 2.6: Electrostatic forces attraction between positively charged nuclei and negatively charged shared electrons [65]

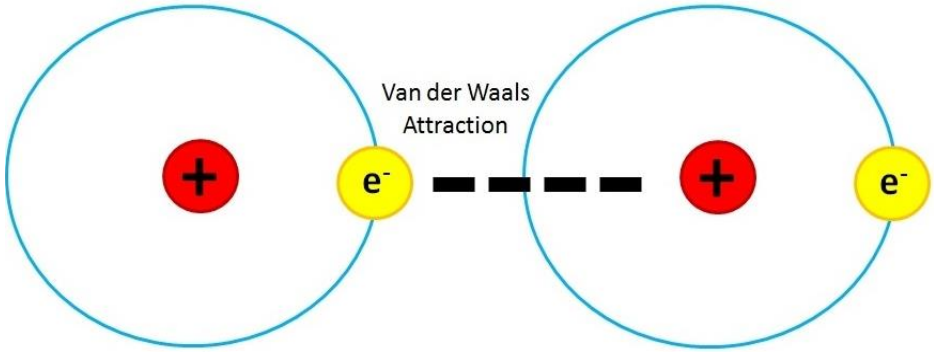

Figure 2.7: Van der Waals forces created by electrostatic particles [65]

2.5.2.5 Interlocking

The interlocking of particles depends on their shape. When the particle shape is suitable to forming closed bonds, a different type of physical bonding known as interlocking or matting can be generated. Fibrous, flat-shaped, and bulky materials are suitable for interlocking. Figure 2.8 shows the simplified interlocking process.

Figure 2.8: Interlocking closed bonds [50]

2.5.3 Materials Used for Wastewater Treatment

2.5.3.1 Algae as Raw Material for Wastewater Treatment

Microalgae is one of the most popular and effective materials used in wastewater treatment. Many studies and experiments have been performed using different types of algae. Zhao et al. [66] studied three different types of microalgae, i.e. *Selenastrum bibraianum*, *Scenedesmus obliquus*, and *Chlorella vulgaris* for high-strength wastewater treatment and potential lipid production. These microalgae were precultured and then added to an Erlenmeyer flask in which 2000 ml of synthetic high-strength wastewater was inoculated. All precultured algae species were cultivated for 7 days in BG-11 medium to obtain stable characteristics. During the 14-day period, chemical oxygen demand (COD), total nitrogen (TN), total phosphorous (TP) and pH were monitored. Table 2.1 shows the initial and final values of those parameters. As can be seen, *Scenedesmus obliquus* provides the better COD, TN, and TP concentrations overall.

TABLE 2.1

INITIAL AND FINAL NUTRIENT CONCENTRATIONS AND FINAL BIOMASS FOR TWO HIGH-STRENGTH WASTEWATERS WITH THREE MICROALGAE [66]

Wastewater used	Algae used	Initial nutrient concentration (mg L^{-1}, day 0)			Final nutrient concentration (mg L^{-1}, day 14)			Final biomass concentration (g L^{-1})
		COD	TN	TP	COD	TN	TP	
High C loading	*Selenastrum bibraianum*	530.08 ± 21.73	102.85 ± 2.16	3.34 ± 0.04	126.46 ± 1.64	85.54 ± 1.85	0.10 ± 0.003	284.25 ± 5.31
	Scenedesmus obliquus	535.70 ± 12.86	100.79 ± 3.43	3.26 ± 0.05	93.81 ± 3.01	39.13 ± 1.10	0.15 ± 0.005	481.99 ± 2.69
	Chlorella vulgaris	533.67 ± 18.14	97.36. ± 3.60	3.39 ± 0.07	130.05 ± 2.73	47.91 ± 1.20	0.14 ± 0.005	546.86 ± 7.28
High N loading	*Selenastrum bibraianum*	168.18 ± 3.53	194.65 ± 5.45	3.45 ± 0.06	49.83 ± 1.69	164.21 ± 4.43	0.15 ± 0.004	249.65 ± 7.87
	Scenedesmus obliquus	168.35 ± 5.56	194.18 ± 6.99	3.51 ± 0.08	33.61 ± 1.38	77.58 ± 2.02	0.11 ± 0.004	465.29 ± 6.14
	Chlorella vulgaris	167.73 ± 4.19	195.91 ± 6.07	3.47 ± 0.07	56.96 ± 2.22	102.47 ± 2.15	0.19 ± 0.007	529.89 ± 4.33

Gutzeit et al. [67] studied algal-bacterial biomass to establish a low-cost wastewater treatment. Symbiotic reaction was the main principle used in this study. Here, the beneficial interactions between photoautotrophic algae and heterotrophic bacteria enhance the exchange of oxygen and carbon dioxide. Simultaneous degradation of organic carbon by heterotrophic bacteria and nutrients has occurred due to the interactions. This study involved the operation of a laboratory scale and a pilot scale reactor system. Two metal halide lamps were installed to irradiate the tank with about 2,000 micro-mol/s-m^2 for a period of 10 to 12 hrs a day. COD, total organic carbon, TN, TP, and ammonium concentrations were studied before and after the operation in wastewater. The mechanism of symbiotic interactions is shown in Figure 2.9, and a comparison of all concentrations characterizing the wastewater is provided in Table 2.2.

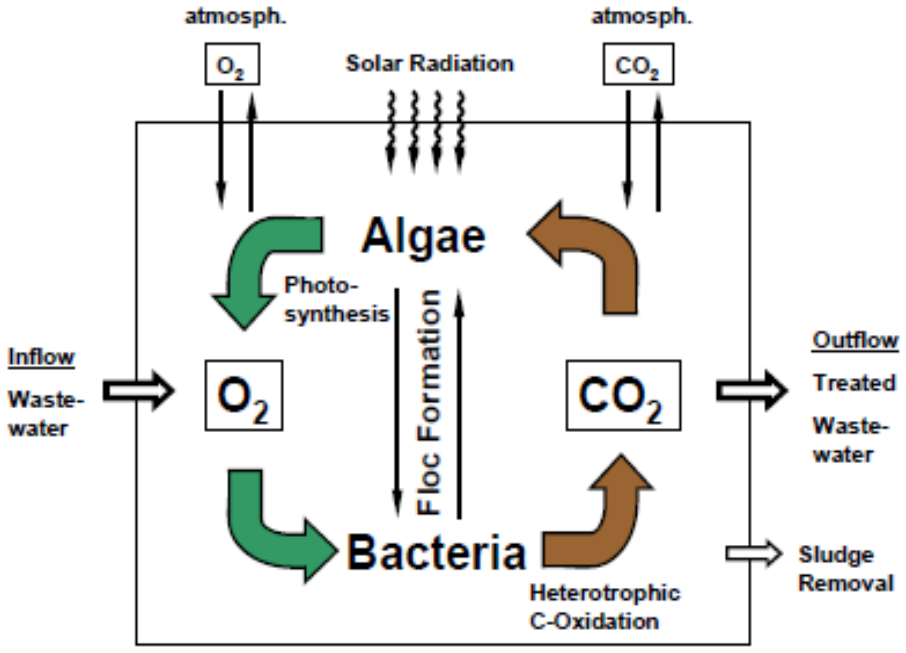

Figure 2.9: Schematic diagram of symbiotic interactions with algal-bacterial biomass [67]

TABLE 2.2

CHARACTERIZATION OF WASTEWATER [67]

Parameter	Unit	Synthetic wastewater	Pre-treated sewage
		Mean (after preparation)	Mean ± s.d.
Chemical oxygen demand	($mgO_2\ l^{-1}$)	420	471.3 ± 90.0
Total organic carbon	($mgC\ l^{-1}$)	195	230.0 ± 40.0
Total nitrogen	($mgN\ l^{-1}$)	75	78.5 ± 10.1
Ammonium	($mgN\ l^{-1}$)	12	53.9 ± 7.6
Total phosphorus	($mgP\ l^{-1}$)	12	10.8 ± 2.0

Ting et al. [68] reviewed the previous work of microalgae cultivation in photobioreactors (PBRs) and their application in wastewater treatment. In this study, PBR configurations, design parameters, and types of wastewater were investigated. The photosynthesis process gives microalgae the ability of CO_2 sequestration and pollutant removal. Various PBRs have been developed for microalgae cultivation: open, closed, and semi-closed vessels. An open PBR is commonly used in commercial applications; however, low yield of biomass and easy contamination are problems associated with this type of PBR. Therefore, closed systems have been used for scientific research. The removal of pollutants such as nitrogen and phosphorous is related to the cultivation environment and growing conditions such as supplementation of light, CO_2, and hydraulic retention time. Using different microalgae species, Ting et al. reviewed the configurations of almost all kinds of closed-system PBRs: suspended, flat panel, tubular, immobilized bead, and biofilm. They analyzed the water quality in terms of the removal of

pollutants such as COD, TN, TP, ammonia, phosphate, acetate, etc. Some schematic diagrams of PBRs for the cultivation of pure microalgae are shown in Figure 2.10.

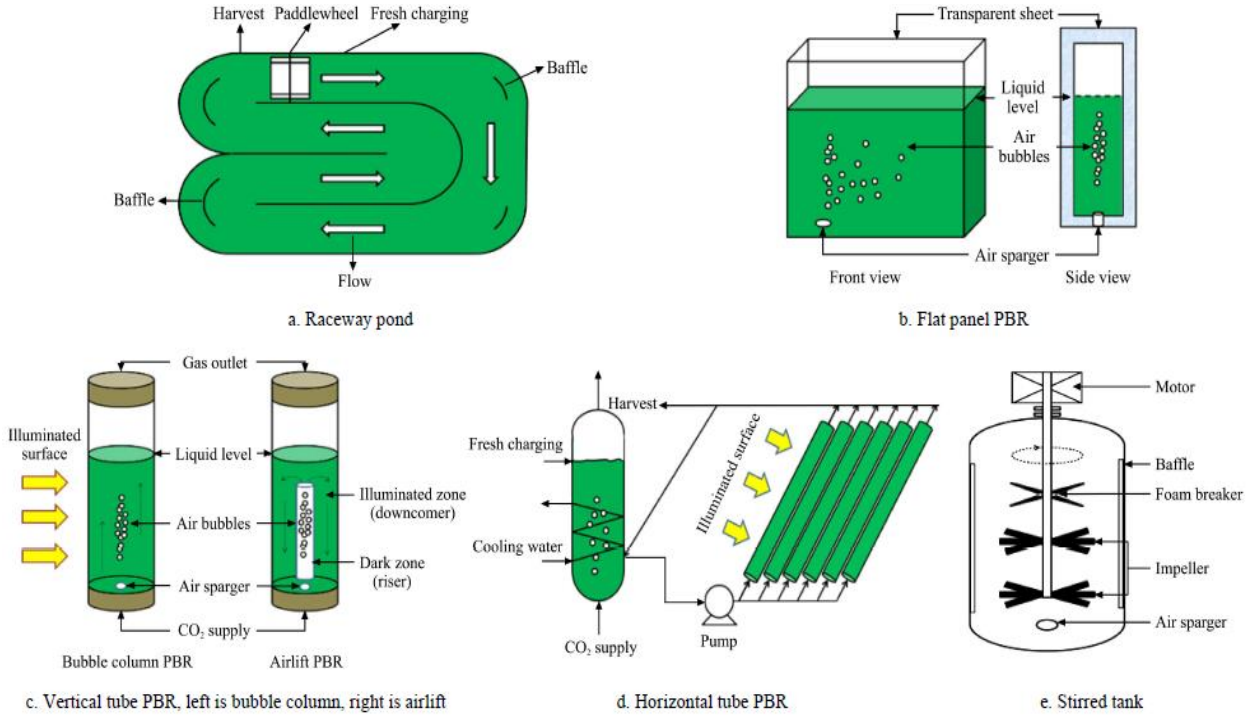

Figure 2.10: Schematics of different types of PBRs for microalgae pure cultivation [68]

Shi et al. [69] studied the nitrogen, phosphorous, and ammonium removal from wastewater using two green microalgae: *Chlorella vulgaris* and *Scenedesmus rubescens*. They used the method of algal cell immobilization in a twin-layer system, with the second layer consisting of macro-porous fibrous tissue. The advantage of twin layers is the ability to separate microalgae from the bulk of their growth medium and yet allow nutrient diffusion. The total procedure was divided into the microalgae culture preparation and the twin-layer setup. Algae cultures were kept at $23 \pm 2^{\circ}C$ using a fluorescent white light with a light/dark period of 14/10 hrs. Cultures were grown in Erlenmeyer flasks with Waris-H medium. After 4–6 weeks, those cultures were moved to another aerated 10L flask. After reaching the sufficient cell density, algal biomass was harvested by centrifugation at 3,000 rpm for 10 minutes and then immobilized. The twin-layer system was

composed of two different porous, ultrathin sheets: one the substrate layer, and the other the source layer, both of which are hydrophilic, wet, and self-adhering. Twin layers were mounted on a board of polyvinyl chloride (PVC) and placed vertically. Wastewater was inserted on the top of the source layer at the PVC board at a speed of 220–240 mL/hr by a peristaltic pump. A schematic of this twin-layer wastewater treatment is shown in Figure 2.11. After 8–9 days, the remaining amount of phosphate, ammonium, and nitrate was less than 10% of their initial concentrations. *Chlorella vulgaris* showed a better removal rate of pollutants at any time than *Scenedesmus rubescens.*

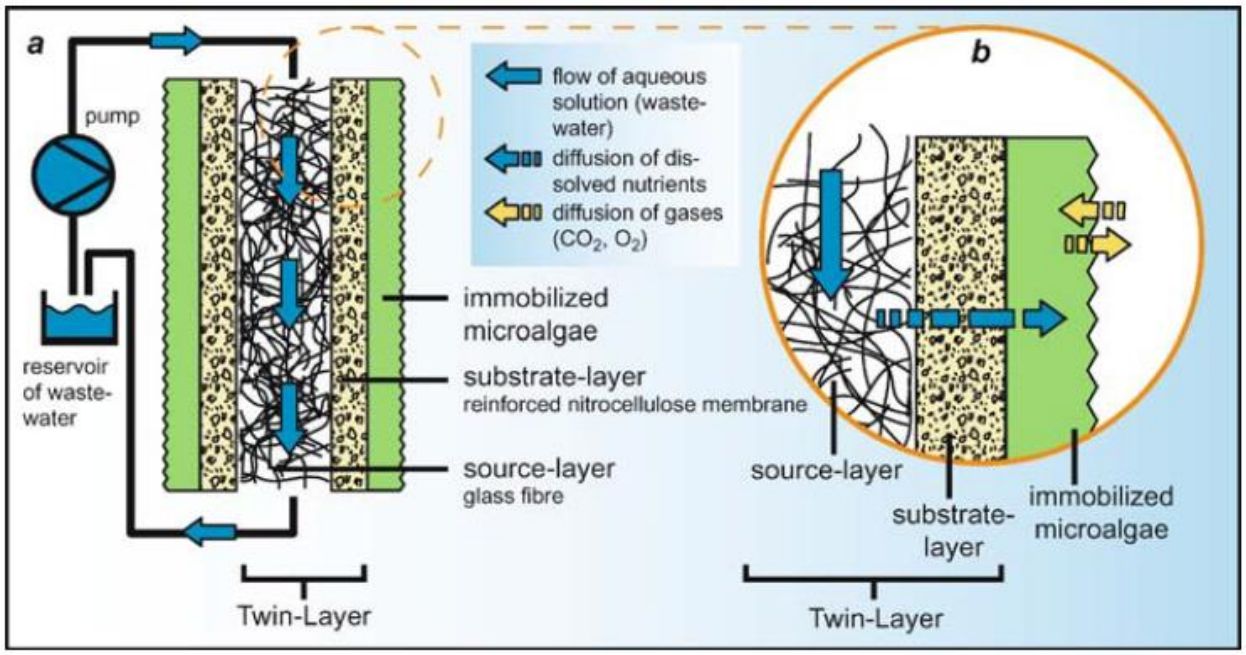

Figure 2.11: Twin layer wastewater treatment [69]

Chan et al. [70] analyzed nutrient removal from the secondary effluent from wastewater by using microalgae. They used *Chlorella vulgaris* (CV), *Spirulina maxima* (SM), and a mixture of *Synechocystis sp.* and *Chlorella sp.* (MIX) as raw materials for the algae strain. The cultures were grown in 250-ml Erlenmeyer flasks after autoclaving at 121°C for 15 minutes at 98–137 KPa. Two sets of bulbs were provided to maintain the temperature of 26°C–28°C. Two trials were performed

using the secondary effluent. One trial, where secondary effluent was added to the autoclaved flasks and inoculated, was referred to as the "untreated" trial. In the other trial, secondary effluent as well as the flask were autoclaved, prior to adding the inoculation, which destroyed all microorganisms. This trial was referred to as the "autoclaved" trial. Microalgae were grown for 3 weeks in the Erlenmeyer flasks. The percent removal of total phosphorous and total ammonia for both trials from this study is shown in Tables 2.3 and 2.4, respectively.

TABLE 2.3

PERCENT REMOVAL OF TOTAL PHOSPHOROUS FOR NORMAL AND AUTOCLAVED TRIALS [70]

	Normal				Autoclaved			
I	II	III	IV	V	II	III	IV	V
Strain	Initial (mg/L)	Final (mg/L)	Day	% Removal	Initial (mg/L)	Final (mg/L)	Day	% Removal
Control	0.148	0.0251	8	83.0	0.132	0.0975	2	26.1
CV	0.987	0.0613	4	93.8	0.687	0.0820	6	88.1
SM	0.951	0.125	4	86.8	0.706	0.0958	6	86.4
MIX	0.937	0.0389	6	95.8	0.654	0.0631	4	90.4

TABLE 2.4

PERCENT REMOVAL OF TOTAL AMMONIA FOR NORMAL AND AUTOCLAVED TRIALS [70]

	Normal				Autoclaved			
I	II	III	IV	V	II	III	IV	V
Strain	Initial (mg/L)	Final (mg/L)	Day	% Removal	Initial (mg/L)	Final (mg/L)	Day	% Removal
Control	30.7	4.51	6	85.3	40.4	24.1	8	40.3
CV	32.1	6.04	6	81.2	37.8	8.91	6	76.4
SM	40.1	2.15	6	94.6	50.0	6.88	8	86.2
MIX	44.4	3.15	8	92.9	53.3	8.13	8	84.7

2.5.3.2 Date as Raw Material for Waste Water Treatment

Date as raw material for activated carbon is gaining popularity due to its availability and price. There are almost 10 million palm trees in the United Arab Emirates alone. A female palm tree bears approximately 200–1000 dates. Therefore, a single tree may provide 600 pounds of date seeds annually on average. For this reason, as a raw material for AC, date seed is a very good

option. Mane et al. [71] studied the removal of phenol from wastewater using AC, where date seeds were considered as raw materials for the preparation of carbon. Phenol removal is necessary because of its toxicity and pungent odor. For the preparation of date seed carbon (DSC), at first the date seeds were dried and grinded. Then the ground small particles were boiled with distilled water and filtered, and eventually dried for the carbonization. Date seeds were heated at 700°C for 1 hr in the presence of limited oxygen. The DSC was washed with distilled water several times, dried at 110°C, and sieved through a 100-mesh screen size. The surface area and pH of the prepared carbon was 66 m^2/gm and 7.75, respectively. An amount of 100 mg of this carbon was added to 50 ml of wastewater, placed in a 250-ml Erlenmeyer flask, and shaken at 180 rpm for 6 hrs to ensure equilibrium. In this study, the adsorption of phenol on the DSC was investigated by changing the concentration from 100 to 200 mg/l. As shown in Figure 2.12, the amount of phenol absorbed increased with the increase in the DSC concentration.

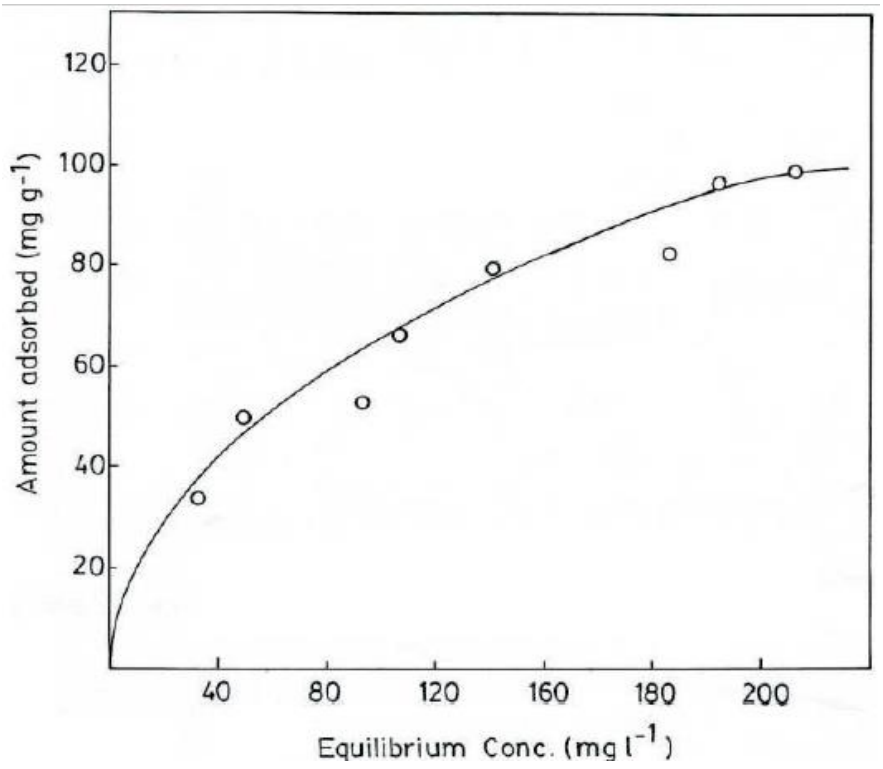

Figure 2.12: Adsorption isotherm of phenol on DSC [71]

Nemr et al. [72] studied activated carbon from date palm seeds to treat wastewater containing toxic chromium. Adsorption is one of the most efficient ways to remove toxic pollutants from a solution. Activated carbon has proven to be an effective adsorbent for the removal of a wide range of organic and inorganic pollutants from different media. In this study, date palm seeds were washed with distilled water and dried in an oven for 24 hrs at 200°C. The dried seeds were milled and sieved to a particle size less than 0.5 mm. The sieved particles were added to sulfuric acid (H_2SO_4) for 5 hrs followed by boiling for 20 hrs in a fume hood. Then the mixture was cooled in an ice bath. The obtained cool carbon was dried in an open oven for 24 hrs at 120°C and then immersed in 5% sodium bicarbonate ($NaHCO_3$). It was ensured that the AC had a pH of 6, then dried at 150°C for 24 hrs, and finally sieved to a particle size less than 0.1 mm. The prepared carbon was mixed with a solution of 5.657 gm of potassium dichromate ($K_2Cr_2O_7$) to make 500 ml and then added to 1,000 ml of distilled water. The concentration of $K_2Cr_2O_7$ was kept in a range of 5–150 mg/l. To adjust the pH value of the solution, 0.1 M HCl or 0.1 M NaOH was applied. From this investigation, it was seen that the chromium removal rate had an inverse relation to the pH values. Also, the chromium removal rate of any concentration increased with time. It was easier to remove the low concentration of chromium than the higher concentration of chromium. These results are shown in Figure 2.13.

Nemr et al. [72] also investigated the chromium removal capacity of DSC using different types of water: distilled water, artificial seawater, natural seawater, and wastewater. These results are shown in Table 2.5.

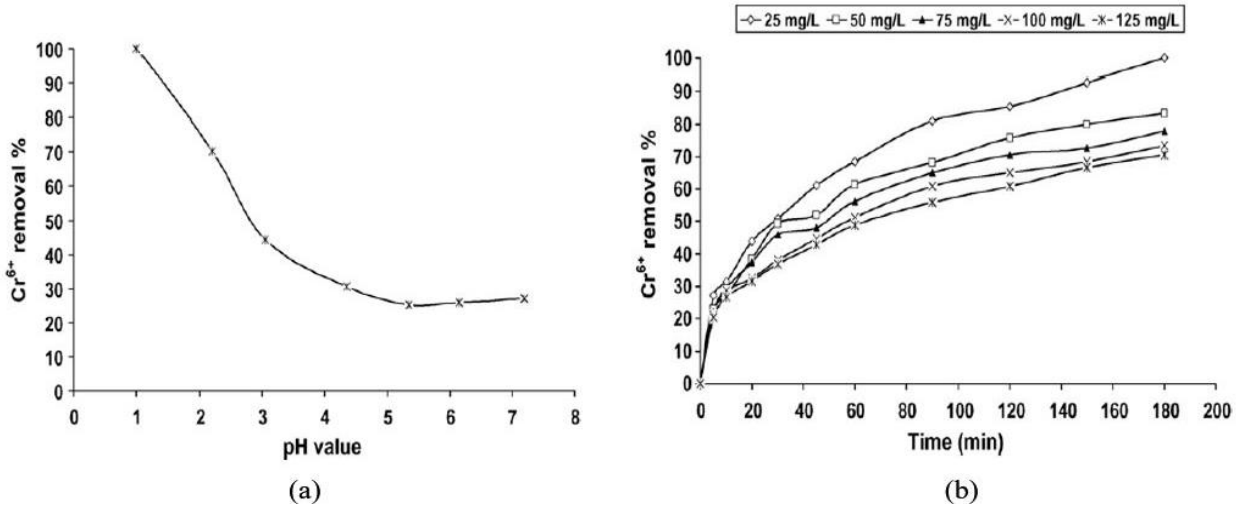

Figure 2.13: Results of DSC to treat chromium wastewater: (a) pH on adsorption of Cr^{+6}, and (b) contact time on removal of different initial concentrations of Cr^{+6} [72]

TABLE 2.5

ADSORPTION OF CHROMIUM (125 MG/L) IN DIFFERENT WATER SOLUTIONS USING DSC (5 G/L) [72]

Solution of chromium used	DSC	
	Removal (%)	Maximum capacity ($mg\ g^{-1}$)
Distilled water	92.43	120.48
Artificial seawater	93.12	121.22
Natural seawater	91.25	118.78
Wastewater	90.84	118.49

Islam et al. [73] prepared activated carbon from palm date seeds (PDSs) to study the mesoporous and adsorptive properties. To convert biomass into char, the hydrothermal carbonization (HTC) method was applied. This thermochemical operation is used to produce carbon from pure carbohydrates or lignocellulosic biomass. HTC can be performed at a comparatively low temperature and is eco-friendly. PDSs were washed several times to remove dirt and flesh, dried at room temperature, and then ground to a size of 1–2 mm. In the HTC reactor,

5 gm of crushed PDS was submerged with 100 ml of distilled water and then heated to 200°C for 5 hrs at a rate of 5°C/min. The brownish hydrochar produced was then cooled to room temperature, washed several times with distilled water, and heated again in an oven at 105°C for 24 hrs. After that, the hydrothermal carbonized PDS was impregnated with NaOH at different ratios to observe the effect and then oven dried again at 105°C for 24 hrs. Finally, the NaOH-hydrochar mixture was heated at 600°C under the flow of N_2 at 150 cm^3/min., at a heating rate of 10°C/min. The AC produced was then rinsed repetitively until the pH of the solution reached 6–7. This wet AC was oven-dried again for 24 hrs at 105°C. Along with the absorption of the pollutants, other parameters such as surface area, BET surface area, micropore surface area, and total pore value were also evaluated, as shown in Table 2.6.

TABLE 2.6

PROPERTIES OF PALM DATE SEED ACTIVATED CARBON [73]

Surface Area	1233.89 m^2/gm
BET Surface Area	1282.49 m^2/gm
Micropore Surface Area	769.81 m^2/gm
Total Pore Volume	0.66 cm^3/gm

2.5.3.3 Olive as Raw Material for Waste Water Treatment

Many studies have been performed on olive seeds and olive waste cake as the raw materials for activated carbon. Skodras et al. [74] studied several raw materials as AC to enhance mercury adsorption. They prepared seven different activated carbons from pine and oak wood, waste tires, and olive seeds. The AC produced from pine and oak wood and waste tires was done by physical activation. The AC produced from olive seeds was done by the chemical activation. In their experiment, samples from pine and oak wood were marked as A and B; three waste tire

samples were marked as C1, C2, and C3; and three olive seed samples were marked as D1, D2, and D3. For the pyrolysis of pine/oak wood and tires, a compact power pyrolysis plant was used. Here the samples were heated at 800°C in an inert environment for 45 min. The produced char was activated at 970°C through the flow of steam for 0.5 and 2 hrs. For olive seeds, dry olive kernels were pyrolyzed in a steel reactor at 800°C for 1 hr with a flow of N_2 at 100 cm^3/min. KOH was impregnated with the precursor in a ratio of 4:1. Mixing was done for 10 min, and the mixture was activated at 800°C with N_2 at 100 cm^3/min for 1 hr and 3 hrs. Following the AC preparation, the BET surface area, total pore volume, and mercury removal per AC mg (Hg adsorptive capacity) were evaluated. The results are shown in Table 2.7. It can be seen that activated carbon prepared from olive provides a higher BET surface area, pore volume, and adsorptive capacity. Among the samples, olive carbon activation for 3 hrs (Sample D2) shows a very high surface area, pore volume, and adsorptive capacity.

TABLE 2.7

PORE STRUCTURE CHARACTERISTICS AND HG ADSORPTIVE CAPACITY OF VARIOUS ACTIVATED CARBONS [74]

Sample	**BET (m^2/gm)**	**V_{tot} (cm^3/gm)**	**Hg (ng/mg AC)**
A (Pine/Oak)	896.7	0.61	421
B (Pine/Oak)	684.4	0.45	379
C1 (Waste Tire)	132.9	0.25	188
C2 (Waste Tire)	251.6	0.26	331
C3 (Waste Tire)	358.5	0.31	342
D1 (Olive, 1 hr Activation)	1058.2	0.66	795
D2 (Olive, 3 hr Activation)	1690	0.9	869

Martinez et al. [75] prepared activated carbon using olive stones and walnut shells to observe the iodine adsorption. The raw materials were cleaned and dried at 100°C and then ground

using a roller mill to obtain a particle size of 1–3 mm. The ground samples were then pyrolyzed in a muffle furnace at 600°C for 1 hr under the constant flow of nitrogen. After that, chemical activation was performed using KOH at two different concentrations (50% and 75%, w/w) in a ratio of 1:1 (KOH/char, w/w). Then the solution was dehydrated for 3 hrs at 300°C and immediately activated at 900°C for 1 hr in an N_2 media. Finally, the activated carbon was washed and dried at 100°C for 2 hrs and cooled. The obtained activated carbon by this process was in a granular form. The iodine adsorption capacity was evaluated and compared with the powder form of activated carbon and commercial carbon. A comparison of iodine adsorption in the olive pit carbon (OPC) is shown in the Figure 2.14.

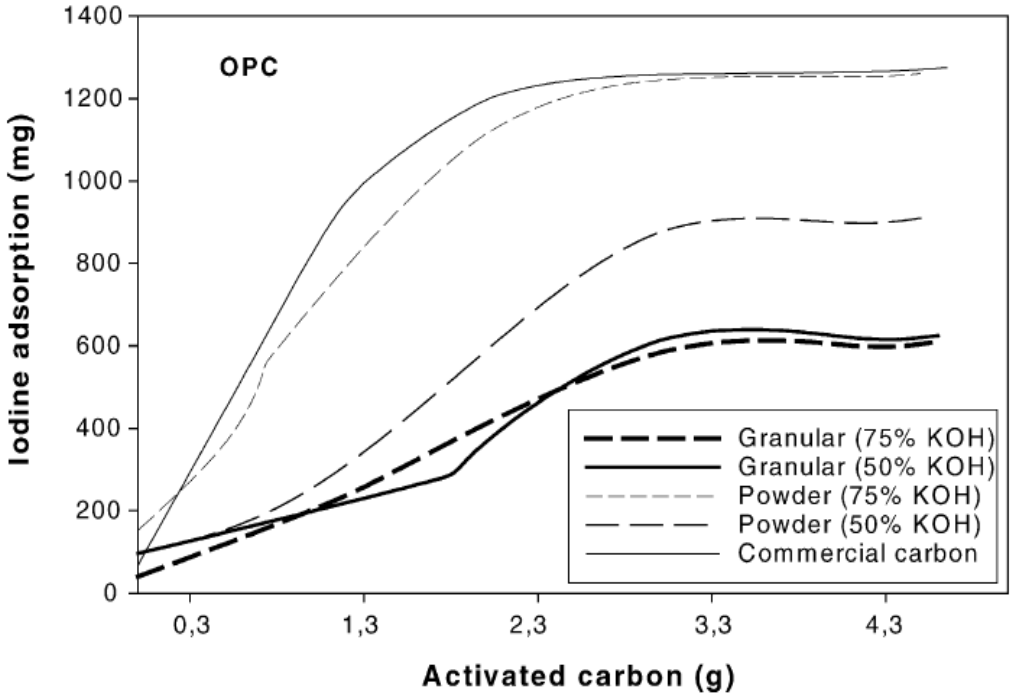

Figure 2.14: Iodine adsorption capacity of olive pit carbon [75]

Baçaoui et al. [76] studied the optimized conditions for producing activated carbon from olive-waste cakes. Activated carbon was produced at different activation temperatures and times to observe the effect. Carbonization was performed in a stainless steel autoclave where the olive-

waste cake was heated at 673K for 1 hr with a nitrogen flow. The activation process was carried out in a thermal silica electric oven. The activation time was varied from 30 to 70 min with a 10-min increasing rate, and the activation temperature was set between 1023 K and 1123 K. Following activation, the carbon was boiled in distilled water for 30 min, then dried and ground to a powder with a particle size smaller than 45 μm. Finally, the powder was dried at 383 K. By varying the activation condition (temperature and time), adsorption capacity, BET surface area, and pore volume, the external surface area was evaluated to find the optimum condition. These results are shown in Table 2.8. As shown, the higher values of adsorption capacity, BET surface area, and micropore volume were obtained at an activation time of 60 min and activation temperature of 1123 K.

TABLE 2.8

EXPERIMENTAL RESPONSES OF ACTIVATED CARBON USING OLIVE-WASTE CAKE [76]

Exp. No.	**Condition (Activation Time/ Temperature)**	**Methylene Blue Adsorption Capacity (m^2/gm)**	**Iodine Adsorption Capacity (m^2/gm)**	**BET Surface Area (m^2/gm)**	**Micropore Volume (cm^3/gm)**	**External Surface Area (m^2/gm)**
1	70/1073	373	1261	1201	0.298	0.557
2	30/1073	115	796	514	0.249	0.238
3	60/1123	490	1495	1271	0.377	0.456
4	40/1023	121	741	687	0.225	0.217
5	60/1023	197	996	700	0.272	0.303
6	40/1123	364	1017	1127	0.317	0.389
7	50/1073	285	930	1025	0.229	0.294

Stavropoulos and Zabaniotou [77] investigated the properties and N_2 removal using activated carbon produced from olive seed waste residue. The residue was first ground and sieved to a particle size of 125–160 μm and then dried at 110°C for 24 hrs. Pyrolysis of the sieved materials was done at 800°C for 1 hr in an inert atmosphere. The flow of N_2 flow was at a rate of 100 cc/min to ensure the inert atmosphere. After carbonization, the remaining chars were mixed with KOH in a ratio of 1:4 (C/KOH), and individually activated at temperatures of 800°C and 900°C for 1, 2, 3, and 4 hrs. Following activation, the residue was mixed with HCl for 1 hr to neutralize the KOH, and then washed with distilled water until a neutral pH was achieved. Finally, the produced activated carbons were dried at 110°C for 24 hrs. BET surface area and total pore volume were evaluated for different conditions. These values are shown in Table 2.9. It can be seen that the activation temperature of 900°C and activation time of 4 hrs resulted in the maximum BET surface area (3049 m^2/gm) and maximum pore volume (1.52 cm^3/gm). A similar result was seen in the N_2 absorption graph shown in Figure 2.15. The higher amount of N_2 absorption was achieved at 900°C and 4 hrs of activation time.

TABLE 2.9

STRUCTURAL PARAMETERS OF OLIVE SEED CARBON [77]

Temperature (°C)	**Time (hrs)**	**BET Surface Area (m^2/gm)**	**Total Pore Volume (cm^3/gm)**
800	1	1339	0.595
800	2	1334	0.580
800	3	2578	1.062
800	4	2431	1.033
900	1	1550	0.679
900	2	1462	0.665
900	3	1798	0.842
900	4	3049	1.52

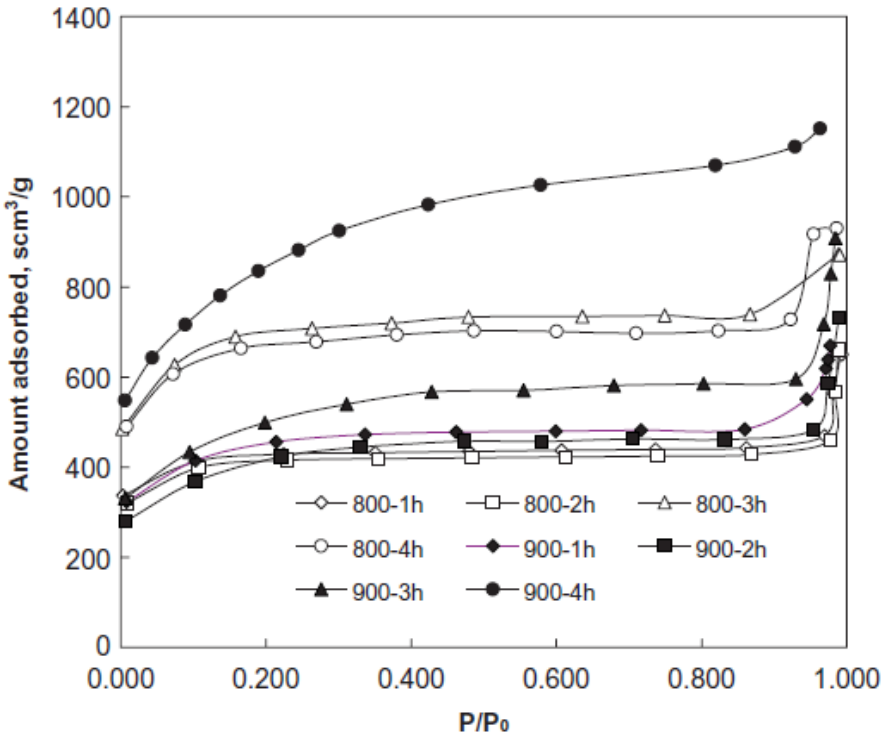

Figure 2.15: N_2 absorption isotherms of carbons from olive seed waste activated with KOH [77]

CHAPTER 3

EXPERIMENT

3.1 Materials and Equipment

Different materials and equipment were used in this study to prepare the activated carbon and study the surface area and adsorption properties. Various waste materials—algae, date seeds, olive seeds, used paper, and waste cotton cloth—were used as raw materials for the activated carbon. The briquetting method was used for the algae, used paper, and waste cotton cloth. Making briquettes requires a binder, and molasses was selected as the binder here. The chemical reagents used for activation were $CaCl_2$ and $ZnCl_2$. The pH was adjusted using HCl and NaOH.

3.1.1 Date Seeds

Dates are very popular in the Middle Eastern region due to their availability and taste. A large amount of date seeds can be recycled every year. The chemical content of date seeds is provided in Table 3.1. Due to the higher percentage of carbohydrate and other contents such as protein and fat in date seeds, they can be considered a very good source of carbon. Dates were purchased from a local store, and the seeds were collected and washed in the laboratory. Collected date seeds are shown in Figure 3.1.

TABLE 3.1

CHEMICAL COMPOSITION OF DATE SEED
(COMPOSITION PERCENTAGE MAY VARY ACCORDING TO TYPE) [78]

Content	Percentage of Chemical Content
Moisture	3–12
Fat	5–13
Protein	3–6
Ash	0.9–2
Carbohydrate	70–85

Figure 3.1: Date seeds

3.1.2 Olive Seeds

Olives are useful for many purposes, i.e., medical treatment, skin care, and nutrition. Along with fat, protein, and carbohydrates, olive seeds contain polyphenols and antioxidants. It is difficult to provide an exact chemical composition of the content of olive seeds. Activated carbon from olive seeds can be a very good mercury, iodine, and nitrogen adsorbent. For this study, olive fruits were purchased from the local market, and the olive seeds were collected in the laboratory. Collected olive seeds are shown in Figure 3.2.

Figure 3.2: Olive seeds

3.1.3 Algae Powder

Algae culture has been used prolifically for many years as a method to clean wastewater. Algae is very effective in the adsorption of nitrogen, phosphorous, and ammonium. In this study, instead of cultivating algae in water, pure algae powder was used to treat wastewater. Spirulina

pure powder, purchased from Herb Store USA, contains protein, a negligible amount of carbohydrate and fat, Vitamin A (beta-carotene), and Vitamin B-12. Molasses was used as a binder to prepare the briquette from the spirulina pure powder (algae), which is shown in Figure 3.3.

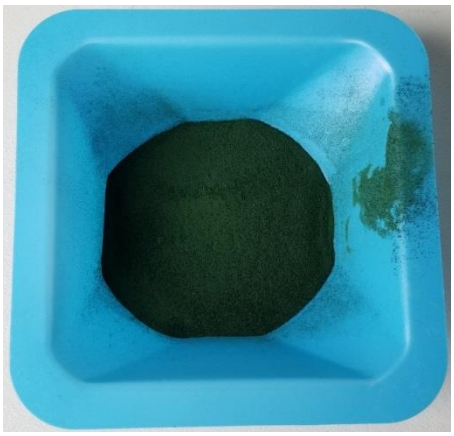

Figure 3.3: Spirulina Pure Powder (Algae)

3.1.4 Waste Paper

In this study, waste paper was chosen as one of the raw materials for activated carbon due to its availability and better surface area. Typically, writing or printing paper consists of cellulose fibers, lignin, some coating and filling materials such as clay, calcium carbonate, titanium oxide, etc., and some chemical additives such as rosin, alum, and starch. The waste paper used in this study is shown in Figure 3.4.

Figure 3.4: Waste paper

3.1.5 Waste Cotton Cloth

Waste cotton cloth was chosen as a raw material for activated carbon because of its porous characteristics. Waste cotton, supposedly containing 99% cellulose, was collected from various sources. Some washing was required before using the cloth. The cloth used in this experiment is shown in Figure 3.5.

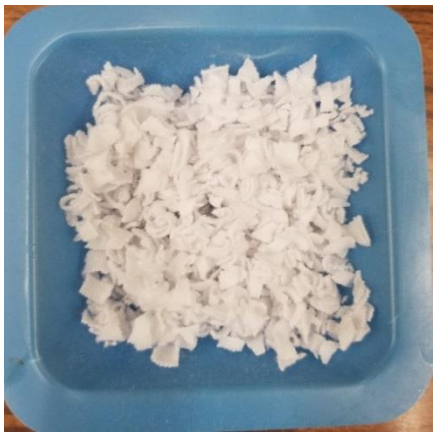

Figure 3.5: Waste cotton cloth

3.1.6 Other Materials and Equipment

Other materials used in this experiment are listed below:

- 25% $ZnCl_2$ solution
- 25% $CaCl_2$ solution
- Deionized (DI) water
- 3 M HCl
- 1 M NaOH
- Molasses
- Argon gas

Other equipment used in this experiment are listed below:

- Weighing Scale (Mettler Toledo, Model: ME 103, maximum capacity: 120 gm)

- Mortar
- Pulsing Vortex Mixer (Fisherbrand, speed: 500–3000 rpm)
- Mold and Die Punch (briquetting tools)
- Hydraulic Press (Dake Utility, Model: B-10, capacity: 10 tons)
- Magnetic Hot Plate Stirrer
- Precision Gravity Convection Oven (Thermo Scientific Thelco, temperature display: 0–250°C)
- Split-Tube Furnace (MTI, Model: OTF 1200X series, maximum temperature: 1200°C)
- Benchtop pH/mV Meter (Sper Scientific, Model: 860031)
- Total Dissolved Solids and Electrical Conductivity Meter (Pancellent)
- Turbidity Meter (Xinrui, Model: WGZ-1B)

3.1.7 Equipment Used for Briquetting

To create briquettes, higher pressure and a mold are required. A cylindrical die and punch mold with a half-inch diameter were designed in a Wichita State University machine shop. Figure 3.6 shows an isometric view of the wireframe of the die and punch mold with some relevant dimensions. The punch part of the mold consists of a punch rod and a flat head to close the die. The punch rod was designed to transfer the load directly to the briquetting samples. The upper part of the punch rod was ground down to 0.01 inch to reduce the friction between the surface contact and the die. The die also consists of two parts, in order to remove the briquette easily. The bottom of the die has an end fitting that is screwed onto the die when the briquette is being pressed, and this end fitting is removed in order to push out the produced briquette. The die and punch of the mold used in the experiment are shown in Figure 3.7.

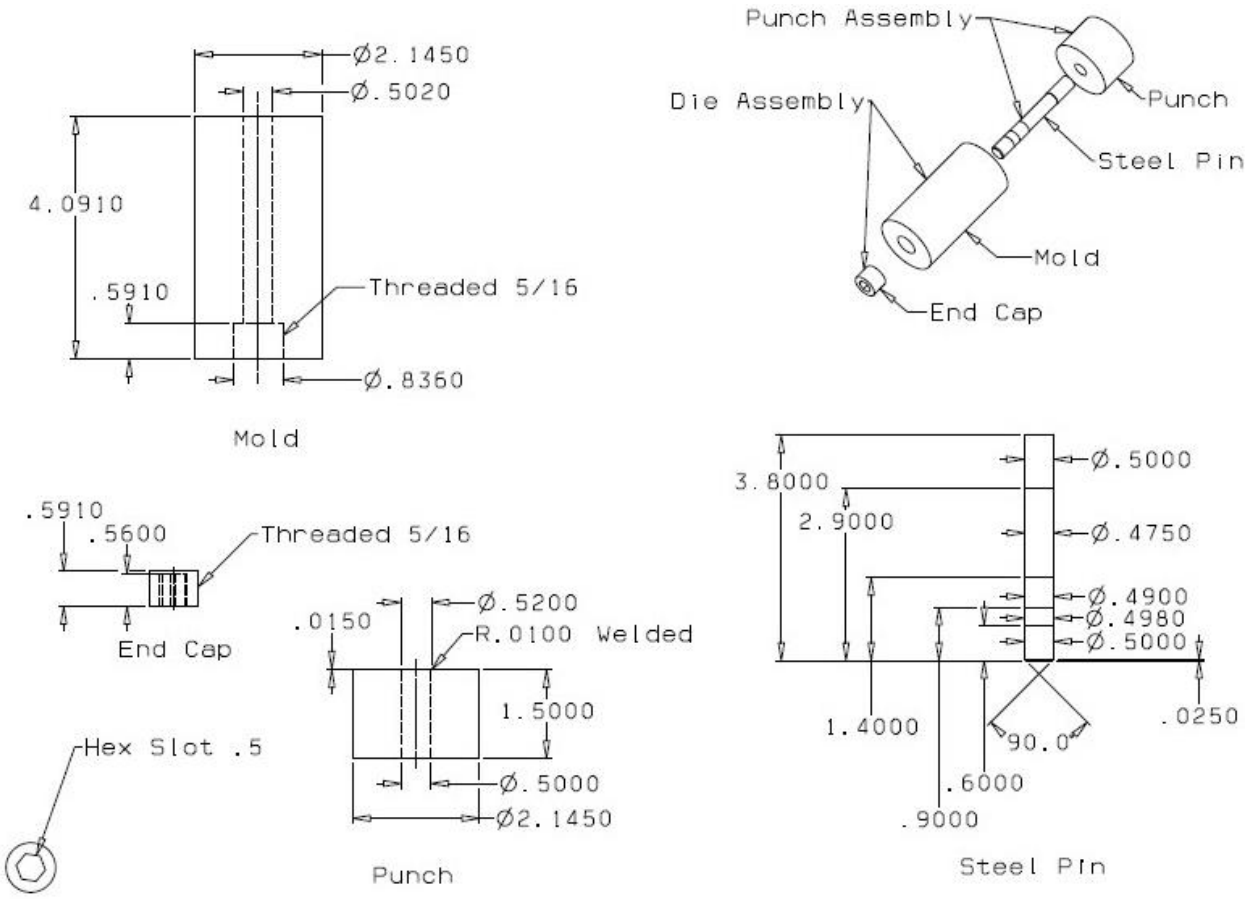

Figure 3.6: Isometric view of wireframe of die and punch mold

Figure 3.7: Die and punch of mold

3.2 Methods

Before carbonization, the different sample materials were prepared. For date and olive seeds, crushing and sieving were necessary. For algae, waste paper, and waste cotton fabric, the briquetting method was applied. Both approaches are discussed elaborately in the following sections.

3.2.1 Preparation of Date and Olive Seeds

3.2.1.1 Crushing and Sieving of Seeds

After collecting the seeds, they were first washed with deionized water and dried for 24 hrs at room temperature. The dried seeds were then crushed and sieved using a hydraulic press and a mortar. Finally, seeds were sieved to a size of 3–4 mm.

3.2.1.2 Impregnation of Seeds with Chemical Agents (Chemical Activation)

For chemical activation, samples must be impregnated with chemical agents. In this study, $ZnCl_2$ and $CaCl_2$ were used separately to achieve the activation and to observe the individual effects. Before impregnation, 25% solutions of $ZnCl_2$ and $CaCl_2$ were prepared using 15 gm of DI water and 5 gm of $ZnCl_2$ and $CaCl_2$ powders. After preparing the solutions, 20 gm of date/olive seeds were impregnated with 20 gm of a $ZnCl_2$/$CaCl_2$ solution and stirred at 85°C for 2 hrs on a magnetic hotplate stirrer. The impregnated solution was then dehydrated at 110°C for 24 hrs in an oven.

3.2.2 Preparation of Algae, Waste Paper, and Waste Cotton Cloth Samples

3.2.2.1 Mixing of Algae, Waste Paper, and Waste Cotton Cloth Samples with Binder

To prepare the briquettes, a binder was used to enhance the adhesive forces in order to hold the materials altogether. In this study, molasses was used as the binder. The goal here was to prepare 3-gm briquettes. To serve this purpose, a 3.2-gm homogeneous mixture of each sample

with binder was prepared, where 94% would be the base material (algae, waste paper, or waste cotton cloth) and 6% would be the binder, meaning approximately 3.008 gm base material and 0.192 gm molasses, which were measured using a weighing scale. The reason behind the 3.2-gm mixture accounts for the loss of material during the briquetting process, so that after loss, there should be a briquette of approximately 3 gm. Waste paper and waste cotton cloth were chopped to a size of 2–3 mm. Then the material and binder were first mixed manually using a stirrer; however, to create a homogeneous mixture, the prepared mixture was further mixed using a vortex mixer for 5 min at 3000 rpm to prepare a uniform mixture. Figure 3.8 shows the vortex mixing process.

Figure 3.8: Vortex mixing process

3.2.2.2 Briquetting of Materials

A negligible amount of vegetable oil was added to the die in order to reduce the friction between the punch rod and the interior of the die wall. The sample mixture was then inserted into the mold, and the punch was inserted into the mold. The die-punch was placed in the hydraulic press, and 5 tons/cm^2 of pressure was applied to the punch. This pressure was kept for 2 min. After

releasing the pressure, the bottom end of the die was opened using an Allen wrench to extract the prepared briquette. The experimental setup for preparing the briquettes and the various prepared briquettes are shown Figures 3.9 and 3.10, respectively.

Figure 3.9: Experimental setup for briquette production

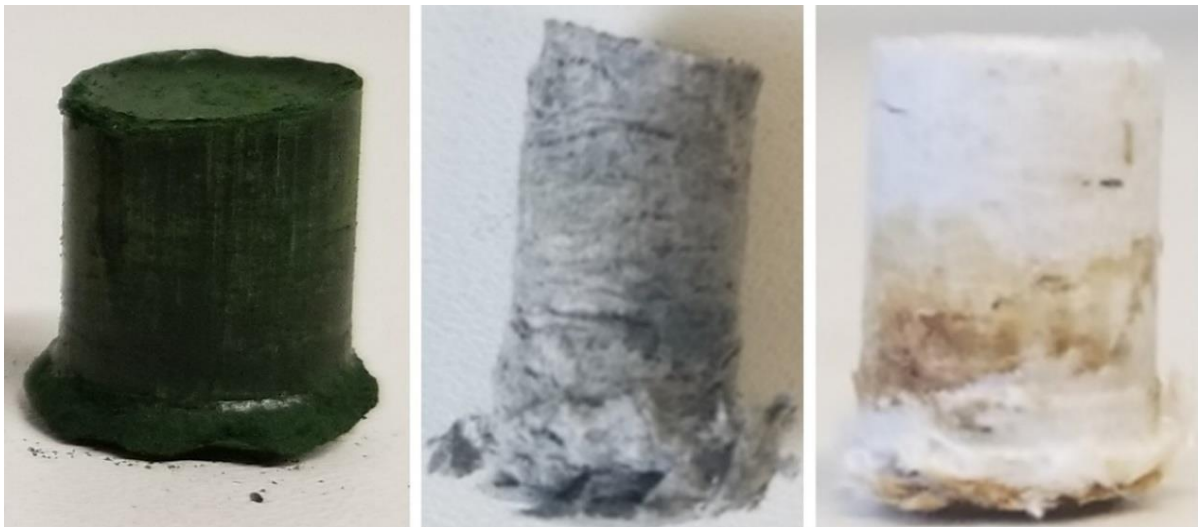

(a) (b) (c)

Figure 3.10: Various briquettes: (a) algae, (b) waste paper, and (c) waste cotton cloth

3.2.2.3 Impregnation of Briquettes with Chemical Agent (Chemical Activation)

This process was quite similar to the impregnation of seeds. Each of the various briquettes was impregnated separately in a large beaker with a 25% solution of $ZnCl_2$/$CaCl_2$ solution. A thin layer of net was used to prevent any loss of materials in the solution. The briquettes were impregnated for 2 hrs at 85°C without any stirring. After that, the impregnated briquettes were dried at 110°C for 24 hrs in an oven.

3.2.3 Pyrolysis of Samples (Carbonization)

The dried samples were placed inside a horizontal tube furnace and pyrolyzed in an inert atmosphere under the flow of argon gas. The temperature was ramped from an atmospheric temperature to 750–850°C at a rate of 10°C/min. For the date and olive samples, a temperature of 850°C was held constant for 1 hr, and for the briquettes, a temperature of 750°C was held constant for 1 hr. The pyrolyzed samples were then cooled at room temperature. The experimental setup for carbonization and its schematic are shown in Figures 3.11 and 3.12, respectively.

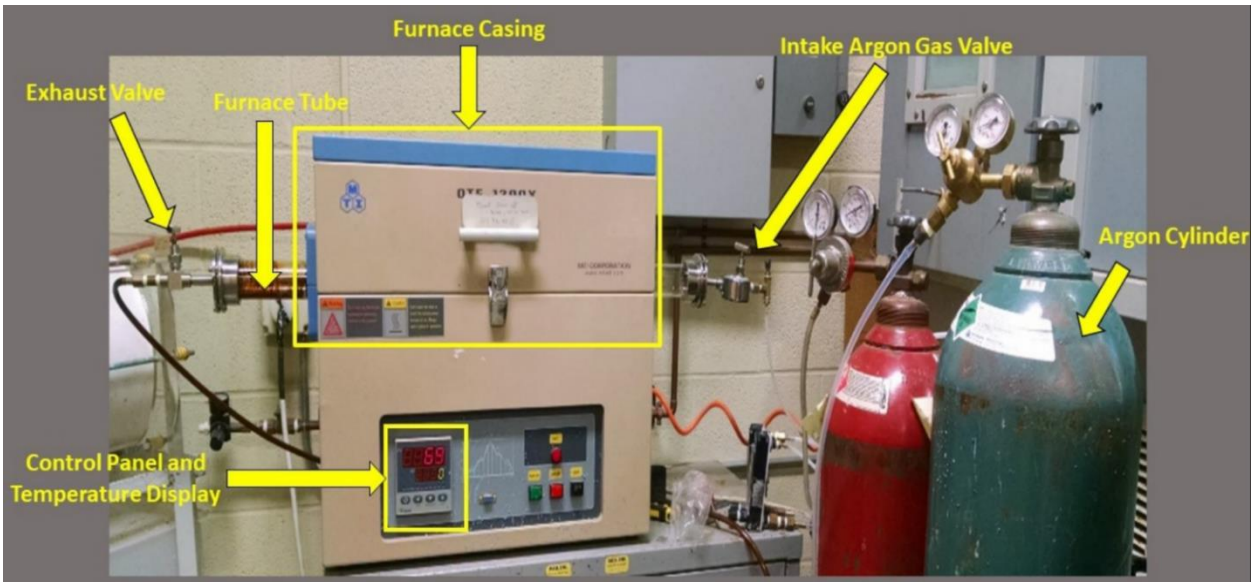

Figure 3.11: Experimental setup for carbonization

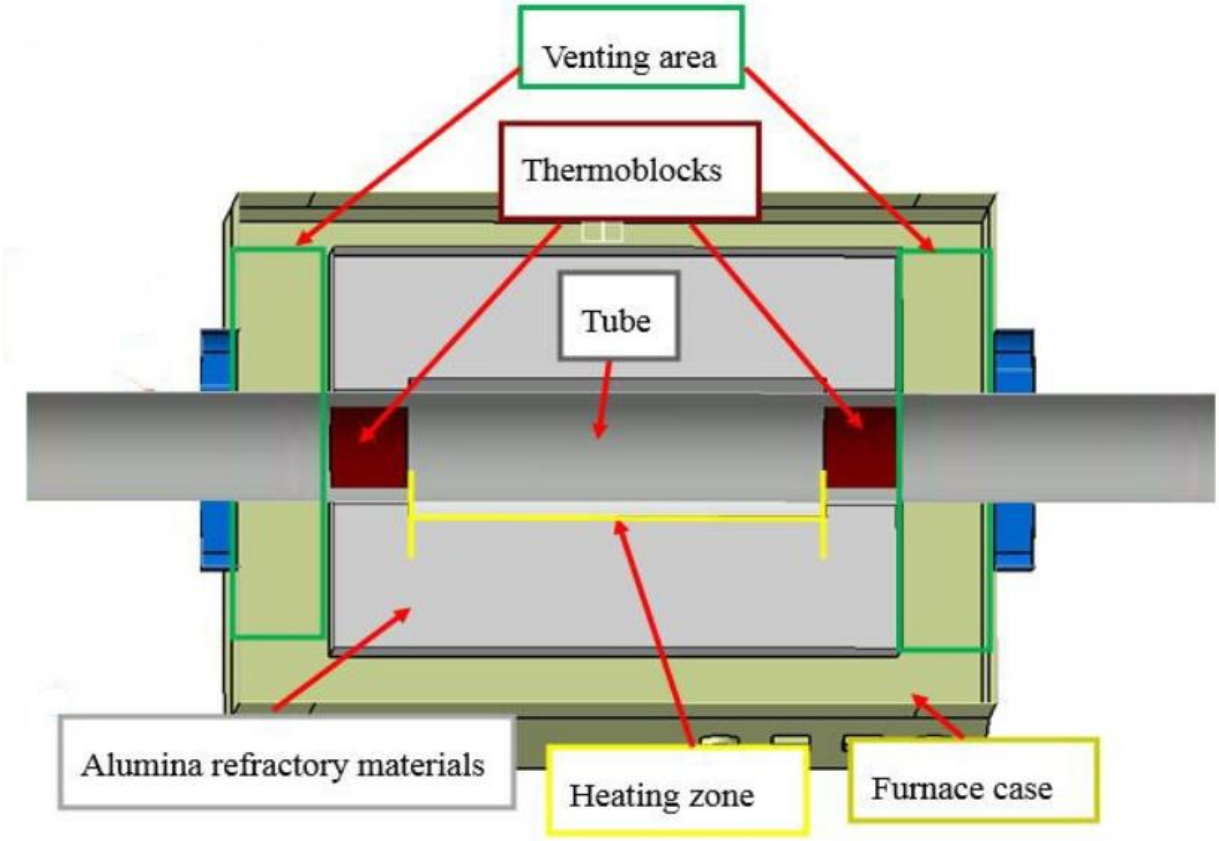

Figure 3.12: Schematic diagram of MTI tube furnace OTF-1200X [79]

3.2.4 Washing and pH Adjustment of Activated Carbon

After cooling the activated carbons, they were washed with a 3M HCl solution by heating to 90°C for 30 min and then filtered. Following that, the carbons were rinsed with DI water until solution pH was almost 7. To neutralize the effect of the concentrated HCl, 1M NaOH was used at the beginning of the rinsing process. After washing and filtering multiple times, the carbon solutions were brought to a pH of 6.7–7. Then the activated carbons were filtered and dried at 105°C for 12 hrs in an oven. Finally, the activated carbons were collected for use in the water column. The final product of each activated carbon is shown in Figure 3.13.

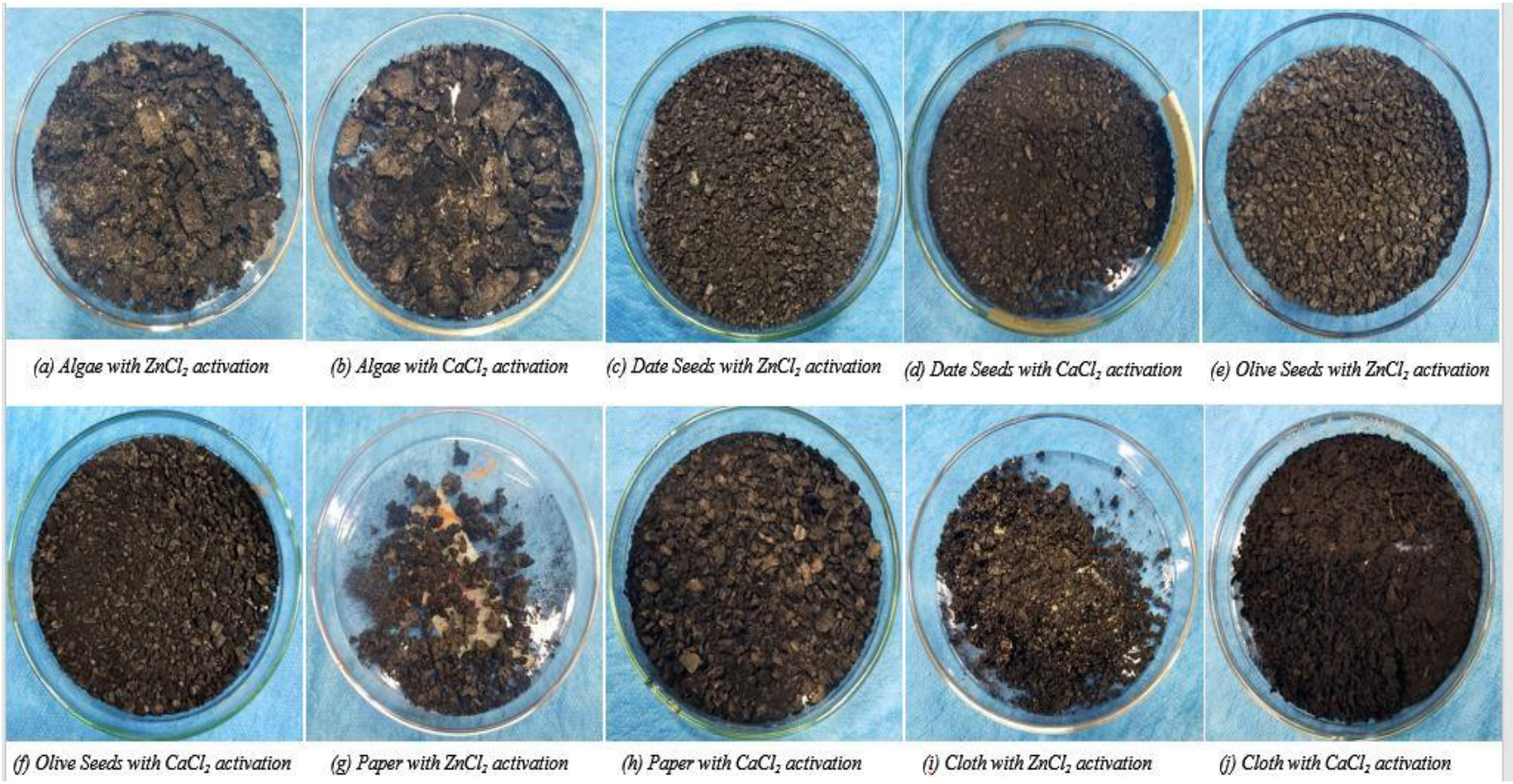

Figure 3.13: Various activated carbon samples prepared by carbonization and chemical activation

3.3 Preparation of Water Column for Filtration

For filtering the water with the produced activated carbon, it was necessary to build a water column. Materials used to make the water column are as follows:

- PVC polymer pipe (3/8 inch outer diameter and 1/2 inch inner diameter)
- Small polymer tube (1/2 inch outer diameter)
- Sand
- Prepared activated carbon
- Clean cotton cloth

The total water column filter was divided into five layers. At the bottom of the PVC polymer pipe, a clean cotton fabric layer was inserted very tightly so that it could hold the other layers properly. A sand layer was added over the cotton cloth layer. Then an activated carbon layer was inserted for purposes of adsorption. Another layer of sand was added over the activated carbon layer. Finally, a clean cotton cloth layer was added very tightly in order to provide rigidity to the entire water column system. Each layer was approximately 2 cm thick.

This filtration system required a vacuum pump to create negative pressure. One end of the water column was submerged under water, and the other end was connected to the vacuum pump via a small polymer tube so that the pump could draw water through the column by creating negative pressure. Another tube was connected to the other part of the vacuum pump to collect the filtered water in a jar.

A schematic design and prototype of the water column filter, as well as the experimental setup of the filtering process are shown in Figures 3.14 and 3.15, respectively.

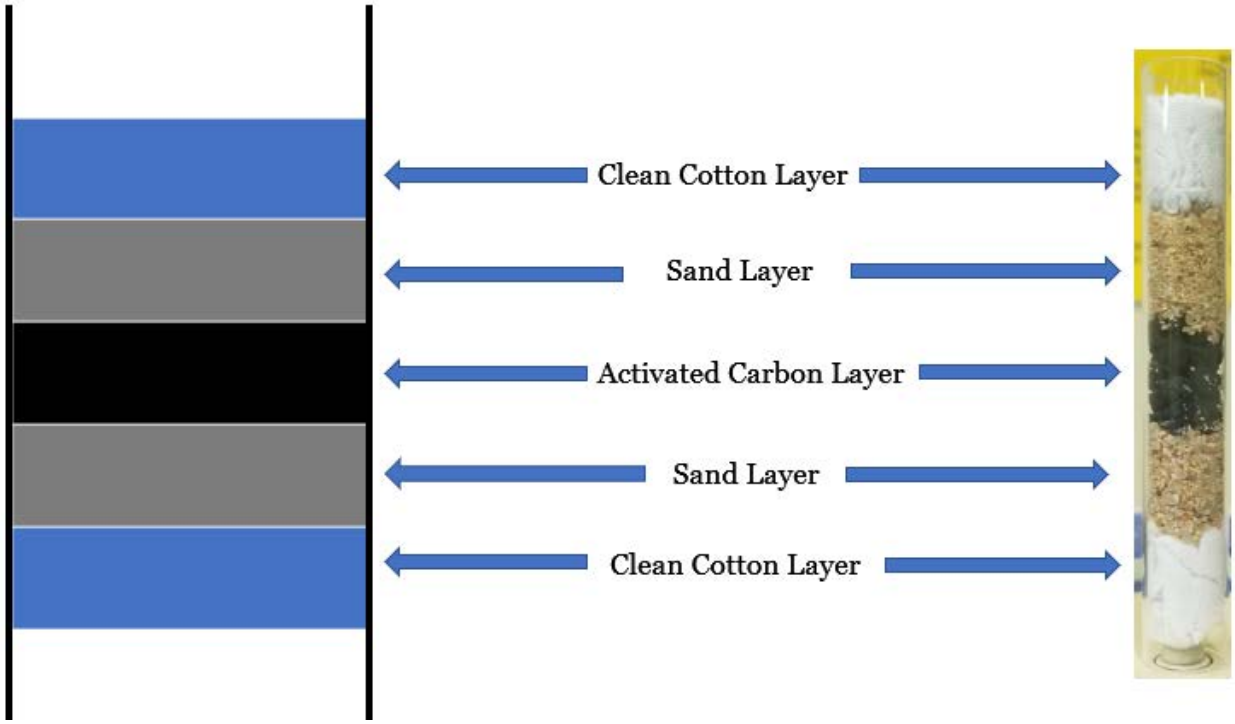

(a) (b)

Figure 3.14: Water column filter: (a) schematic design, and (b) prototype

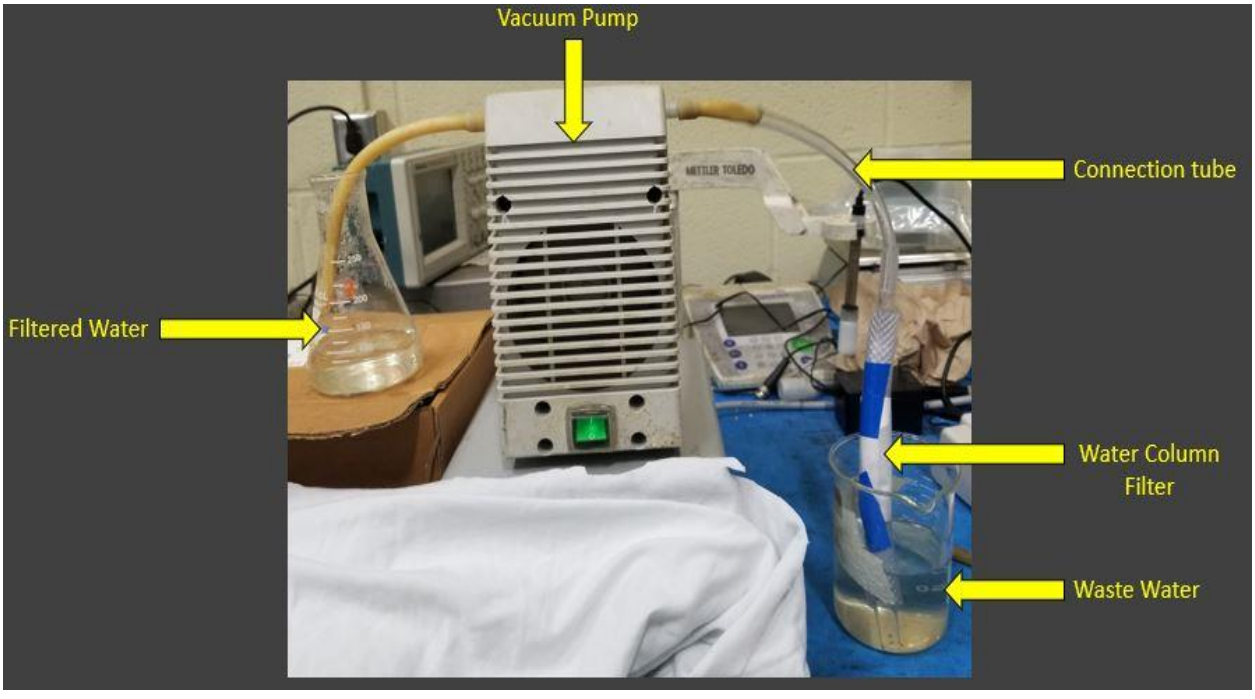

Figure 3.15: Experimental setup of water filtration process

CHAPTER 4

RESULTS AND DISCUSSION

The activated carbons produced from different sources were analyzed using different parameters such as pore volume, surface area, SEM images, and adsorption. To realize the porosity of a substance, the International Union of Pure and Applied Chemistry (IUPAC) divides pores into three categories:

- Micropores: less than 2 nm in diameter
- Mesopores: between 2 and 50 nm in diameter
- Macropores: larger than 50 nm in diameter

4.1 Low-Pressure Nitrogen Adsorption

Low-pressure nitrogen adsorption is generally performed to investigate microporous and mesoporous materials. In this experiment, nitrogen adsorption and desorption isotherms were collected at 77 K (–196°C). Before obtaining the isotherm data, it was necessary to de-gas the samples in order to remove any traces of gas and moisture. From low-pressure nitrogen adsorption, information such as specific pore volume (cm^3/gm), pore shape, specific surface (m^2/gm) can be obtained.

4.1.1 Analysis of Nitrogen Adsorption

The adsorption isotherm is used to evaluate the amount of gas adsorbed at different relative pressures (P/P_o), where P is the gas vapor pressure, and P_o is the saturation pressure of the adsorbent. A desorption isotherm is evaluated by measuring the gas removal quantities from the samples when the pressure is lowered. According to Brunauer et al. [80], in actual testing, five types of standard isotherms are mostly observed, as shown in Figure 4.1 (Type I–Type V).

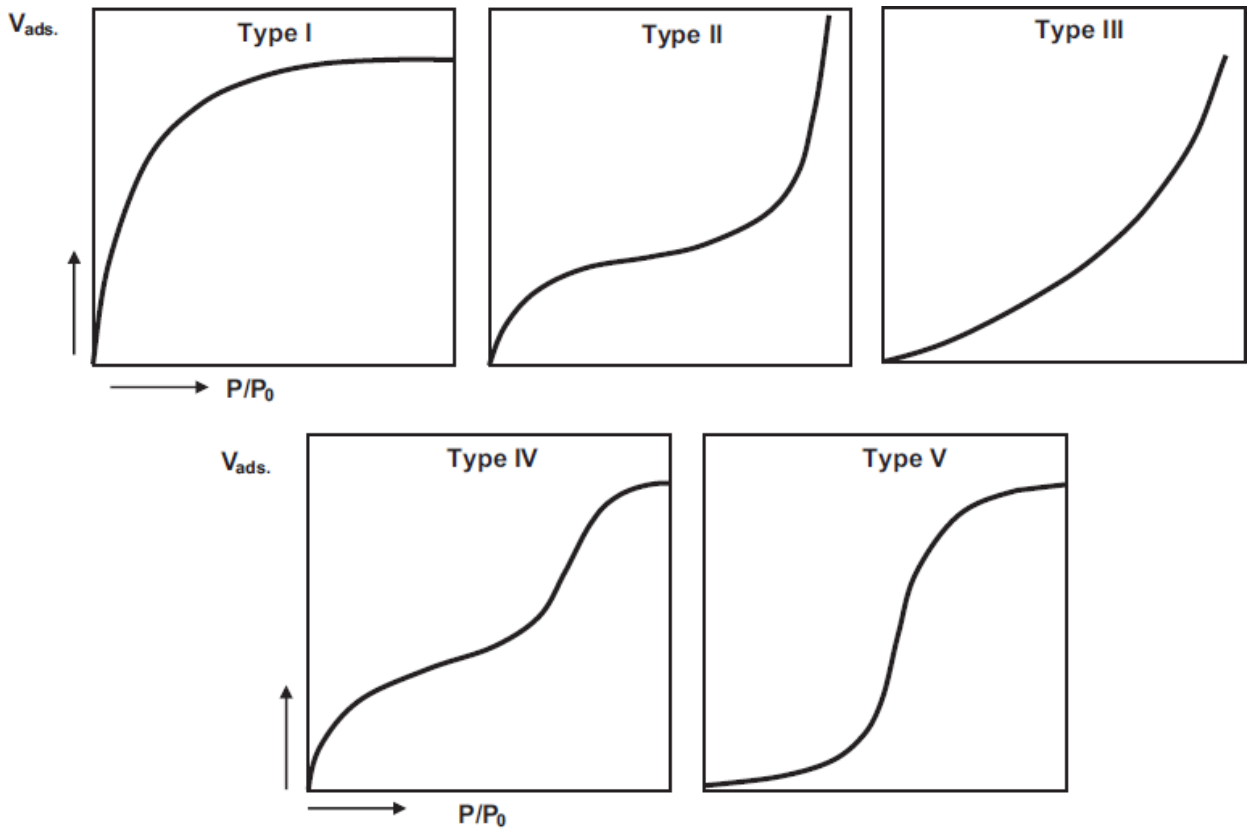

Figure 4.1: Adsorption isotherm types [80]

From Figure 4.1, it can be seen the adsorption in Type I adsorption isotherms increases at a very high rate at low relative pressure (P/P_o), and the adsorption rate slows down at moderate pressure. It shows almost a steady adsorption from moderate- to high-pressure ratio, revealing that the adsorbent consists of micropores and mesopores. For Type II adsorption isotherms, adsorption increases sharply at a very low relative pressure, and then the adsorption rate increases at a steady rate during the moderate pressure ratio. Again, the rate increases drastically when the relative pressure ratio is close to 1 (0.9–1). This isotherm reflects the dominance of micropore filling. Type III adsorption isotherms show weak relations between the adsorbent and the adsorbate, indicating a convexly curved relation between relative pressure and adsorption. Type IV adsorption isotherms are somewhat similar to Type II isotherms, but there is a sharp increase in adsorption from the moderate-pressure to high-pressure ratio. Finally, at the higher pressure, adsorption is almost

constant, reflecting various-sized pores, and considerable micropore and mesopores. Type V adsorption isotherms increase at a very slow rate and at a low relative pressure, which reveals poorly developed micropores, and then they sharply increase at moderate pressure, revealing mesopore development and non-macropores.

Generally, adsorption isotherms are not reversible. As a result, they exhibit hysteresis. From previous research, five types of hysteresis loops correlated to pore shape are seen. Different hysteresis loops and their corresponding pore shapes are shown in Figure 4.2. Type A hysteresis is associated with cylindrical pores. Type B hysteresis produces slit-shaped pores. Types C and D hysteresis are attributed to wedge-shaped pores. Type E hysteresis shows bottleneck pores.

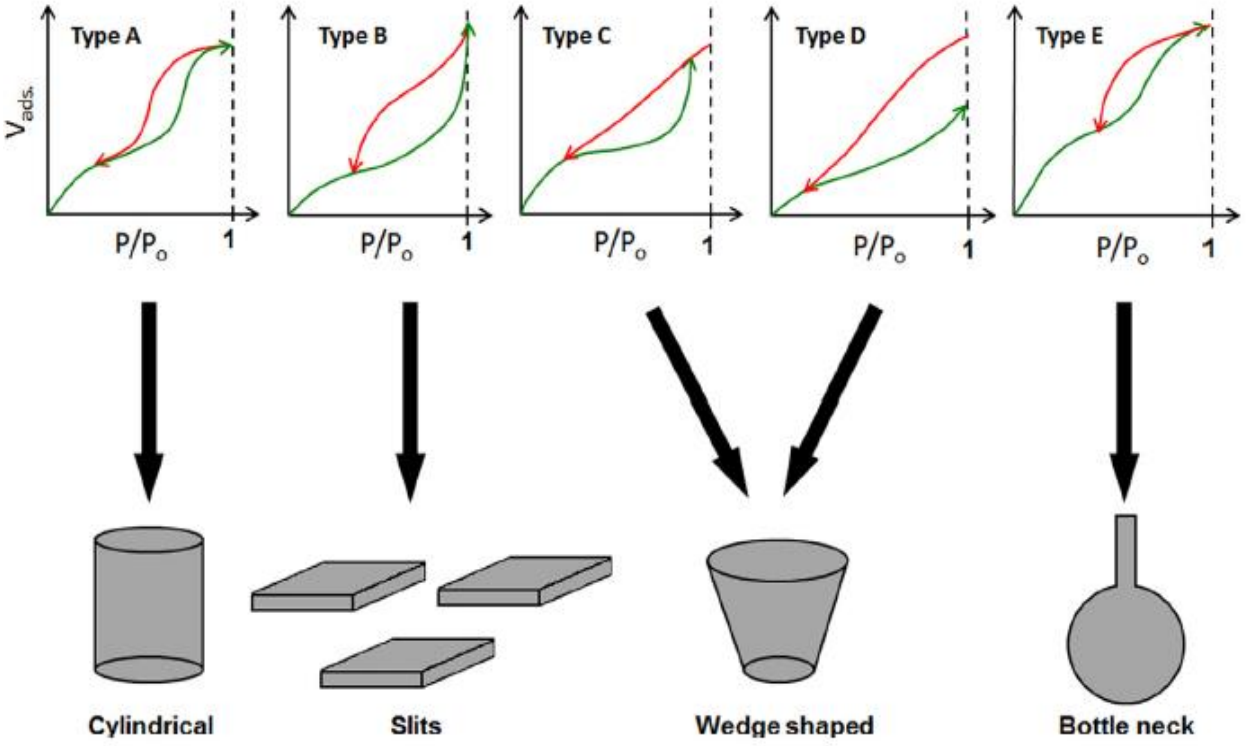

Figure 4.2: Five types of hysteresis loops and their related pore shapes [81]

4.2 Analysis of Activated Carbon Produced by Algae

4.2.1 Adsorption Isotherms of Algae-Based Activated Carbon

Figure 4.3 shows a comparison of three adsorption isotherms for algae-based activated carbon: algae-produced carbon using chemical activation, algae-produced carbon chemically activated with $ZnCl_2$, and algae-produced carbon activated with $CaCl_2$.

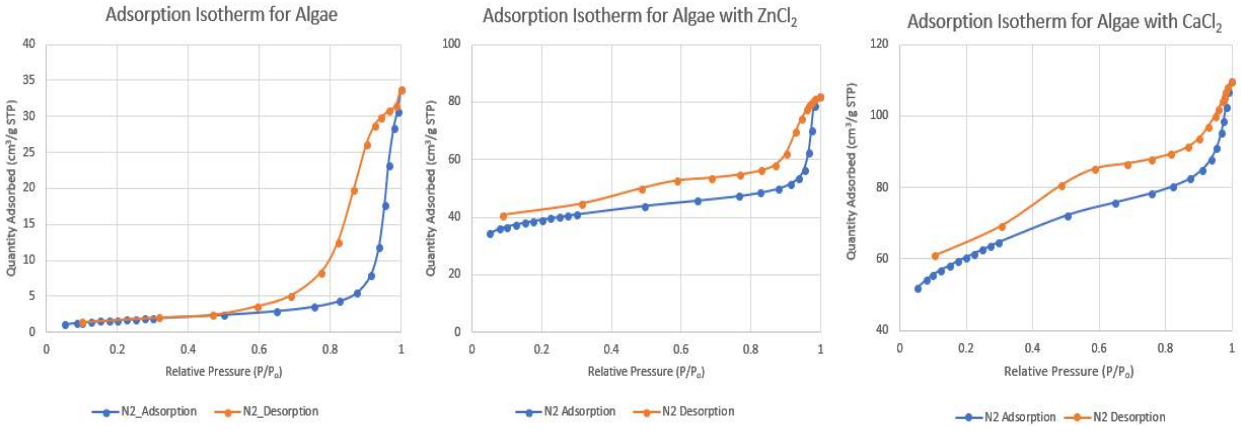

Figure 4.3: Comparison of adsorption isotherms for algae-based activated carbon

The shapes of the isotherm curves for algae without chemical activation and for algae with $ZnCl_2$ activation suggest Type II isotherms, and the shape of the isotherm curve for algae with $CaCl_2$ activation is actually a combination of Types II and III isotherms. In terms of quantity of adsorption, the isotherm of algae without chemical activation shows very low adsorption at both low and moderate pressures. A sudden increase in adsorption occurred at a higher relative pressure (0.9–1.0). The highest adsorption quantity was approximately 34 cm^3/gm. Development of mesopores can be observed at higher pressure ratios. Isotherms of algae activated with $ZnCl_2$ showed higher adsorption quantity at a lower relative pressure, and there was a steady increase in adsorption with lower to moderate pressure ratios. At a relative pressure ratio of 1, the adsorption quantity was 82 cm^3/gm. Isotherms of algae activated with $CaCl_2$ showed better adsorption. Adsorption quantity increased at a higher rate from the low relative pressure ratio to the moderate

pressure ratio. The maximum quantity adsorbed was noticed at a relative pressure ratio of 1, which was 109.6 cm^3/gm. All curves showed hysteresis, which indicates the development of micropores and mesopores. In the case of algae, it can be said that based on the adsorption isotherm, chemical activation with $CaCl_2$ provides better porosity and adsorption.

4.2.2 Pore Volume of Algae-Based Activated Carbon

Figures 4.4 and 4.5 provide a comparison of pore volume and pore radius among the algae-based activated carbon materials.

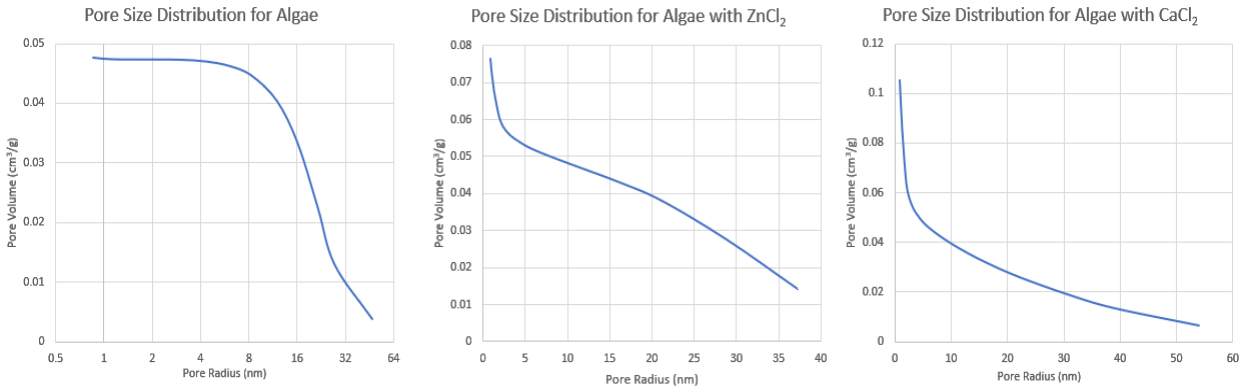

Figure 4.4: Pore volume vs. pore radius for algae-based activated carbon

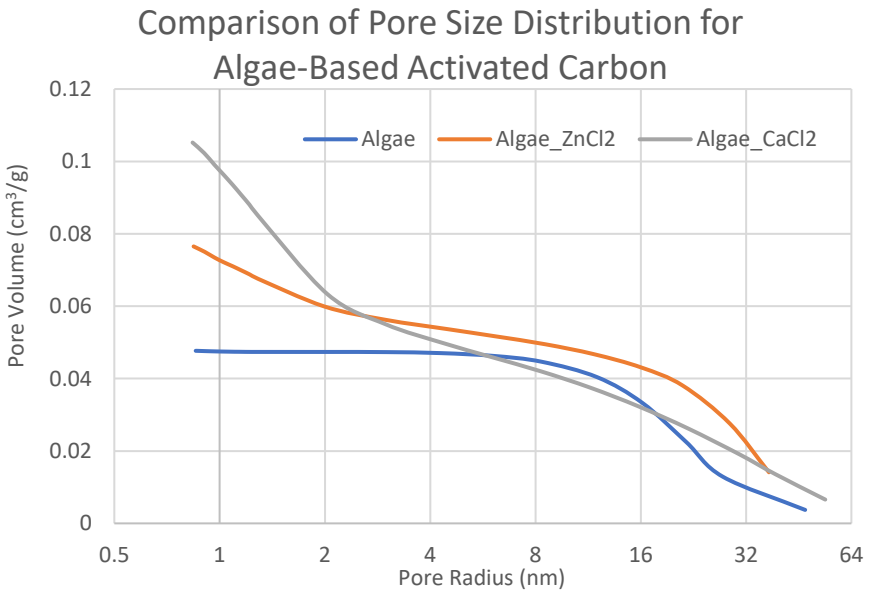

Figure 4.5: Comparison of pore volume and pore radius for algae-based activated carbon

It is a normal analogy that pore volume will decrease with an increase in pore radius. From the pore size distribution (PSD) of algae without any activation, the maximum pore volume was less than 0.05 cm^3/gm. Pore volume remained almost similar for the 1 to 8 nm pore radius. After that, pore volume decreased sharply with the increase in pore radius. The PSD of algae with $ZnCl_2$ activation showed a better pore volume in the micropore region. Maximum pore volume was approximately 0.076 cm^3/gm. Pore volume decreased at a linear rate in the mesopore region with the increase in pore radius. Pore size distribution of algae with $CaCl_2$ activation showed higher pore volume than the other samples. Maximum pore volume was approximately 0.105 cm^3/gm. In the micropore region, pore volume decreased drastically. After a pore radius of 3–4 nm, pore volume decreased with the increase in pore radius at almost a linear rate. Figure 4.5 shows the comparison of pore volume of these three types of carbon. It can be seen that $CaCl_2$-activated carbon shows better pore volume in the micropore region. After the pore radius of 3.5 nm, $ZnCl_2$-activated carbon shows a higher pore volume than the $CaCl_2$-activated carbon. This reflects better pore volume achieved at the meso- and macro-pore regions. Char produced from algae without any activation shows a lower pore volume than char produced from algae with any other activation, as expected.

4.2.3 Pore Size Distribution of Algae-Based Activated Carbon

The Barrett-Joyner-Halenda (BJH) method for determining pore volume was used to observe the pore size distribution. Here, incremental pore volume was plotted against the pore radius. Figures 4.6 and 4.7 provide a comparison of pore size distribution defined by incremental pore volume at low-pressure nitrogen adsorption.

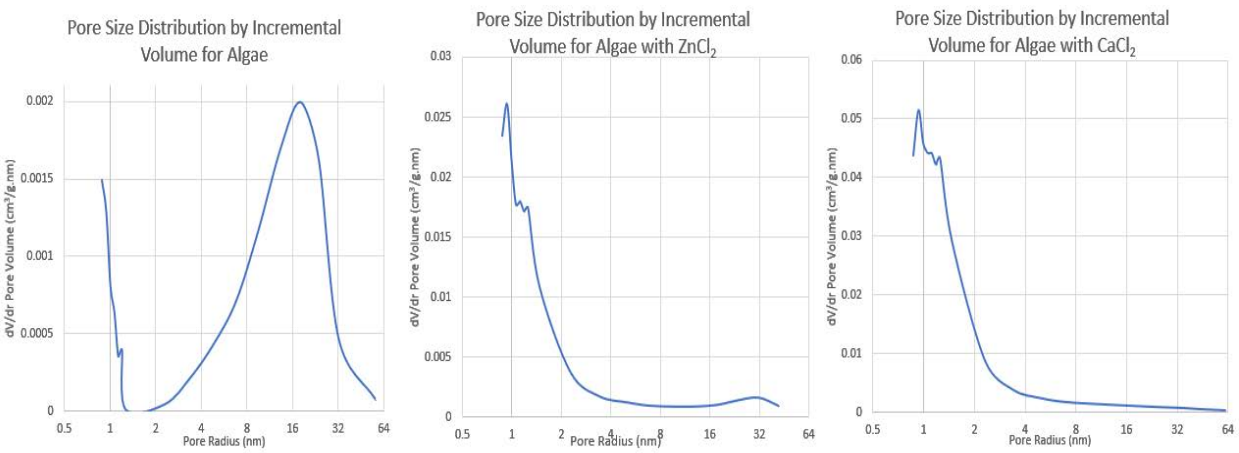

Figure 4.6: Pore size distribution defined by incremental pore volume for algae-based activated carbon

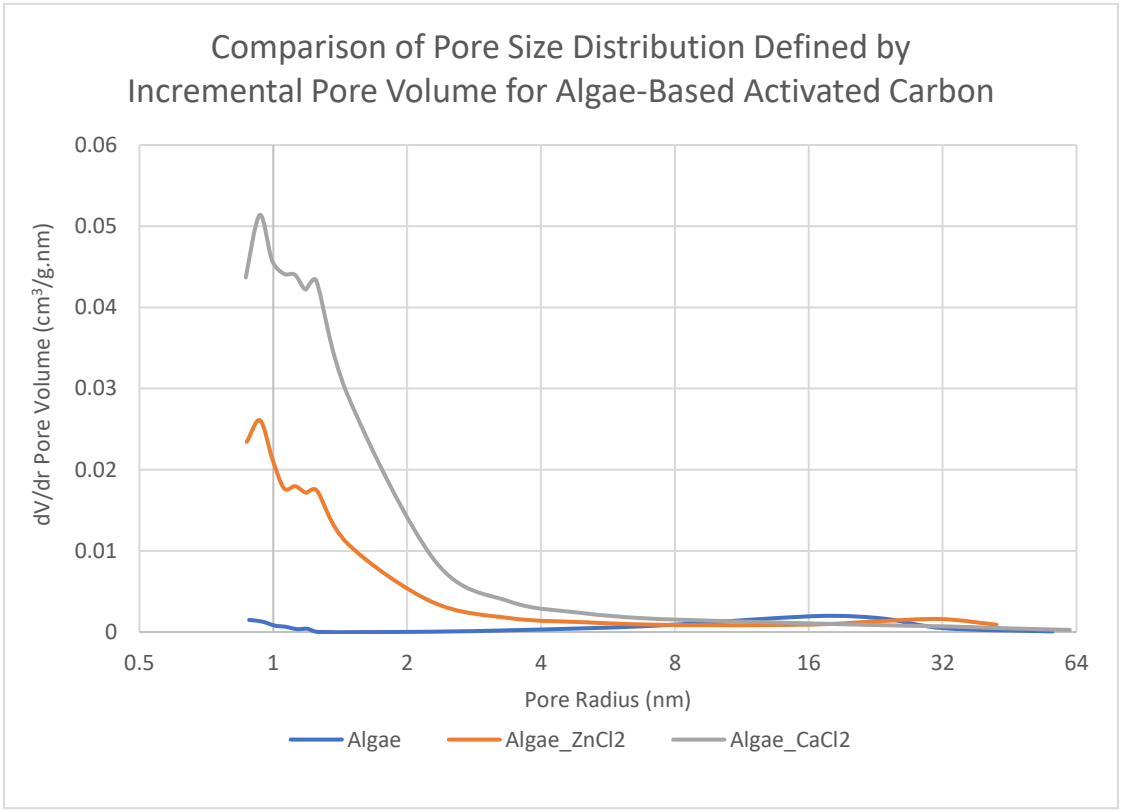

Figure 4.7: Comparison of pore size distribution defined by incremental pore volume for algae-based activated carbon

The PSD of algae without chemical activation shows an irregular pattern. A pore radius of 1.3 to 1.8 nm shows that the incremental pore volume was close to zero. After a pore radius of

2 nm, at the mesopore region, the incremental pore volume starts to increase with the pore radius. A pore radius of 18 to 20 nm indicates that the maximum incremental pore volume is observed, which is close to 0.002 cm^3/gm. Then it starts to decrease with the increase in pore radius. The PSD of algae with $ZnCl_2$ and $CaCl_2$ activation show a similar curve pattern. Here, the average incremental pore volume is found near 1.3 nm, with some slight ups and down in the curve in a very small region. The average pore volume for $ZnCl_2$-activated carbon is approximately 0.018 cm^3/gm and for $CaCl_2$-activated carbon is approximately 0.044 cm^3/gm. Figure 4.7 shows the comparison of incremental pore volume with pore radius of three types of algae-based carbon on the same scale. The three curves exhibit the same pattern with amplitude. At a smaller pore radius, there was a frequent change of pore volume with pore radius, exhibiting a slight zig-zag shape from 0.8 nm to 1.5 nm pore radius (approximately). After that, the change in pore volume decreased with the increase in pore volume. $CaCl_2$-activated algae carbon provided a higher incremental pore volume than the other two. The change in pore volume with pore radius was almost zero, which represents poor porosity. At a higher pore radius (> 6 nm), the change in pore volume with respect to pore radius was almost zero, regardless of the type of carbon produced.

4.2.4 BET Surface Area and BJH Pore Volume of Algae-Based Activated Carbon

Figure 4.8 shows the difference between the BET surface area and the cumulative BJH pore volume of algae-based activated carbon. It can be seen that a better surface area and cumulative volume of pores was found when $CaCl_2$ was used as the chemical agent during activation. The $CaCl_2$-based activation for algae provided 31 times better surface area than the $ZnCl_2$-based activation, which provided only 20 times better surface area than the char produced without activation. A similar situation was seen in the pore volume. Approximately 2.1 times more

pore volume was achieved with $CaCl_2$-based activated carbon, while almost 1.76 times more pore volume was achieved with $ZnCl_2$-based activated carbon.

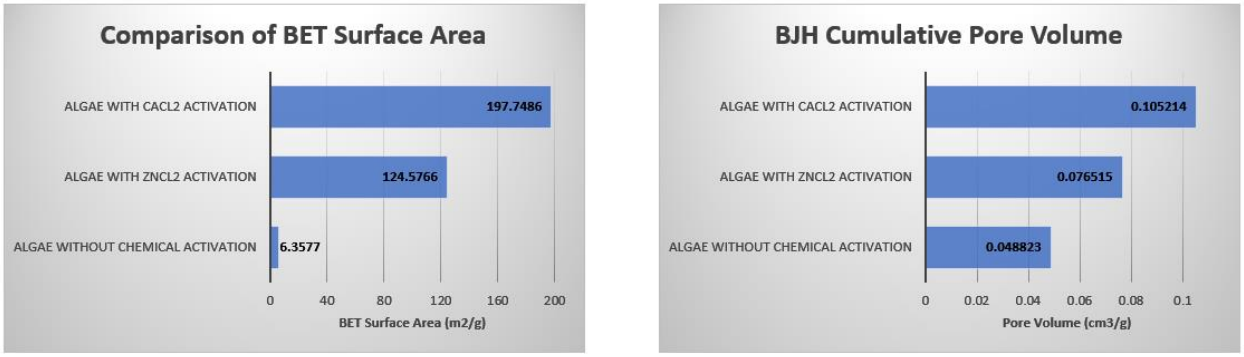

(a) (b)

Figure 4.8: Comparison of algae-based activated carbon: (a) BET surface area, and (b) BJH cumulative pore volume

4.2.5 Scanning Electron Microscopy Analysis of Algae-Based Activated Carbon

Figure 4.9 shows SEM images of various treated algae-based carbons. It can be seen that there is almost no porosity in the algae structure when there is no chemical activation, only char. On the other hand, algae-based activated carbon by $ZnCl_2$ and $CaCl_2$ showed porous structures of the activated carbon samples at 100X magnification. Activation with $CaCl_2$ showed better pore size, as expected from the adsorption isotherm and PSD analysis.

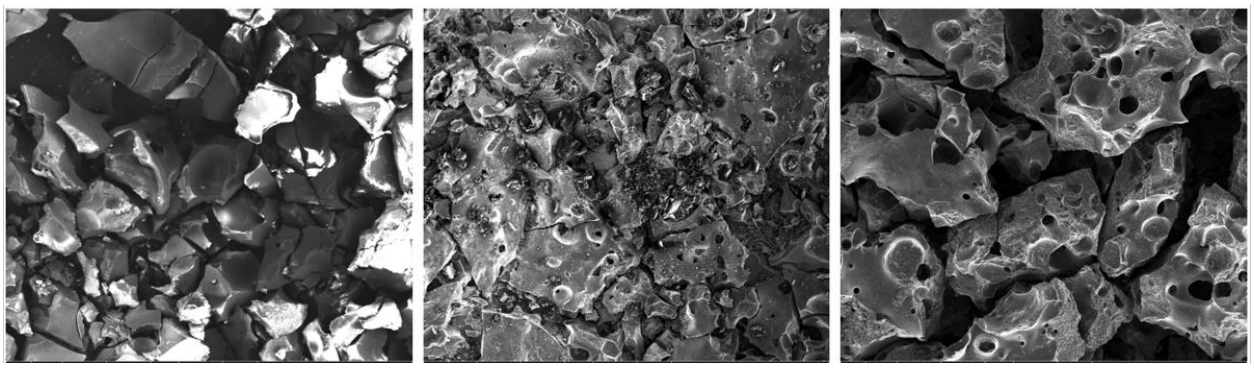

(a) (b) (c)

Figure 4.9: SEM images: (a) algae without chemical activation (b) algae with $ZnCl_2$ activation, and (c) algae with $CaCl_2$ activation (100X)

Pore structure can be seen more clearly in higher-magnification SEM images. Figure 4.10 shows SEM images of algae carbon activated by $ZnCl_2$ at a magnification of 22807X and algae carbon activated by $CaCl_2$ at a magnification of 6277X. The slit-type mesopore structure can be seen in the algae carbon activated by $ZnCl_2$. On the other hand, a combination of slit and wedge-shaped pores can be seen in the algae carbon activated by $CaCl_2$, as expected. Better adsorption is expected by using $CaCl_2$ as the activating agent for algae.

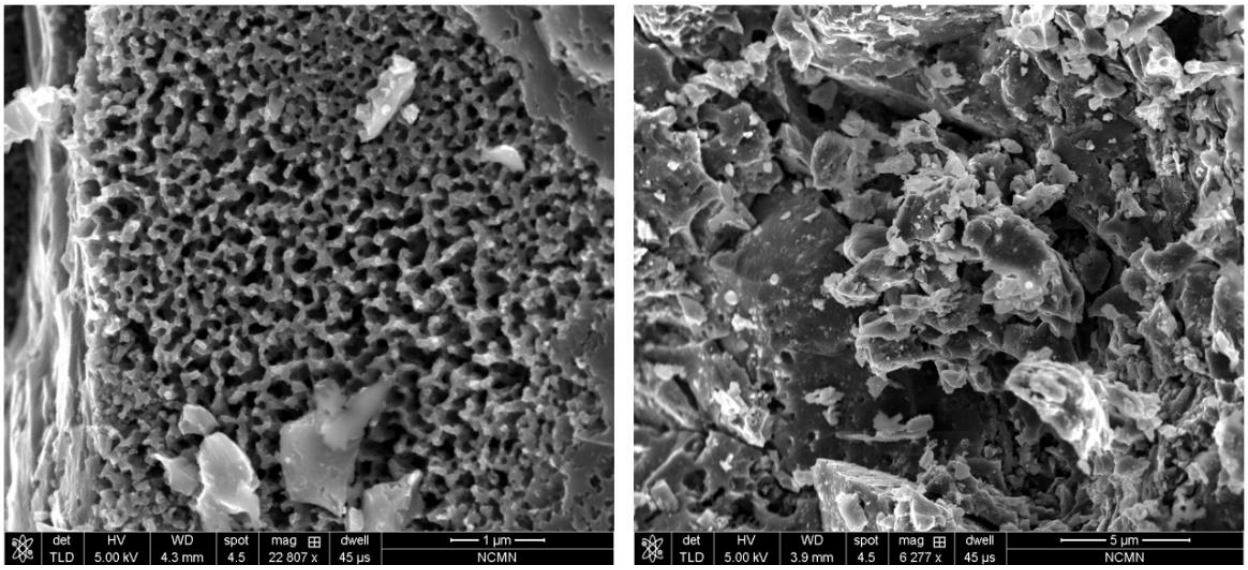

(a) (b)

Figure 4.10: SEM images: (a) algae with $ZnCl_2$ activation (22807X), and (b) algae with $CaCl_2$ activation (6277X)

4.3 Analysis of Activated Carbon Produced by Date Seeds

4.3.1 Adsorption Isotherms of Date Seed-Based Activated Carbon

Figure 4.11 shows a comparison of nitrogen adsorption isotherms from date seed-based carbon. The first curve shows the adsorption isotherm from char produced by date seeds without any activation. Regardless of the change in the relative pressure ratio, the value of the quantity adsorbed was almost similar, fluctuating from approximately 5.2 cm^3/gm to 7 cm^3/gm. The adsorption isotherm is very similar to the Type II isotherm. From the value of the quantity

adsorbed, it can be said that the surface is not very porous. In the second curve, the shape of the adsorption isotherm of the date seed-based carbon activated with $ZnCl_2$ is similar to the Type I isotherm. One exception is that there is no sharp increase in adsorption value when the relative pressure ratio started to increase from zero. From moderate to high pressure, there was a steady slow increase in adsorption. The third curve showing $ZnCl_2$-activated date seed carbon indicated high adsorption. At a lower pressure ratio, the value of the quantity adsorbed was 162.54 cm^3/gm, and at a higher-pressure ratio (close to 1), the value of the quantity adsorbed was approximately 212.62 cm^3/gm.

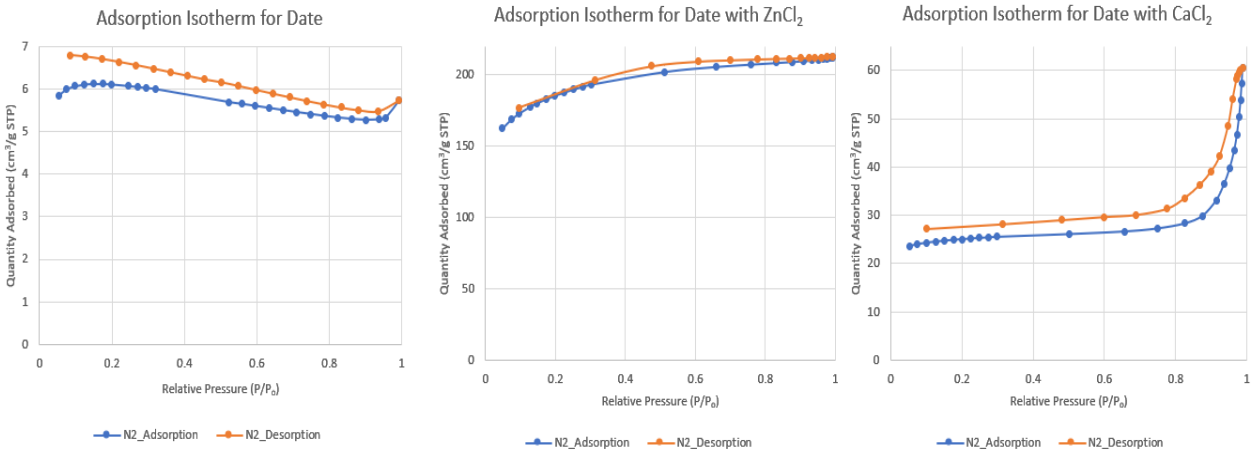

Figure 4.11: Comparison of adsorption isotherms for date seed-based activated carbon

No significant hysteresis formation was observed from the adsorption and desorption isotherms. Cylindrical-shaped pores were expected from the isotherm analysis. The shape of the adsorption isotherm of date seed-based carbon activated with $CaCl_2$ is similar to the Type II isotherm, with one exception: there was no sharp increase in adsorption at the lower pressure ratio. From the lower to the moderate pressure ratio (0.8), the adsorption quantity did not change much. At a higher-pressure ratio, there was a sudden sharp increase in the adsorption quantity. At a lower pressure ratio, the value of quantity adsorbed was 23.68 cm^3/gm, and the maximum adsorption

found at a higher pressure ratio (0.989) was 60.62 cm^3/gm. Slit-type pore structures were expected here.

4.3.2 Pore Volume of Date Seed-Based Activated Carbon

Figures 4.12 and 4.13 show the change in pore volume with pore radius for various activated date seed-based carbons.

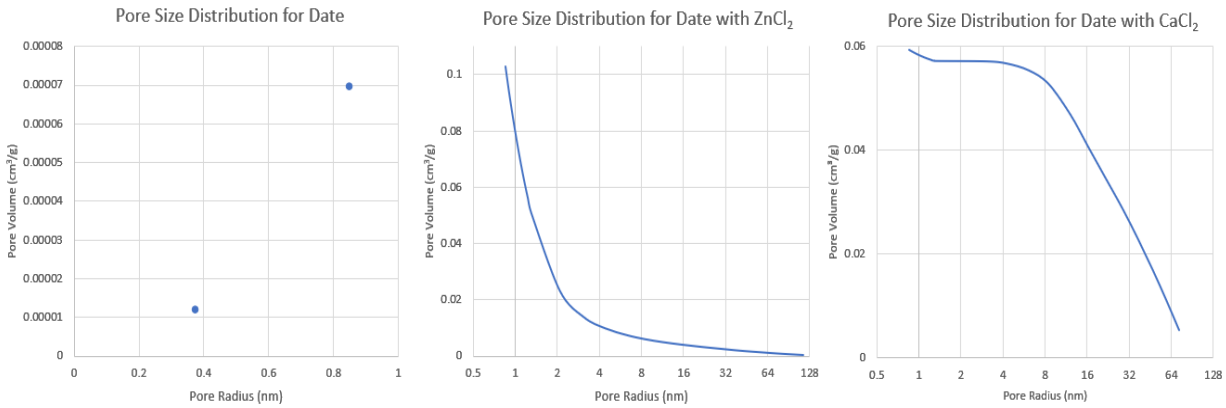

Figure 4.12: Pore volume vs. pore radius for date seed-based activated carbon

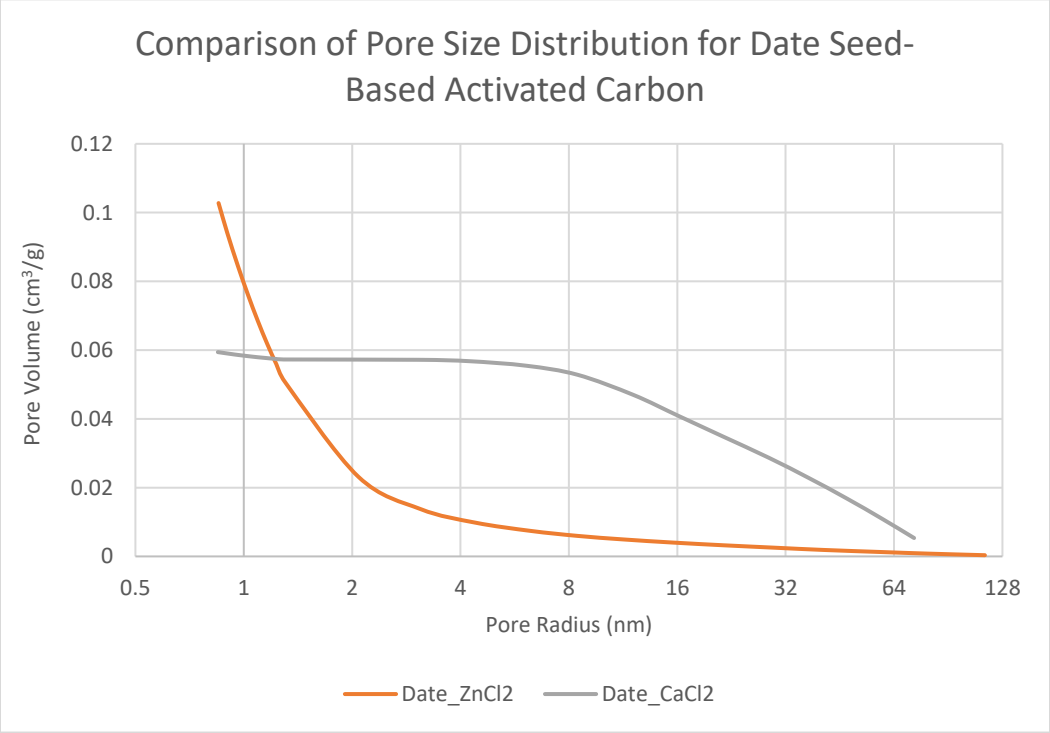

Figure 4.13: Comparison of pore volume and pore radius for date seed-based activated carbon

The char produced from date seeds without any chemical activation after the degassing process did not reveal enough data about pore volume. Therefore, it can be concluded that less porosity would be observed from this char microscopic structure. Pore size distribution of date seed-based activated carbon showed better pore volume in the micropore region. The maximum pore volume was 0.103 cm^3/gm at a pore radius of approximately 0.85 nm. In the beginning, pore volume was decreased at a drastic rate from 0.85 nm to 2 nm. At 2 nm, the pore volume was approximately 0.022 nm. In the mesopore region, pore volume decreased at a slower rate. After a pore radius of 16 nm, the pore volume was almost zero. From the graph of pore volume vs. pore radius of date seed-based activated carbon with $CaCl_2$, it can be seen that the pore volume remained almost constant with the pore radius 0.84 nm to 6 nm. After a pore radius of 8 nm, the pore volume decreased at a higher rate and approached zero at a pore radius of approximately 72 nm. The maximum pore volume of 0.0594 cm^3/gm. was observed at a pore radius of 0.847 nm. Figure 4.13 provides a comparison of the change in pore volume with pore radius at the same scale. Initially the pore volume of $ZnCl_2$-activated carbon was higher. However, with the increase in pore radius, this decreased quite sharply. On the other hand, pore volume remained almost constant for $CaCl_2$-activated carbon up to a pore radius of 8 nm and then slowly started to decrease. This reflected meso- and macro-pore formation.

4.3.3 Pore Size Distribution of Date Seed-Based Activated Carbon

Figures 4.14 and 4.15 show the pore size distribution defined by incremental pore volume at low pressure nitrogen adsorption using BJH methods for date seed-based activated carbon and their comparison.

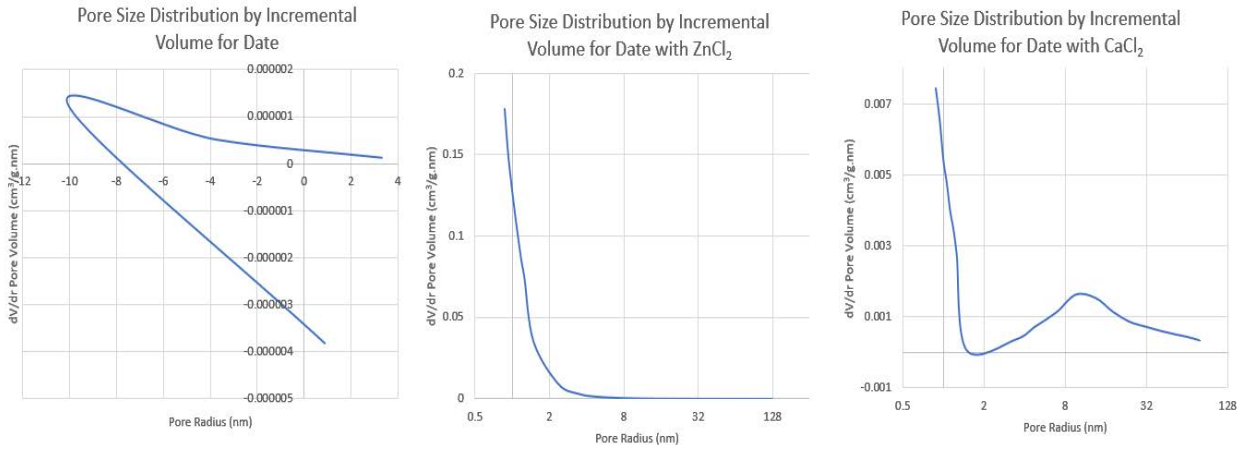

Figure 4.14: Pore size distribution defined by incremental pore volume for date seed-based activated carbon

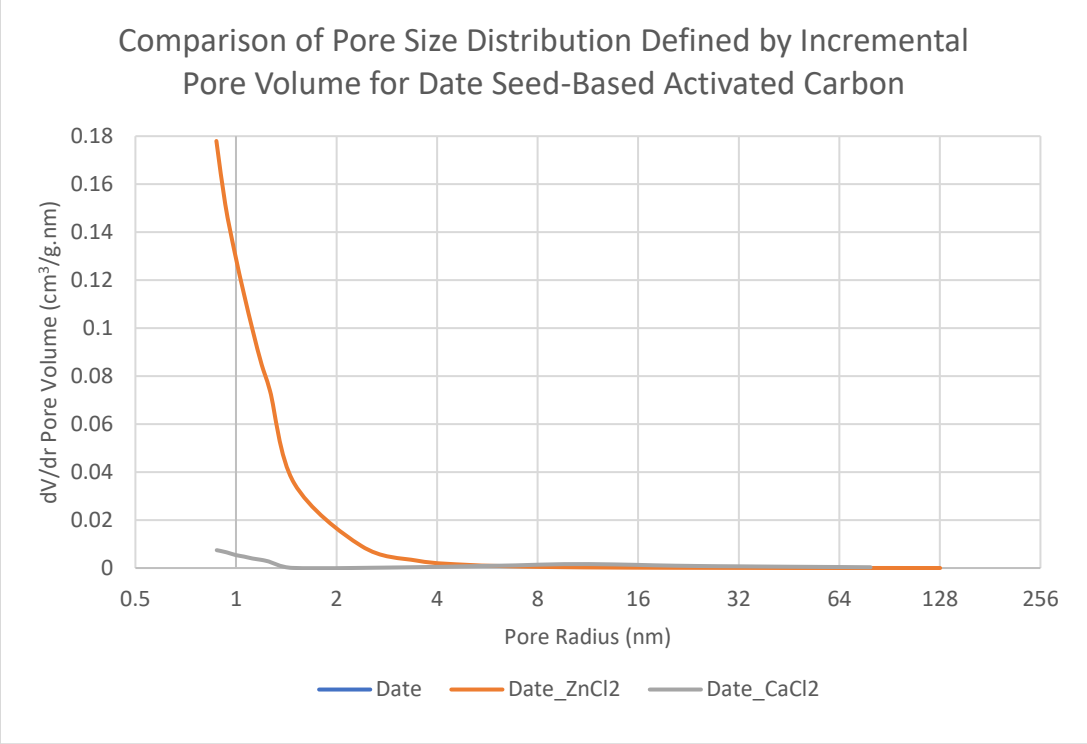

Figure 4.15: Comparison of pore size distribution defined by incremental pore volume for date seed-based activated carbon

From the pore distribution of char produced from date seeds, it can be seen that there were two negative pore radius values. The reason behind that was the poor porosity of the char from date seeds. Some measurement errors could affect the process after degassing. From the pore

distribution of date seed-based activated carbon with $ZnCl_2$, incremental pore volumes were decreased at a very sharp rate from 0.85 nm to 2 nm. Average incremental pore volumes were close to 0.12 cm^3/gm. After the pore radius of 6 nm, incremental pore volumes were almost zero. This reflected the lack of mesoporosity in the activated carbon structure. Maximum incremental pore volume was 0.178 cm^3/gm. Pore size distribution of date seed-based activated carbon with $CaCl_2$ showed less incremental pore volume than the $ZnCl_2$ activated carbon. Maximum incremental pore volume was 0.0075 cm^3/gm. Average incremental pore volume was approximately 0.004 cm^3/gm. In the beginning, from 0.87 nm to 1.4 nm pore radius, incremental pore volumes were decreased at a drastic rate. From 1.4 nm to 5 nm pore radius, incremental pore volumes were almost 0. After that, incremental pore volumes started to increase with the increase of the pore radius. Another pick in the curve had been found at a pore radius of 9.59 nm where the pore volume was 0.0016 cm^3/gm approximately. After that pick, incremental pore volumes were decreased at a steady rate. Mesoporous structures were expected from this analysis. From Figure 4.15, it can be seen that there was no apparent change in pore volume with the change the change of pore radius. Incremental pore volume was almost zero after 1.5 nm pore radius. The incremental pore volume of date seeds-based carbon without any activation was so negligible that it couldn't be shown in the graph. $ZnCl_2$ activated carbon showed a higher incremental pore volume initially. But there was a similar decreasing pattern with the increase of pore radius. And a change of pore volume with the change of pore radius was almost zero after 4 nm pore radius.

4.3.4 BET Surface Area and BJH Pore Volume of Date Seed-Based Activated Carbon

The BET surface area and BJH cumulative pore volume are shown in Figure 4.16. From the comparison of BET surface areas, it can be seen that date seed-based carbon with $ZnCl_2$ chemical activation provided the highest surface area. The BET surface areas achieved by date

seed char, $ZnCl_2$ activation, and $CaCl_2$ activation were 18.1671 m^2/gm, 591.4278 m^2/gm, and 76.9446 m^2/gm, respectively. $ZnCl_2$ activation provided 32 times better surface area than a char without any activation and almost 7.68 times better surface area than $CaCl_2$-activated carbons. The BJH adsorption cumulative pore volume showed almost the similar pattern. BJH cumulative pore volumes achieved by date seed char, $ZnCl_2$ activation, and $CaCl_2$ activation were 0.00007 cm^3/gm, 0.102766 cm^3/gm and 0.059418 cm^3/gm, respectively6. $ZnCl_2$-activated carbon provided 1468 times more cumulative pore volume than a char of date seeds without any activation and almost 1.8 times more cumulative pore volume than $CaCl_2$-activated carbon.

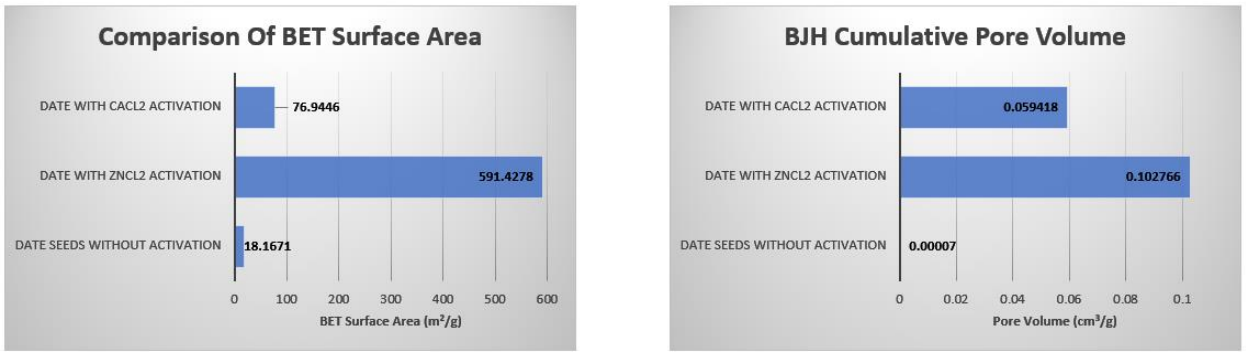

(a) (b)

Figure 4.16: Comparison of date seed-based activated carbon: (a) BET surface area, and (b) BJH cumulative pore volume

4.3.5 Scanning Electron Microscopy Analysis of Date Seed-Based Activated Carbon

SEM images of char prepared from date seeds and two types of date seed-based activated carbon are shown in Figure 4.17. As can be seen, the SEM images of char produced from date seeds showed a structure with a very low pore volume, which was expected. The 411X magnification image is shown here for better understanding. From the adsorption isotherm and BET surface area analysis of $ZnCl_2$-activated carbon from date seeds, a good microporous surface was expect ed. From the SEM image at 333X magnification, a porous structure was found, and a dominant amount of micropore formation was observed. Higher magnification might be required

to explain this porosity. From the SEM image of $CaCl_2$-activated carbon at a magnification of 532X, a discontinuous and rough mesoporous surface can be observed.

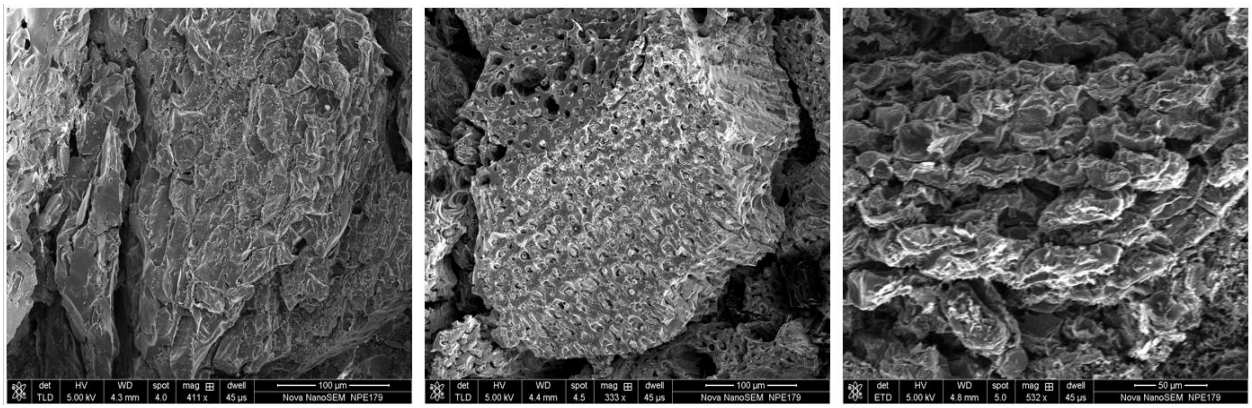

(a) (b) (c)

Figure 4.17: SEM images: (a) date seeds without chemical activation (411X), (b) date seeds with $ZnCl_2$ activation (333X), and (c) date seeds with $CaCl_2$ activation (532X)

It is easier to analyze details of the pore structure of the date seed-based activated carbon at higher magnification. Figure 4.18 shows the SEM image of $ZnCl_2$ activated carbon at a magnification of 14048X and SEM image of $CaCl_2$ activated carbon at a magnification of 2947X.

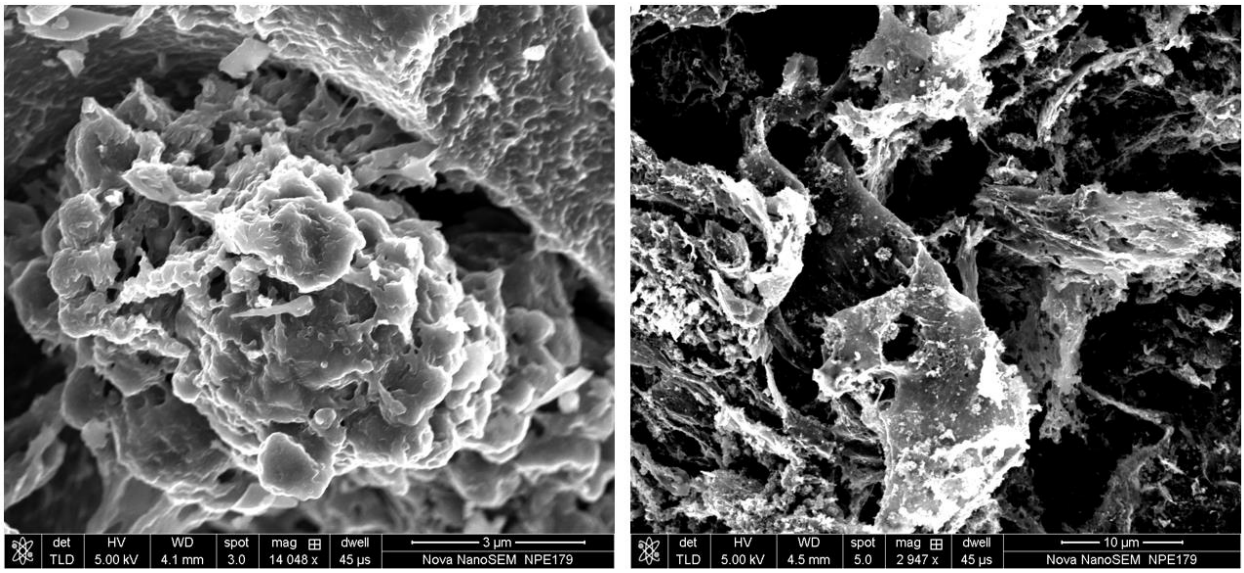

(a) (b)

Figure 4.18: SEM images: (a) date seeds with $ZnCl_2$ activation (14048X), (b) date seeds with $CaCl_2$ activation (2947X)

A rough cylindrical micropore structure can be observed from the SEM image showing $ZnCl_2$ activation. From the SEM image of carbon activated by $CaCl_2$ that is 2947X magnified, micro- and mesoporous structures can be seen. Some macropore formation is also noticed.

4.4 Analysis of Activated Carbon Produced by Olive Seeds

4.4.1 Adsorption Isotherms of Olive Seed-Based Activated Carbon

Figure 4.19 shows a comparison of nitrogen adsorption isotherms from different olive seed-based carbon. The first isotherm curve is of the olive-based char without any activation. Initially, the adsorption values were higher. Then the values of quantity adsorbed started to decrease with the increase in the relative pressure ratio. When the relative pressure ratio 0.933441 was reached, the values of quantity adsorbed started to increase with the pressure ratio. The value of adsorption quantity was 3.247 cm^3/gm at a relative pressure ratio of 0.994153. The maximum adsorption quantity of 3.6628 cm^3/gm was found at a pressure ratio of 0.124882. This adsorption curve was similar to the Type II isotherm. The desorption curve did not follow the same path as expected. The desorption values were higher as the pressure ratio decreased, which leaves hysteresis in the isotherm plot. Considering the adsorption and desorption values, a weak porous structure was expected.

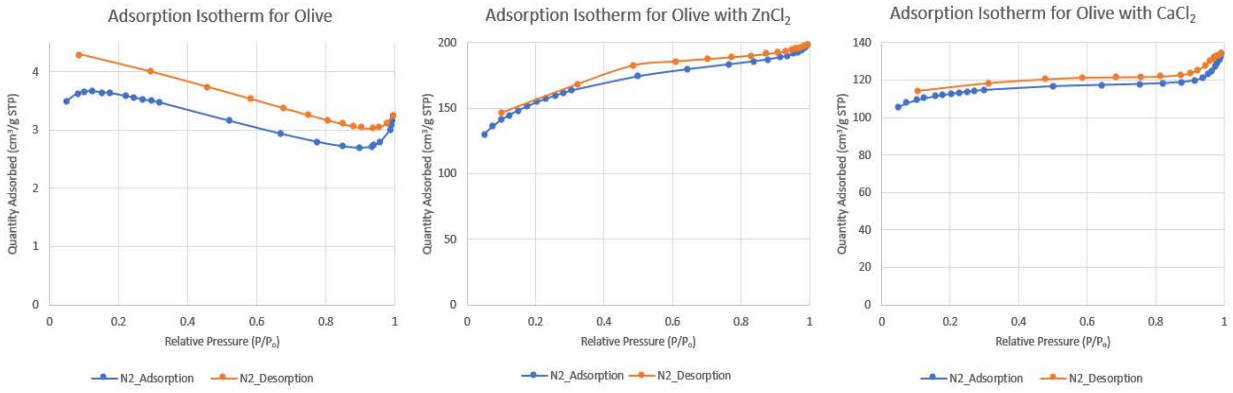

Figure 4.19: Comparison of adsorption isotherms for olive seed-based activated carbon

The second curve shown in Figure 4.19 is the isotherm of olive seed-based carbon activated with $ZnCl_2$. Here the adsorption quantity increased at a steady rate with the increase in the relative pressure ratio. The maximum adsorption value of 197.94 cm^3/gm was found at a pressure ratio of 0.995038. The desorption curve followed almost a similar path as the adsorption curve. A very narrow hysteresis was formed. Here the pattern of adsorption curve is actually the combination of Types I and II isotherms. Therefore, a cylindrical or slit-type pore structure was expected in the SEM image. The last curve in Figure 4.19 is the isotherm of olive-based activated carbon with $CaCl_2$. The adsorption quantity increased at a very low rate with a low to moderate pressure ratio. At a moderate pressure ratio, the values of quantity adsorbed remained almost constant. At a higher pressure ratio, the adsorption quantity again started to increase sharply. The maximum value of adsorption was 134.2964 cm^3/gm at a relative pressure ratio of 0.992476. The desorption curve followed a similar pattern with a little offset path. A small hysteresis formed. This curve reflected a Type II isotherm, and a slit-type pore structure was expected for this reason.

4.4.2 Pore Volume of Olive Seed-Based Activated Carbon

Figures 4.20 and 4.21 show the change in pore volume with pore radius for differently treated olive seed-based carbon.

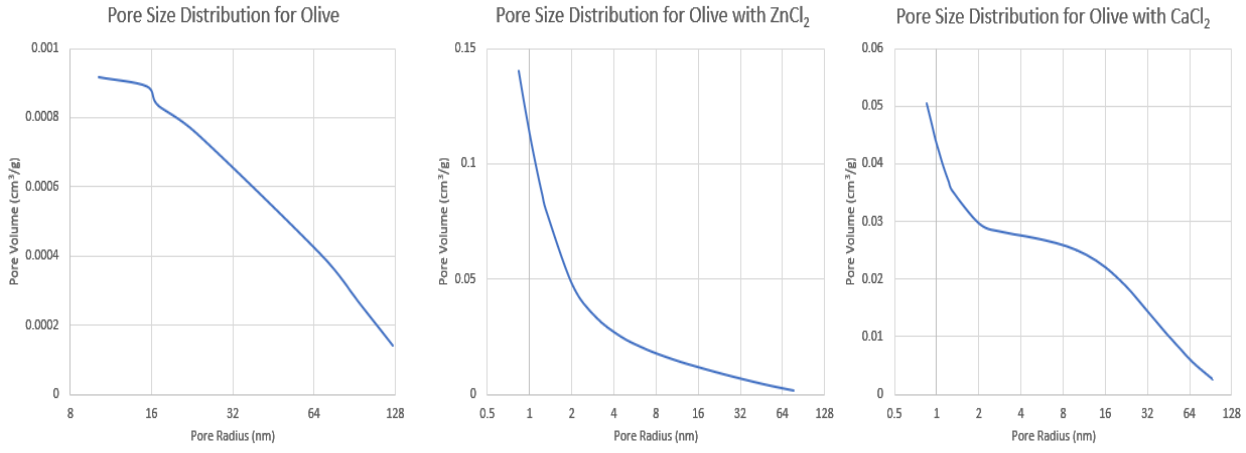

Figure 4.20: Pore volume vs. pore radius for olive seed-based activated carbon

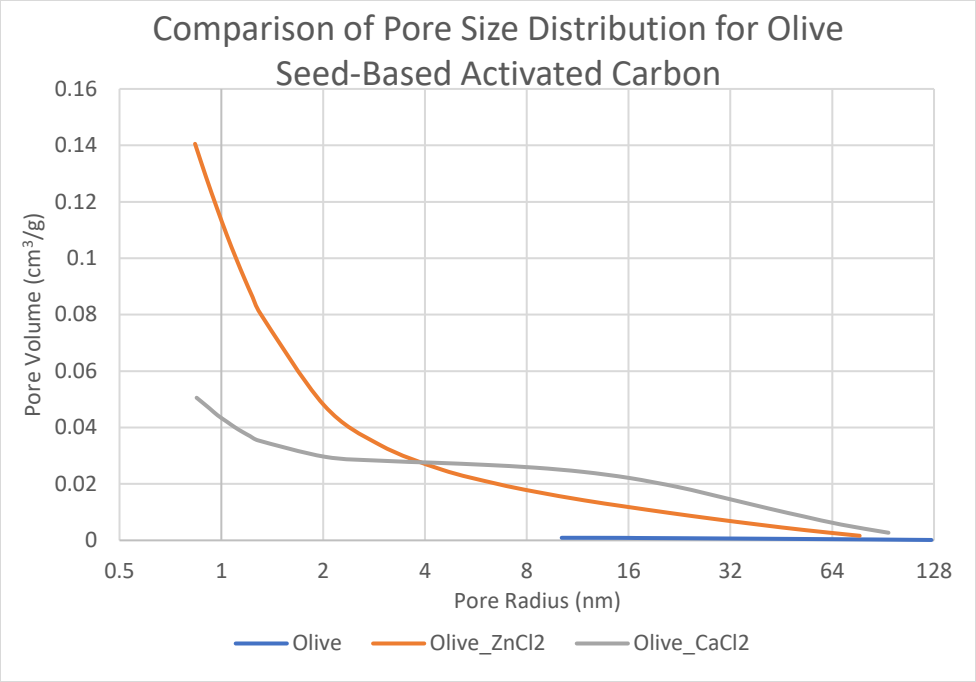

Figure 4.21: Comparison of pore volume and pore radius for olive seed-based activated carbon

The first curve in Figure 4.20 represents the interaction of pore volume and a corresponding pore radius of olive seed-based char without any chemical activation. From pore radius 10 nm to 16 nm, the pore volume did not change much. The average pore volume of that region was approximately 0.0084 cm^3/gm. After that, with the increase in pore radius, the pore volume decreased at a steady rate in the meso- and macro-pore regions. Overall, the pore volume was very low, regardless of the pore radius. A better pore volume was found from the olive seed-based carbon activated with $ZnCl_2$, as shown in the second curve in Figure 4.20. The maximum pore volume was 0.140547 cm^3/gm at a pressure ratio of 0.836273. At the micropore region (0–2 nm pore radius), the pore volume decreased at a very sharp rate. After the pore radius of 2 nm, the pore volume decreased at a smaller rate with the increase in pore radius, which reflected mesopore formation in the structure. The third curve in Figure 4.20 represents the pore size distribution of olive seed-based carbon activated with $CaCl_2$. Here the maximum pore volume of approximately 0.05055 cm^3/gm was achieved at the 0.879 nm pore radius. From pore radius 0.87 nm to 2 nm, the

pore volume decreased substantially. In the mesoporous region in the beginning, pore volumes decreased at a lower rate until the pore radius of 14 nm. After that, the pore volume again started to decrease at a higher rate with the increase in pore radius. The average pore volume in the mesoporous region was approximately 0.024 cm^3/gm.

Figure 4.21 shows a comparison of pore volume vs. pore radius for olive seed-based carbon activated on the same scale. The pore volume of olive seed-based carbon activated with $ZnCl_2$ showed a higher pore volume than the others, but it decreased at a higher rate with the increase in pore radius. However, the pore volume of the olive seed-based carbon activated with $CaCl_2$ showed an almost constant pore volume with a pore radius of 2 to 12 nm. After the pore radius of 4 nm, the pore volume of olive seed-based carbon activated with $ZnCl_2$ decreased at a faster rate than the $CaCl_2$-activated carbon. Char produced from olive seeds without any activation showed no micropores. Here the pore volume was almost zero, regardless of the pore radius.

4.4.3 Pore Size Distribution of Olive Seed-Based Activated Carbon

Figures 4.22 and 4.23 provide a comparison of the pore size distribution defined by incremental pore volume at low-pressure nitrogen adsorption using BJH methods for olive seed-based activated carbon.

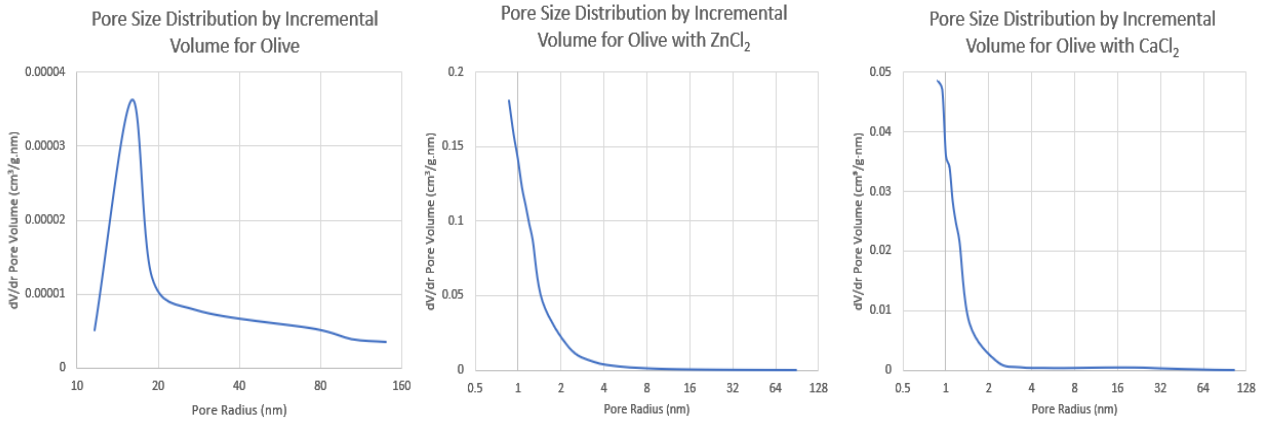

Figure 4.22: Pore size distribution defined by incremental pore volume for olive seed-based activated carbon

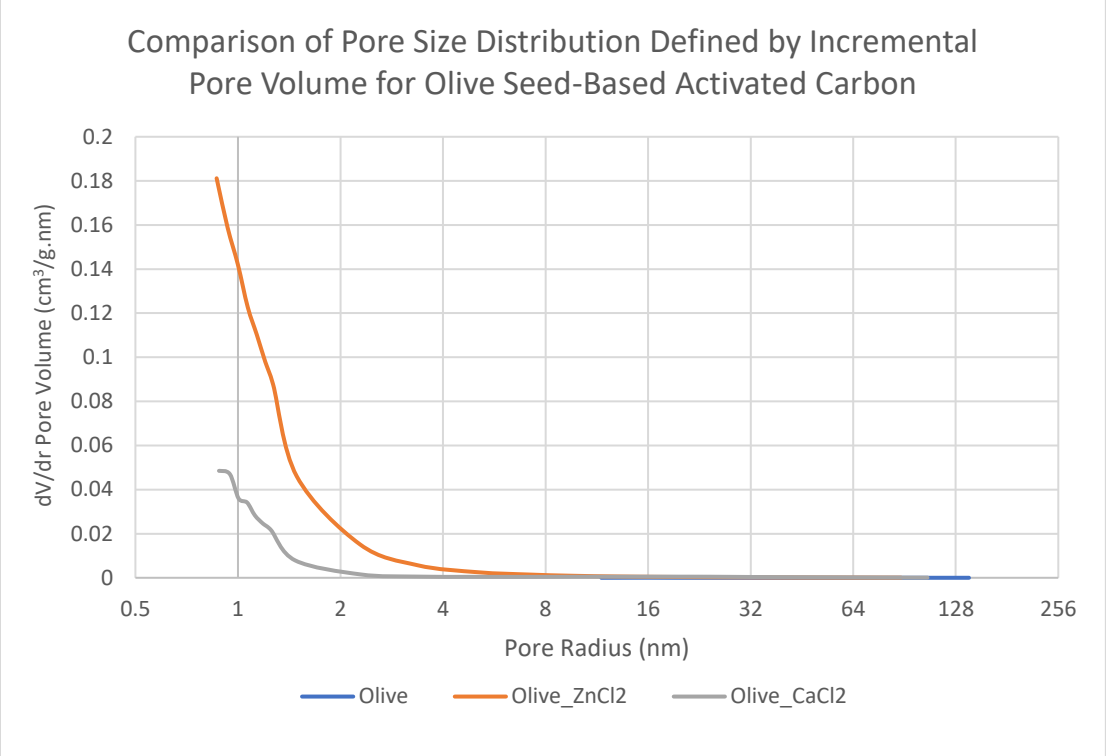

Figure 4.23: Comparison of pore size distribution defined by incremental pore volume for olive seed-based activated carbon

From the pore size distribution of char produced from olive seeds, an unexpected increase in incremental pore volume was observed, as can be seen in the first curve of Figure 4.22. From a pore radius of 10 to 16 nm, there was a drastic increase in incremental pore volume. Maximum incremental pore volume was found at 15.9954 nm pore radius, and the incremental pore volume at that point was 0.0000362 cm^3/gm. After that, from 16 to 20 nm pore radius, there was a similar drastic decrease in incremental pore volume. At that point, incremental pore volume was approximately 0.0000123 cm^3/gm. Weak meso- and macro-pore structures were expected. From the PSD of for olive seed-based carbon activated with $ZnCl_2$, as shown in the second curve of Figure 4.22, a sharp decrease in incremental pore volume was seen in the micropore region (0–2 nm pore radius). The average incremental pore volume was approximately 0.096 cm^3/gm in the micropore region. After that, it decreased at a slower rate with the increase in pore radius. After a

pore radius of 6 nm, the incremental pore volume became almost zero. Therefore, pore volume did not change much with the change in pore radius. The third curve shown in Figure 4.22 indicates the pore size distribution defined by incremental pore volume of $CaCl_2$-activated carbon. As can be seen, in the beginning, there was almost the same incremental pore volume regardless of the increase in pore radius (from 0.85 to 1 nm). Then there was a sudden sharp decrease until a pore radius of 1.5 nm. The average incremental pore volume in the micropore region was 0.028 cm^3/gm. The maximum incremental pore volume was 0.049 cm^3/gm. After the pore radius of 3 nm, there was not much change in pore volume with the change in pore radius. Figure 4.23 shows a comparison of these three types of incremental pore volume on the same scale. Olive seed-based carbon activated with $ZnCl_2$ showed a good response in the change of pore volume with the change in pore radius. But that difference changed at a higher rate with the change in pore radius. The difference in pore volume with respect to the change in pore radius was much smaller for olive seed-based carbon activated with $CaCl_2$ compared to the $ZnCl_2$-activated carbon. The difference in pore volume with respect to the change in pore radius was so small in the case of char produced from olive seeds that it was not visible on the curve at this scale.

4.4.4 BET Surface Area and BJH Pore Volume of Olive Seed-Based Activated Carbon

Figure 4.24 provides a comparison of BET surface area and BJH pore volume of char produced from olive seeds and two types of olive seed-based activated carbon. From the comparison of BET surface area, carbon with $ZnCl_2$ chemical activation showed the maximum surface area for olive seeds. The BET surface areas achieved by olive seed char, $ZnCl_2$ activation, and $CaCl_2$ activation were 10.1841 m^2/gm, 501.4492 m^2/gm, 340.5691 m^2/gm, respectively. There was an almost 49 times increase in the BET surface area using $ZnCl_2$ as the chemical activation

agent and almost 33 times increase using $CaCl_2$ as the chemical activation agent. Of the two chemical agents, $ZnCl_2$ activation provided better BET surface area than $CaCl_2$ activation.

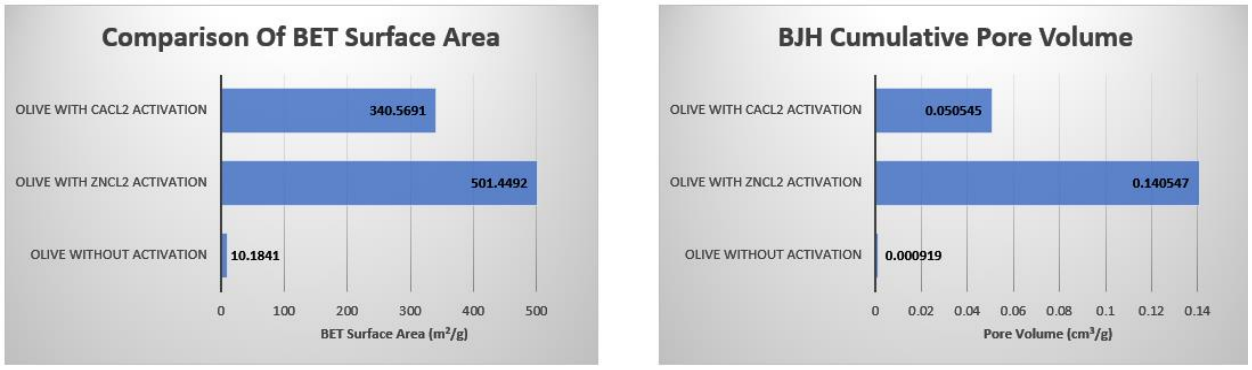

(a) (b)

Figure 4.24: Comparison of olive seed-based activated carbon: (a) BET surface area, and (b) BJH cumulative poor volume

The BJH cumulative pore volume analysis reflected a similar outcome. BJH cumulative pore volumes achieved by olive seed char, $ZnCl_2$ activation, and $CaCl_2$ activation were 0.000919 cm^3/gm, 0.140547 cm^3/gm and 0.050545 cm^3/gm, respectively. The $ZnCl_2$-activated carbon provided almost 153 times and the $CaCl_2$-activated carbon provided about 55 times more cumulative pore volume than the olive seed char without any activation. The $ZnCl_2$-activated carbon showed 2.78 times better pore volume than the $CaCl_2$-activated carbon.

4.4.5 Scanning Electron Microscopy Analysis of Olive Seed-Based Activated Carbon

Figure 4.25 shows SEM images of char prepared from olive seeds and two different chemically activated olive seed-based carbons. The first SEM image of char produced from olive seeds at a magnification of 368X shows the visible formation of some meso- and macropores, which did not comprise a higher pore volume. From isotherm analysis, some slit-type pores were visible from the structure, which was expected. The second SEM image of olive-based carbon activated with $ZnCl_2$ at a magnification of 327X indicates a porous surface. The porosity of the surface is not visible on the third SEM image of the olive-based carbon activated with $CaCl_2$ taken

at a magnification of 392X. To explain the porosity of the activated carbon structure, a much higher magnification is required.

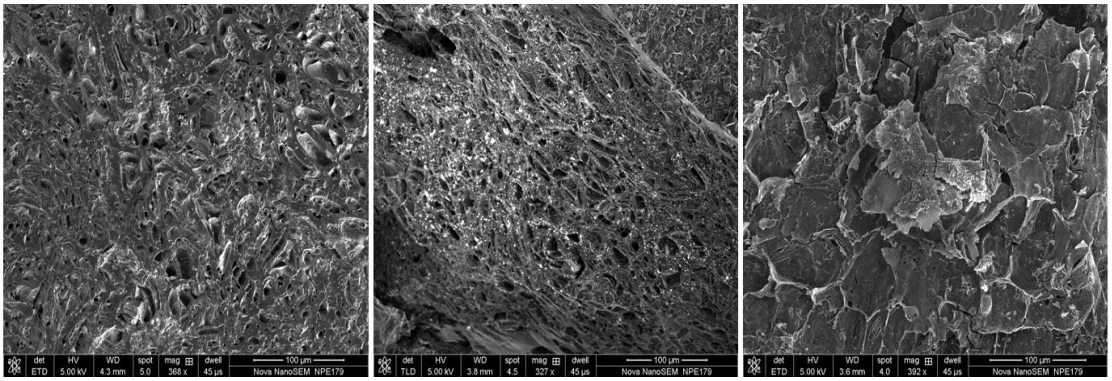

(a) (b) (c)

Figure 4.25: SEM images: (a) olive seeds without chemical activation (368X), (b) olive seeds with $ZnCl_2$ activation (327X), and (c) olive seeds with $CaCl_2$ activation (392X)

Figure 4.26 shows SEM images of olive seed-based carbon activated with $ZnCl_2$ at a higher magnification of 3142X and activated with $CaCl_2$ at a higher magnification of 5268X. Micro- and mesopores in the $ZnCl_2$-activated carbon are easily seen. Both cylindrical and slit-type pores are visible. From the SEM image of $CaCl_2$-activated carbon at 5268X magnification, the porous structure is visible. According to the adsorption isotherm, slit-type pores were expected. Rough, micro- and mesopore surfaces were found in both cases. However, the pore structure of $ZnCl_2$-activated carbon was more convincing for the adsorption.

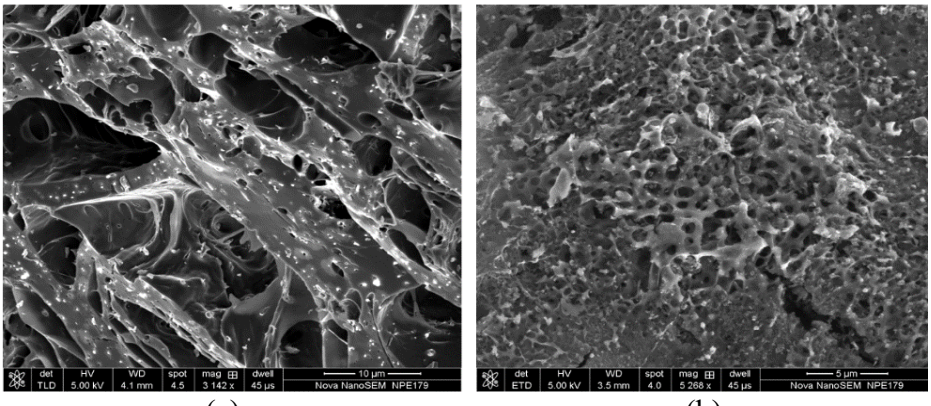

(a) (b)

Figure 4.26: SEM images: (a) olive seeds with $ZnCl_2$ activation (3142X), and (b) olive seeds with $CaCl_2$ activation (5268X)

4.5 Analysis of Activated Carbon Produced by Waste Paper

4.5.1 Adsorption Isotherms of Waste Paper-Based Activated Carbon

Figure 4.27 shows a comparison of adsorption isotherms for three different cases: char produced from waste paper, waste paper-based carbon activated with $ZnCl_2$, and waste paper-based carbon activated with $CaCl_2$.

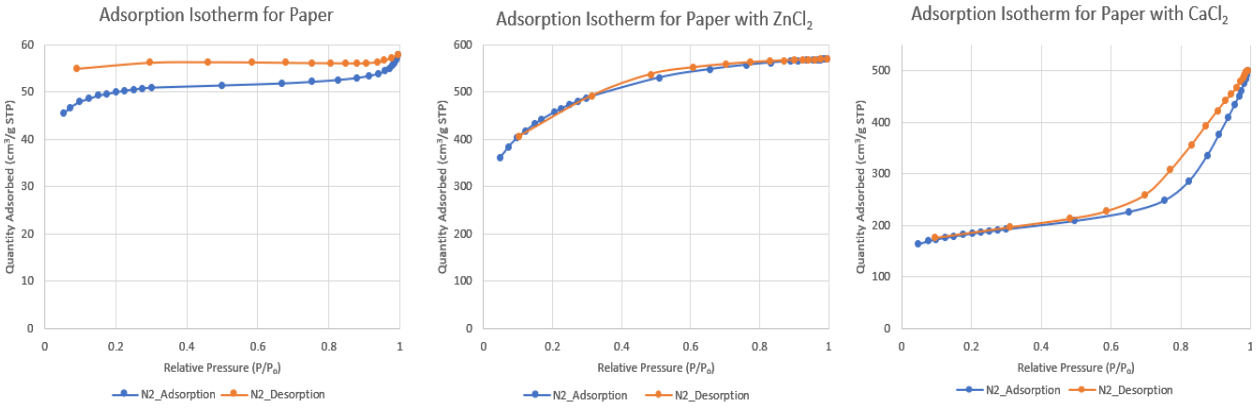

Figure 4.27: Comparison of adsorption isotherms for waste paper-based activated carbon

Three different curves showing three different patterns can be seen. The adsorption isotherm of char produced from waste paper suggests a Type II isotherm with a small exception. At a lower pressure ratio (0–0.18), there was a small sharp increase in adsorption quantity. After that, there was a linear relationship between the adsorption and relative pressure at a moderate pressure ratio. Then at a higher-pressure ratio, there was a slight increase in the adsorption quantity. The maximum quantity adsorbed was 57.94 cm^3/gm at a relative pressure ratio of 0.9956 (approximately). The minimum adsorption quantity was found at a pressure ratio of 0.54 with a value of 45.52 cm^3/gm. The desorption isotherm did not follow the exact path of the adsorption isotherm. A definite hysteresis was observed. A higher adsorption quantity was seen in the waste paper-based carbon activated with $ZnCl_2$. The shape of the isotherm was similar to a Type I isotherm. The adsorption quantity increased with the increase in relative pressure ratio; however,

the progression rate was higher from the lower to moderate pressure ratio, the progression rate increased at a steady rate from the moderate to higher pressure ratio, and the adsorption quantity increased at a steady rate. The maximum quantity adsorbed was 570.62 cm^3/gm at a relative pressure ratio of 0.9944 (approximately). The minimum adsorption quantity was found at a pressure ratio of 0.048 with a value of 361.69 cm^3/gm. The desorption isotherm curve followed the same path as the adsorption isotherm. No hysteresis formed. A cylindrical pore structure was expected from the isotherm analysis. The higher adsorption quantity was also seen in the waste paper-based carbon activated with $CaCl_2$. The shape of the isotherm was similar to a Type III isotherm. A steady increase of quantity adsorbed was seen from the low to the moderate pressure ratio. At a higher-pressure ratio (0.8–1), there was a sharp increase in adsorption quantity. The maximum quantity adsorbed was 500.33 cm^3/gm at a relative pressure ratio of 0.9914 (approximately). The minimum adsorption quantity was found at a pressure ratio of 0.048 and a value of 164.2 cm^3/gm. The desorption isotherm followed almost the same path as that of the adsorption isotherm. A small deviation was noticed from the moderate to higher pressure ratio (0.65–1). As a result, a small hysteresis formed. The wedge-shaped porous structure shown in this analysis was expected.

4.5.2 Pore Volume of Waste Paper-Based Activated Carbon

The interaction of pore volume and pore radius and comparison among the waste paper-based activated carbon and char are shown in Figures 4.28 and 4.29. As shown in the first curve of Figure 4.28, a small pore volume was observed from the char produced by the waste paper. A sharp decrease in pore volume can be seen from pore radius 0.8 to 1.3 nm. After that, the pore volume decreased at a slower steady rate. In the micropore region, the average pore volume was approximately 0.015 cm^3/gm.

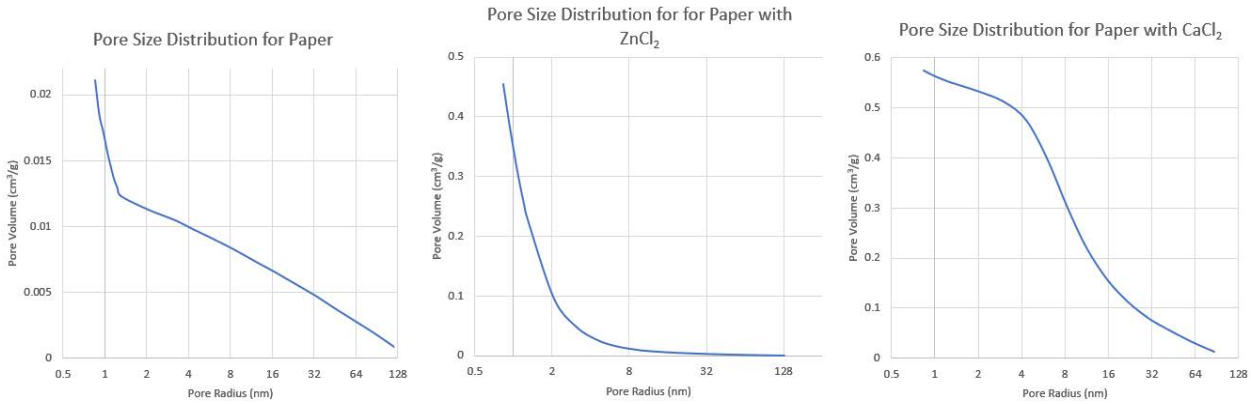

Figure 4.28: Pore volume vs. pore radius for waste paper-based activated carbon

The second curve in Figure 4.28 represents the relationship between the pore volume and pore radius for waste paper-based carbon activated with $ZnCl_2$. As shown, an inverse exponential relation exists between the pore volume and pore radius. An exponential decrease in pore volume was observed in the micropore region. The average pore volume in the micropore region was approximately 0.3 cm^3/gm. The maximum pore volume was 0.455 cm^3/gm at a pore radius of 0.84 nm. After the pore radius of 8 nm, the pore volume was close to zero. The third curve in Figure 4.28 shows the relationship between pore volume and pore radius for waste paper-based carbon activated with $CaCl_2$. From the pore radius of 0.87 to 4 nm, the pore volume decreased at a steady (almost linear) rate. In the micropore region, the average pore volume was 0.045 cm^3/gm. The maximum pore volume was 0.0776 cm^3/gm at a pore radius of 0.87 nm. From the pore radius of 4 to 20 nm, the pore volumes decreased at a steeper rate with the increase in pore radius. Then again after the pore radius of 20 nm, the pore volume decreased at a slower rate with the increase in pore radius. The minimum value found was 0.012 cm^3/gm at a pore radius of 87.19 nm.

From a comparison of these three types of activated carbon, it can be seen in Figure 4.29 that the pore volume of the waste paper-based carbon activated with $CaCl_2$ was higher than the other two and that it decreased initially at a slow rate with the increase in pore radius. However,

the pore volume of the waste paper-based carbon activated with $ZnCl_2$- decreased at a higher rate with pore radius. The pore volume was almost zero after 8 nm. For waste paper-based char without activation, the pore volume was close to zero throughout the change in pore radius.

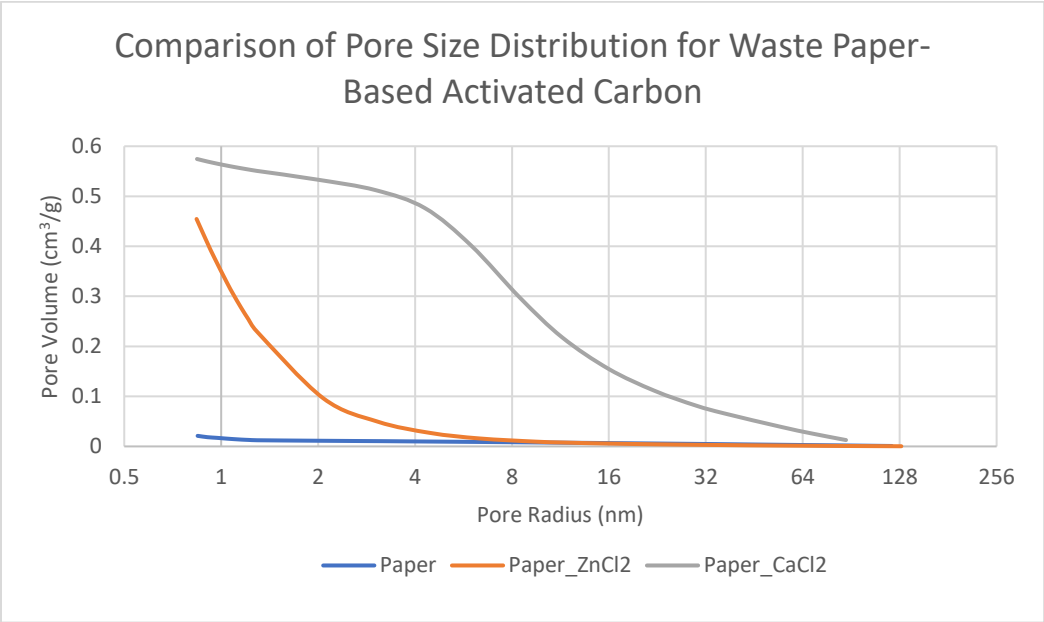

Figure 4.29: Comparison of pore volume and pore radius for waste paper-based activated carbon

4.5.3 Pore Size Distribution of Waste Paper-Based Activated Carbon

Figure 4.30 shows the different pore size distributions defined by incremental pore volume of waste paper-based activated carbon at low-pressure adsorption.

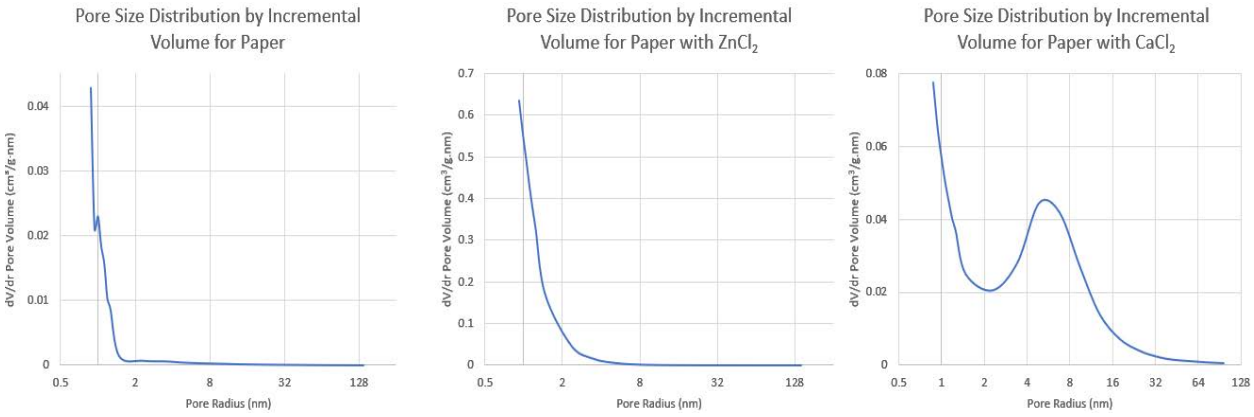

Figure 4.30: Pore size distribution defined by incremental pore volume for waste paper-based activated carbon

As shown in the first cure in Figure 4.30, the PSD of char produced from waste paper showed a drastic decrease in incremental pore volume in the micropore region (pore radius < 1nm). At a pore radius of 0.873 nm, the incremental pore volume was 0.042751 cm^3/gm, and at a pore radius of 0.9347 nm, the incremental pore volume was 0.021015 cm^3/gm. It can be seen that for a small change in pore radius, the incremental pore volume changed by half. There was a small amount of discontinuity in the curve. From pore radius 0.9347 nm to 0.996381 nm, the incremental pore volume increased slightly. Then, again, the incremental pore volume decreased at a high rate (smaller than the initial rate). After the pore radius of 1.47 nm, incremental pore volume was close to zero. This change indicates that the rate of change of pore volume does not depend much on the pore radius after a pore radius of 1.5 nm. The second curve in Figure 4.30 shows the relationship between incremental pore volume and pore radius for waste paper-based carbon activated with $ZnCl_2$. Here, the incremental pore volume decreased at an exponential rate. From the 0 to 2 nm pore radius, the incremental pore volume decreased rapidly. The maximum incremental pore volume was 0.712027 cm^3/gm, which was observed at a pore radius of 0.868774 nm. After the pore radius of 3 nm, there was no significant change in pore volume with the change in pore radius. The third curve in Figure 4.30 shows the relationship between incremental pore volume and pore radius for waste paper-based carbon activated with $CaCl_2$. This curve shows a slight variation over the other two: a sharp decrease at first, then a sudden increase, and finally a non-linear decrease in incremental pore volume with the increase in pore radius. From a pore radius of 0.87 to 2.3 nm, the incremental pore volume decreased with the change in pore radius. From a pore radius of 2.3 to 6.8 nm, the pore volume increased at a higher rate. After that, the pore volume decreased again with the increase in pore radius in a non-linear way. The patterns for waste paper-based carbon activated with $CaCl_2$ and the waste paper-based carbon without activation were similar. The only

difference was the amplitude. The waste paper-based carbon activated with $ZnCl_2$ showed a significant change in pore volume with respect to the change in pore radius. However, this change was almost zero with the increase in pore radius. Figure 4.31 provides a comparison of the three types of incremental pore volumes on the same scale.

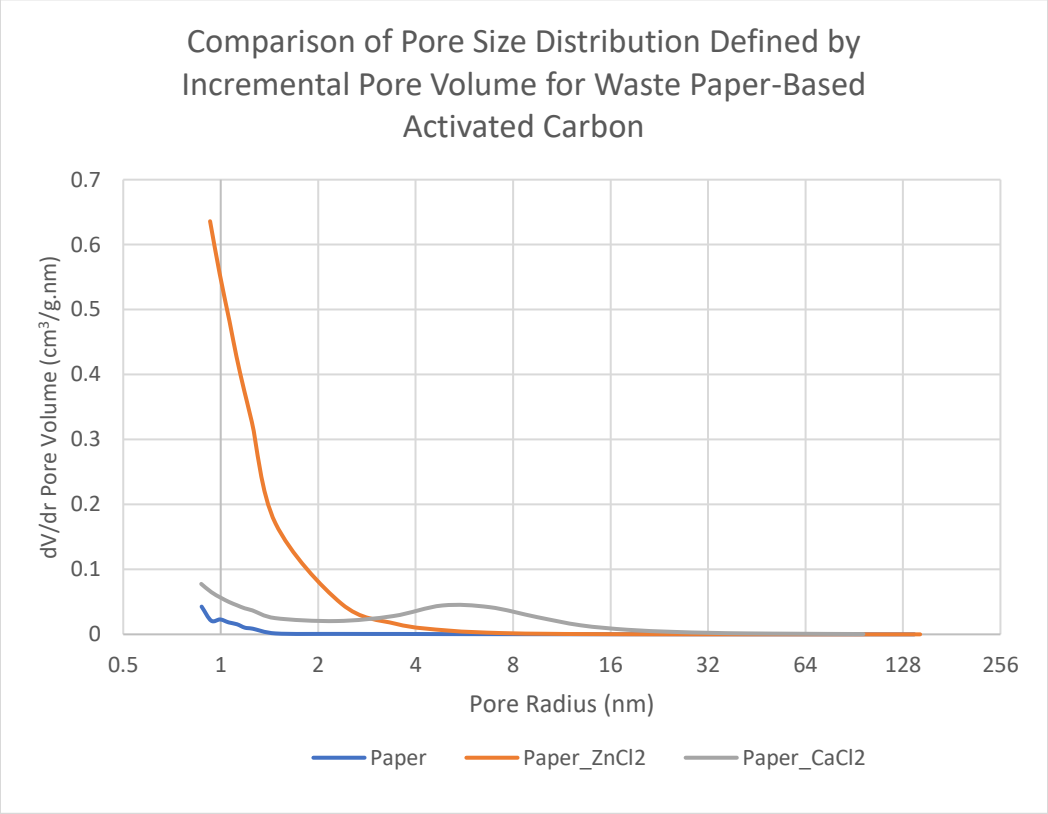

Figure 4.31: Comparison of pore size distribution defined by incremental pore volume for waste paper-based activated carbon

4.5.4 BET Surface Area and BJH Pore Volume of Waste Paper-Based Activated Carbon

Figure 4.32 provides a comparison of BET surface area and BJH cumulative pore volume of different waste paper-based activated carbons and char. From the BET surface area diagram, it can be seen that waste paper-based carbon activated with $ZnCl_2$ provides a better surface area. The BET surface areas of char from waste paper, waste paper-based carbon activated with $ZnCl_2$, and waste paper-based carbon activated with $CaCl_2$ were 158.8533 m^2/gm, 1496.97 m^2/gm, and

577.0856 m^2/gm, respectively. $ZnCl_2$ activation provided 9.4 times better surface area, and $CaCl_2$ activation provided 3.6 times better surface area than the char produced from waste paper without any activation. In other words, $ZnCl_2$ activation provided almost 2.6 times better surface area than $CaCl_2$ activation.

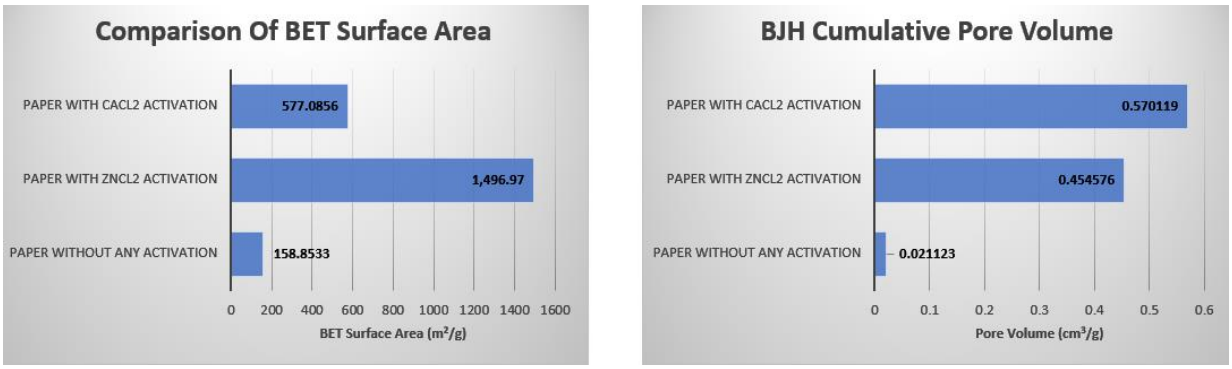

(a) (b)

Figure 4.32: Comparison of waste paper-based activated carbon: (a) BET surface area, and (b) BJH cumulative pore volume

The BJH cumulative pore volume comparison shows an interesting exception. Generally, a higher BJH pore volume means a higher cumulative pore volume. The case of waste paper-based carbon activated with $CaCl_2$ showed a higher cumulative pore volume. The BJH cumulative pore volumes of char from waste paper, waste paper-based carbon activated with $ZnCl_2$, and waste paper-based carbon activated with $CaCl_2$ were 0.021123 cm^3/gm, 0.454576 cm^3/gm, and 0.570119 cm^3/gm, respectively. The $ZnCl_2$ activation provided 21.5 times better cumulative pore volume and the $CaCl_2$ activation provided almost 27 times higher cumulative pore volume than the char produced from waste paper without any activation. The $CaCl_2$ activation provided almost 1.25 times higher pore volume than $ZnCl_2$ activation.

4.5.5 Scanning Electron Microscopy Analysis of Waste Paper-Based Activated Carbon

SEM images of paper-based activated carbon and carbon from paper without any activation are shown in Figure 4.33.

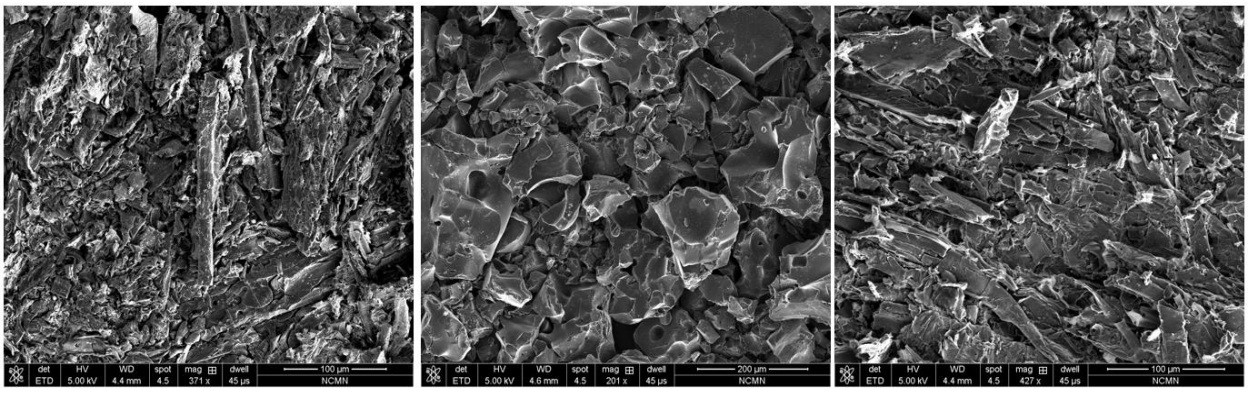

(a) *(b)* *(c)*

Figure 4.33: SEM images: (a) waste paper without chemical activation (371X), (b) waste paper with $ZnCl_2$ activation (201X), and (c) waste paper with $CaCl_2$ activation (427X)

The first SEM image of char produced from waste paper without any activation shows some porosity in the structure. According to the adsorption isotherm, a slit-type pore structure was expected, and the 371X magnification was employed here for better understanding. The second SEM image in Figure 4.33 shows waste paper-based carbon activated with $ZnCl_2$. From the BET surface area analysis, $ZnCl_2$-activated carbon should have a higher porosity. This SEM image reflects that same conclusion. A highly porous surface can be seen in this image, which was taken at a magnification of 201X. The third SEM image shows the waste paper-based carbon activated with $CaCl_2$. The BET surface area analysis indicates that a moderate porosity would be observed. This image, taken at a magnification of 427X, shows little porosity in the structure. A higher magnification is required to observe the details.

Figure 4.34 shows the higher magnification SEM images of waste paper-based carbon activated with $ZnCl_2$ and $CaCl_2$. From the 501X magnified image of waste-paper based carbon activated by $ZnCl_2$, a clean porous structure can be seen. From the adsorption isotherm, a Type I isotherm reflecting the cylindrical pore type was observed. The higher-magnification image shows the cylindrical pore structure, which matches the expectation. The SEM image of waste paper-based carbon activated with $CaCl_2$ was taken at a magnification of 849X to observe the porosity

of the structure. At this higher magnification, a rough pore structure can be seen. According to the adsorption isotherm, a Type III isotherm representing a wedge-shaped structure is observed. From the SEM images, slit and wedge-shaped irregular pore structures are observed.

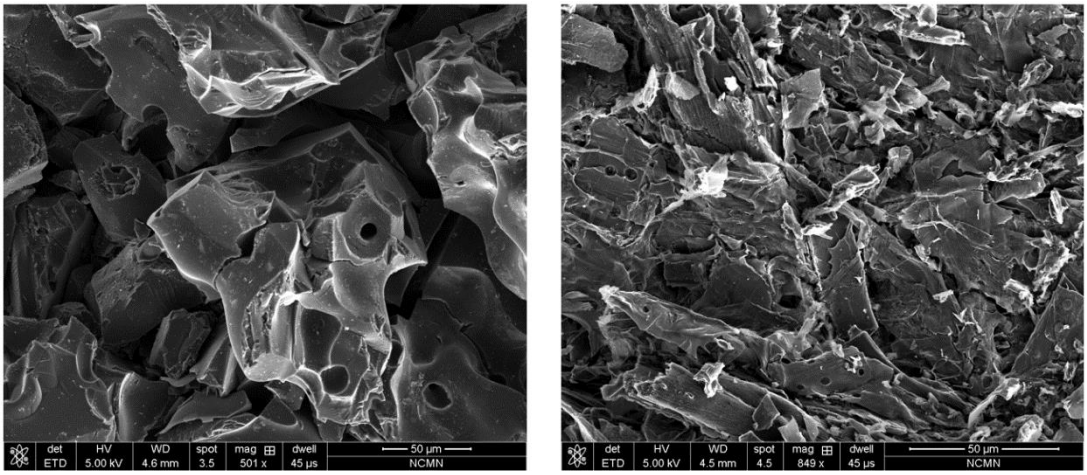

(a) (b)

Figure 4.34: SEM images: (a) waste paper with $ZnCl_2$ activation (501X), and (b) waste paper with $CaCl_2$ activation (849X)

4.6 Analysis of Activated Carbon Produced by Waste Cotton Cloth

4.6.1 Adsorption Isotherms of Waste Cotton Cloth-Based Activated Carbon

Figure 4.35 shows the comparison of a low-pressure nitrogen adsorption isotherm for different cotton cloth-based activated carbon.

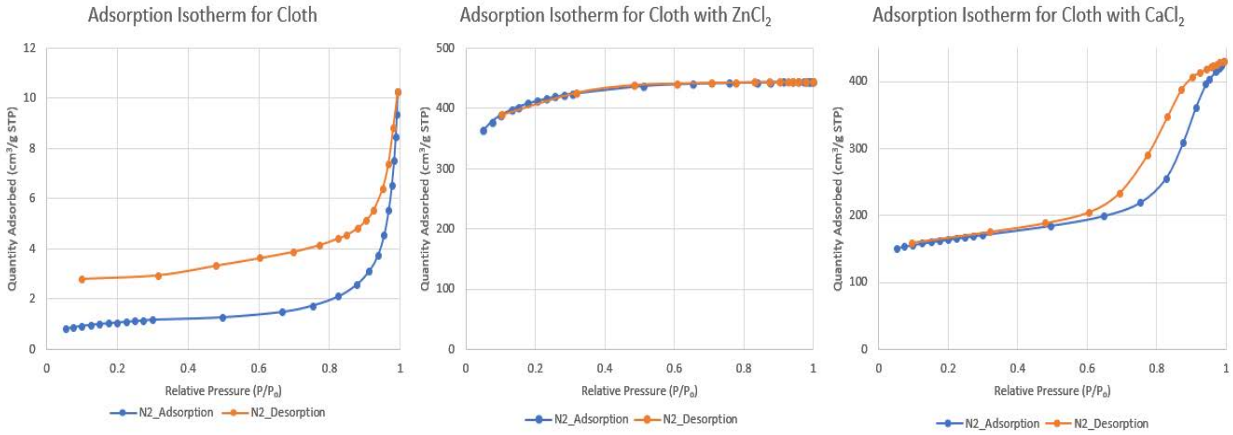

Figure 4.35: Comparison of adsorption isotherms for waste cotton cloth-based activated carbon

Here, the pattern of adsorption isotherm curves is similar to the adsorption isotherm of waste paper-based activated carbon. Three curves show three different patterns. The first curve in Figure 4.35 showing the adsorption isotherm of char produced from waste cotton cloth without any activation suggests a Type II isotherm. At low relative pressure ratio, the adsorption quantity was low. From a lower to moderate pressure ratio, the amount of quantity adsorbed increased almost linearly at a smaller rate with the increase in pressure ratio. From a moderate to higher pressure ratio, there was a sudden sharp increase in quantity adsorption with the increase in pressure ratio (0.82–1.0). The maximum adsorbed quantity was observed at a pressure ratio of 1 at a value of 10.26 cm^3/gm. The slit-type pore structure here was expected. The desorption isotherm did not follow the same path of the adsorption isotherm. A diverging hysteresis formed as the relative pressure ratio was lowered. The second curve in Figure 4.35 represents the adsorption isotherm of waste cotton cloth-based carbon activated with $ZnCl_2$. A higher adsorption quantity can be seen at the lower pressure ratio. This adsorption isotherm follows the trend of a Type I isotherm. From a 0 to 0.4 pressure ratio, there was a small increase in adsorption quantity. After that, the adsorption quantity became almost constant with the change in relative pressure ratio. The minimum adsorption quantity was found at a relative pressure ratio of 0.0487 at a value of 362.93 cm^3/gm. Maximum adsorption quantity was found at a relative pressure of 0.994753 and a value of approximately 444.61 cm^3/gm. This adsorption isotherm is similar to a Type I isotherm, hence the cylindrical pore structure as expected. The desorption isotherm followed the exact path of the adsorption isotherm, so no hysteresis was observed. The third curve in Figure 4.35 represents the adsorption isotherm of waste cotton cloth-based carbon activated with $CaCl_2$. The higher adsorption quantity was achieved at a higher relative pressure ratio, which follows a combination of Types III and IV isotherms. From a relative pressure ratio of 0.05–0.7, adsorption quantity increased at a slower linear rate with the

increase in pressure ratio. After that, there was a sudden increase in adsorption quantity at a steeper rate. The minimum adsorption quantity was found at a relative pressure ratio of 0.0538 at a value of 150.52 cm^3/gm. The maximum adsorption quantity was found at a relative pressure of 0.993874 at a value of approximately 429.986 cm^3/gm. The desorption isotherm followed almost the similar path with a slight variation in the middle. A small hysteresis formed at the relative pressure ratio from 0.6 to 1.0. A wedge-shaped pore structure, as expected, resulted from this adsorption isotherm.

4.6.2 Pore Volume of Waste Cotton Cloth-Based Activated Carbon

The interaction between pore volume and pore radius for different types of waste cotton cloth-based activated carbon and their comparison are shown in Figures 4.36 and 4.37.

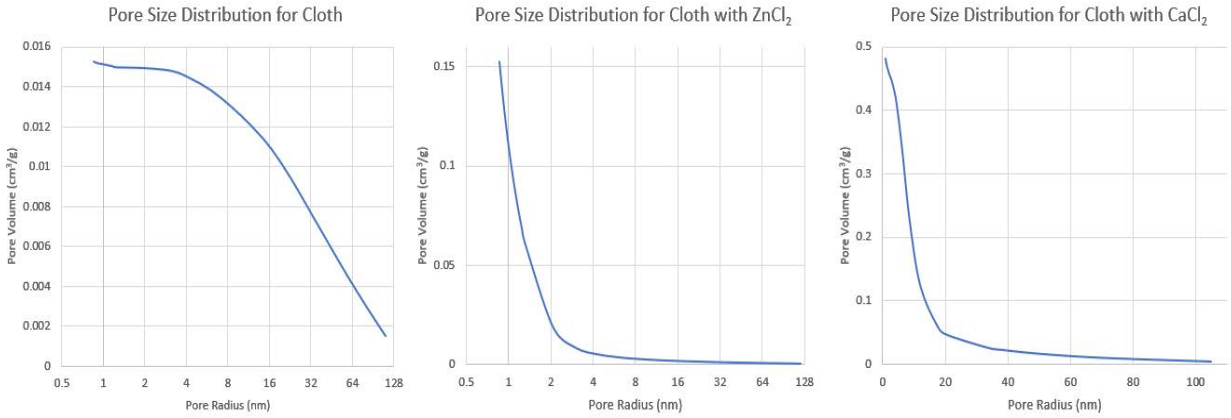

Figure 4.36: Pore volume vs. pore radius for waste cotton cloth-based activated carbon

The first curve represents the relation between pore volume and pore radius of the char produced from waste cotton cloth without any chemical activation. In the beginning, from a pore radius of 0.84 to 4 nm, the pore volume remained almost constant. The average pore volume in the micropore region was approximately 0.015 cm^3/gm. From a pore radius of 5 to 16 nm, the pore volume decreased in a non-linear way with the increase in pore radius. After that, the pore volume decreased linearly at a steady rate. The second curve in Figure 4.36 represents the relationship

between pore volume and pore radius of waste cotton cloth-based carbon activated with $ZnCl_2$. This shows an inverse exponential relationship between pore volume and pore radius. From a pore radius of 0.854 to 2 nm, the pore volume decreased at a drastic rate. The average pore volume in this region was approximately 0.08 cm^3/gm. After that, the pore volume decreased at a slower rate. The pore volume was almost zero after a pore radius of 16 nm. The maximum pore volume was found at a pore radius of 0.854 nm at a value of 0.152621 cm^3/gm. The third curve in Figure 4.36 shows the relationship between pore volume and pore radius of waste cotton cloth-based carbon activated with $CaCl_2$. A constant pore volume can be seen from a pore radius of 0.84 to 4.5 nm. The average pore volume in that region was approximately 0.47 cm^3/gm. After that, a drastic decrease can be seen from a pore volume of 6 to 20 nm. After a pore radius of 20 nm, the pore volume decreased at a steady rate. The higher pore volume was achieved through $CaCl_2$ chemical activation, and the maximum pore volume was approximately 0.482 cm^3/gm.

Figure 4.37 shows the comparison of these three types of waste cotton cloth activated carbon on the same scale. Waste cotton cloth-based carbon activated with $CaCl_2$ showed higher pore volume at any pore radius than the others. Pore value was almost constant until a pore radius of 5 nm. After that, the pore volume decreased with the increase in pore radius. The pore volume of waste cotton cloth-based carbon activated with $ZnCl_2$ decreased at a sharp rate with pore radius. The pore volume of the waste cotton cloth-based carbon without activation showed almost a similar value until a pore radius of 16 nm. After a pore radius of 2.5 nm, higher pore values were observed from the carbon without any activation over the carbon activated with $ZnCl_2$.

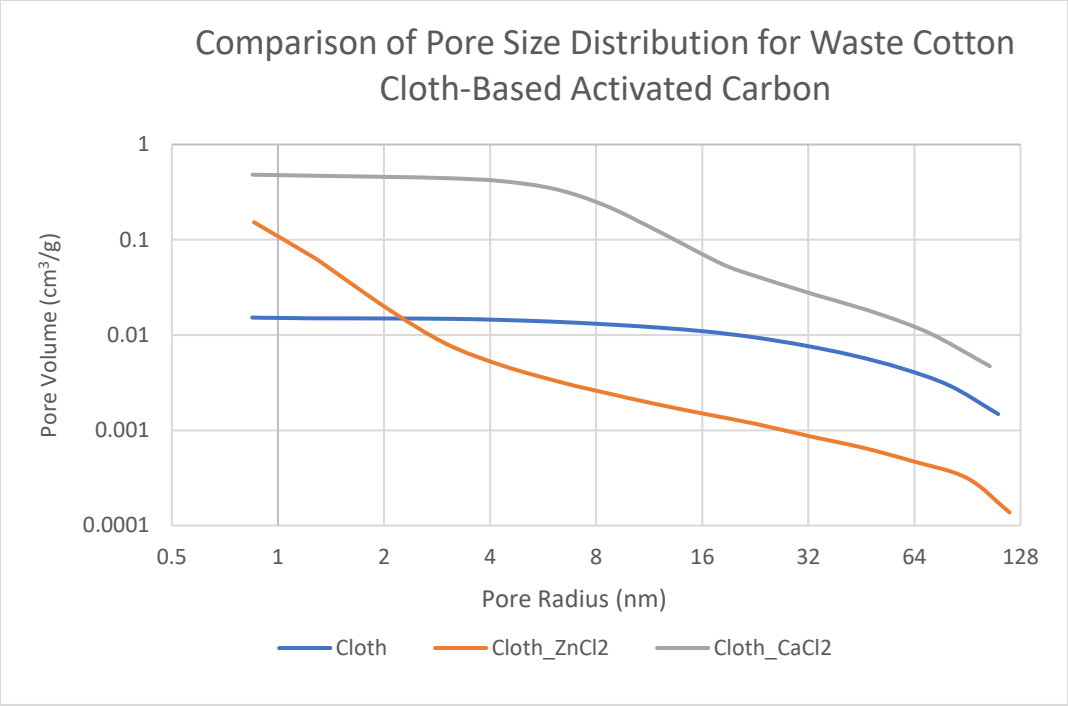

Figure 4.37: Comparison of pore volume and pore radius for waste cotton cloth-based activated carbon

4.6.3 Pore Size Distribution of Cloth-Based Activated Carbon

A comparison of pore size distribution by incremental pore volume of different types of waste cotton cloth-based activated carbon is shown in Figures 4.38 and 4.39.

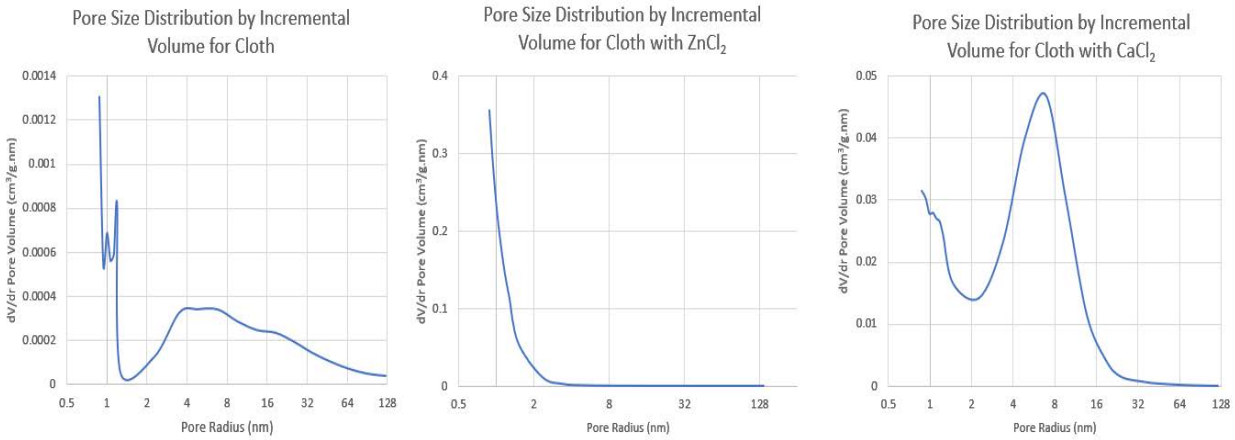

Figure 4.38: Pore size distribution defined by incremental pore volume for waste cotton cloth-based activated carbon

From the first curve in Figure 4.38, it can be seen that the pore size distribution of char produced from waste cotton cloth demonstrates a discontinuous shape in the incremental pore volume vs. pore radius curve. A steep decrease in the incremental pore volume occurred from a pore radius of 0.873 to 1.12 nm. Then there was a sudden increase in pore volume with the increase in pore radius. After that, a sharp decrease and a zig-zag shape in the curve can be seen. This reflected the more frequent change in pore volume with pore radius. The average incremental pore volume in this region was close to 0.00065 cm^3/gm. At a pore radius of 1.25 nm, the incremental pore volume was almost zero. After that, the incremental pore volume started to increase for a certain period, i.e., until a pore radius of 6.8 nm. The value of the incremental pore volume was 0.00034 cm^3/gm at a pore radius of 6.8 nm. After that, the rate of change of pore volume with pore radius decreased at a steady rate. The second curve in Figure 4.38 represents the relationship between incremental pore volume and pore radius of waste cotton cloth-based carbon activated with $ZnCl_2$. As shown, there was a decrease in incremental pore volume with pore radius at a steeper rate from 0.87 to 2 nm. After that, the incremental pore volume became almost zero, regardless of the change in pore radius, which means that no significant change in pore volume occurred with the change in pore radius. The third curve shown in Figure 4.38 of the incremental pore volume vs. pore radius of waste cotton cloth-based carbon activated with $CaCl_2$ indicates an exceptional pattern. Here, with the increase in pore radius, the corresponding change in pore volume sometimes increased and sometimes decreased. In the beginning, from a pore radius of 0.875 to 2.29 nm, the incremental pore volume decreased with the increase in pore radius. After that, the rate of change of pore volume increased at a steeper rate with the increase in pore radius. The maximum incremental pore volume was found at a pore radius of 6.9 nm at a value of approximately 0.047 cm^3/gm. After this,

the incremental pore volume started to decrease at a sharp rate again with the increase in pore radius.

Figure 4.39 provides a comparison of these three types waste cotton cloth-based activated carbon on the same scale. The change in pore volume with the change in pore radius for activated carbon was abrupt. There were ups and downs, as discussed earlier. The change in pore volume rate with respect to pore radius was higher for waste cotton cloth-based activated with $ZnCl_2$ at the beginning, but the incremental pore volume decreased at a steady rate with the increase in pore radius.

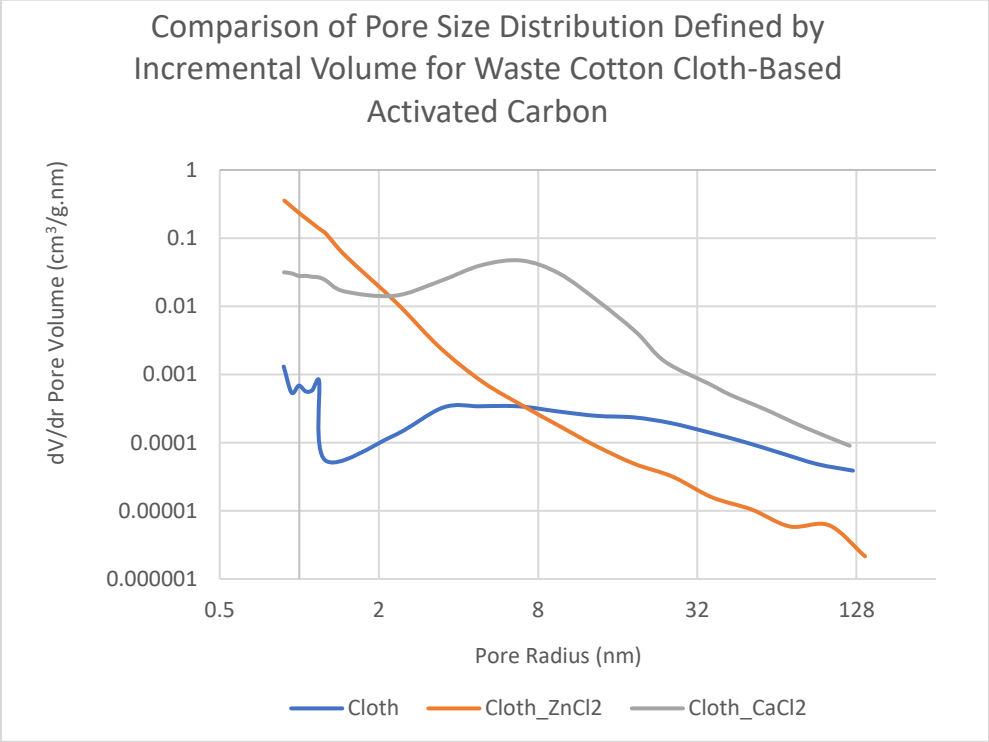

Figure 4.39: Comparison of pore size distribution defined by incremental pore volume for waste cotton cloth-based activated carbon

4.6.4 BET Surface Area and BJH Pore Volume of Waste Cotton Cloth-Based Activated Carbon

Figure 4.40 shows the comparison of BET surface area and BJH cumulative pore volume of different waste cotton cloth-based activated carbon and char.

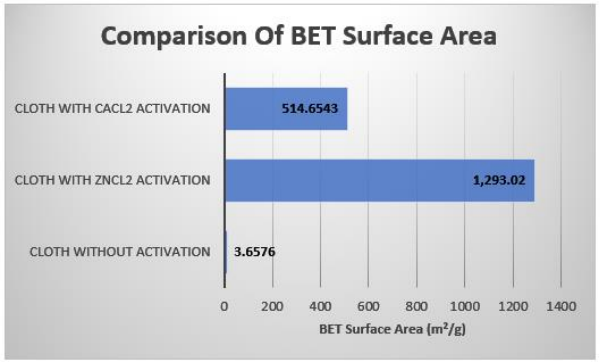

(a)

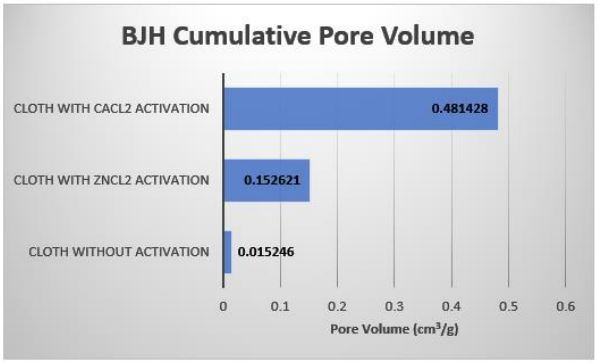

(b)

Figure 4.40: Comparison of waste cotton cloth-based activated carbon: (a) BET surface area, and (b) BJH cumulative pore volume

As can be seen, the BET surface areas achieved by the waste cotton cloth-based char, waste cotton cloth-based carbon activated with $ZnCl_2$, and waste cotton cloth-based carbon activated with $CaCl_2$ were 3.6576 m^2/gm, 1293.02 m^2/gm, and 514.6543 m^2/gm, respectively. A huge improvement can be seen after the chemical activation. $ZnCl_2$ activation provided 353 times better surface area, and $CaCl_2$ activation provided almost 141 times more surface area than the char without any activation. The $ZnCl_2$ activation resulted in an almost 2.5 times improved surface area than that with $CaCl_2$ activation. BJH cumulative pore volume achieved by the waste cotton cloth-based char, waste cotton cloth-based carbon activated with $ZnCl_2$ activation, and waste cotton cloth-based carbon activated with $CaCl_2$ activation were 0.015246 cm^3/gm, 0.152621 cm^3/gm, and 0.481428 cm^3/gm, respectively. In the case of cumulative pore volume, $CaCl_2$-activated carbon provided better pore volumes than the $ZnCl_2$-activated carbon. The $ZnCl_2$ activation provided 10 times better cumulative pore volume and $CaCl_2$ activation provided almost 32 times more cumulative pore volume than the waste cotton cloth-based char without any activation. The $CaCl_2$ activation showed almost 3 times improved pore volume over the $ZnCl_2$ activation.

4.6.5 Scanning Electron Microscopy Analysis of Waste Cotton Cloth-Based Activated Carbon

SEM images of char prepared from two types of waste cotton cloth-based activated carbon are shown in Figure 4.41.

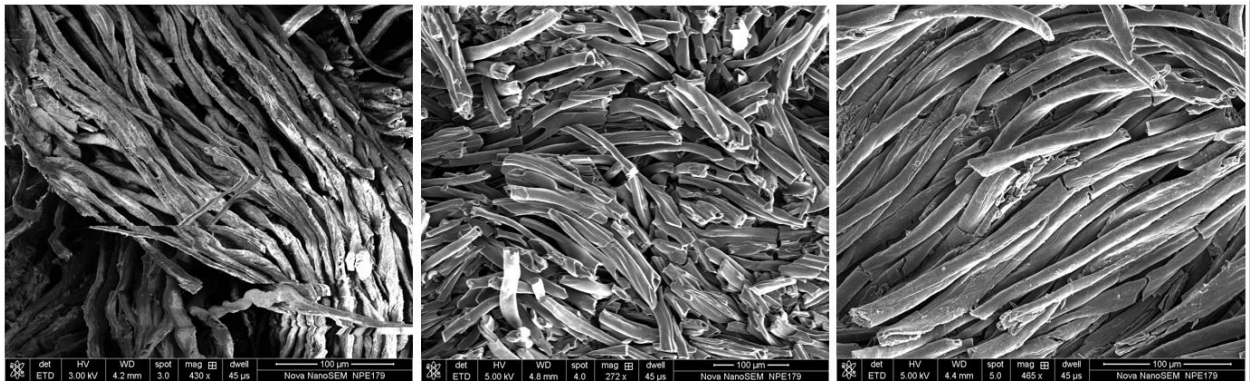

(a) (b) (c)

Figure 4.41: SEM images: (a) waste cotton cloth without chemical activation (430X), (b) waste cotton cloth with $ZnCl_2$ activation (272X), and (c) waste cotton cloth with $CaCl_2$ activation (465X)

From the first SEM image of carbon produced from waste cotton cloth without any activation, the fibrous structure of the cloth can be seen easily. This image was taken at a magnification of 430X. According to the adsorption isotherm, a Type II isotherm was determined. Therefore, the slit-type pore structure was expected. From this SEM image, some pore structure can be seen in between the fibers. The second SEM image shows waste cotton cloth-based carbon activated with $ZnCl_2$ at 272X magnification. The more fibrous surface can be observed here. From the adsorption isotherm, a Type I isotherm was noticed, thus indicating the cylindrical pore structure inside the fibrous structure, as expected. The third SEM image is of waste cotton cloth-based carbon activated with $CaCl_2$ at a magnification of 465X. According to the adsorption isotherm, a combination of Type III and IV isotherms was observed; therefore, wedge-shaped porous structure were expected. To observe the porosity of the structure, higher magnification is required.

Figure 4.42 shows SEM images of $ZnCl_2$-activated carbon and $CaCl_2$-activated carbon at higher magnification, which allows the inside part of the fiber to be visible. With 2513X magnification, the waste cotton cloth-based carbon activated with $ZnCl_2$ shows a detailed pore surface. A better pore structure can also be seen in the waste cotton cloth-based carbon activated with $CaCl_2$. This pore structure inside the fiber is visible at 5456X magnification.

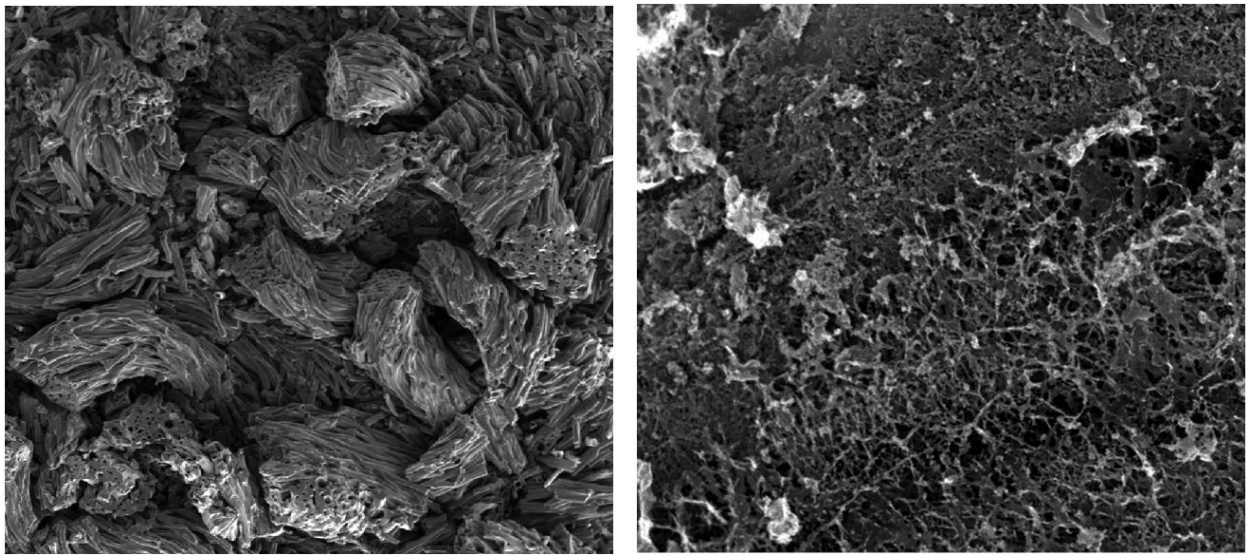

(a) (b)

Figure 4.42: SEM images: (a) waste cotton cloth with $ZnCl_2$ activation (2513X), and (b) waste cotton cloth with $CaCl_2$ activation (5456X)

4.7 BET and BJH Cumulative Pore Volume of Different Conditions and Materials

Tables 4.1 and 4.2, respectively, provide BET surface areas and BJH cumulative pore volumes of different materials under different conditions. It turns out that different activation processes are effective for different materials to obtain a better surface area and therefore porosity.

TABLE 4.1

BET SURFACE AREA OF DIFFERENT MATERIALS UNDER DIFFERENT CONDITIONS

	BET Surface Area (m^2/gm)		
Materials	**Without Chemical Activation**	**Activation with $ZnCl_2$**	**Activation with $CaCl_2$**
Algae	6.3577	124.5766	197.7486
Date Seeds	18.1671	591.4278	76.9446
Olive Seeds	10.1841	501.4492	340.5691
Waste Paper	158.8533	1496.97	577.0856
Waste Cotton Cloth	3.6576	1293.02	514.6543

TABLE 4.2

BJH PORE VOLUME OF DIFFERENT MATERIALS UNDER DIFFERENT CONDITIONS

	BJH Cumulative Pore Volume (cm^3/gm)		
Materials	**Without Chemical Activation**	**Activation with $ZnCl_2$**	**Activation with $CaCl_2$**
Algae	0.048823	0.076515	0.105214
Date Seeds	0.00007	0.102766	0.059418
Olive Seeds	0.000919	0.140547	0.050545
Waste Paper	0.021123	0.454576	0.570119
Waste Cotton Cloth	0.015264	0.152621	0.481428

4.8 Water Purification

4.8.1 Parameters and Standard Values for Water

To inspect the quality of the water after cleaning with an activated carbon filter, the following parameters were chosen:

- Total Dissolved Solids
- Electroconductivity
- pH Level
- Turbidity

4.8.1.1 Total Dissolved Solids

The total dissolved solids are comprised of inorganic and organic substances that can be dissolved in water. Different inorganic salts such as sodium, potassium, bicarbonates, chlorides, sulfates, phosphates, calcium, and nitrates can be dissolved in different concentrations in water [82]. These substances can be dissolved in ionized, molecular, colloidal, or granular form. TDS is referred to as the sum of the concentration of the individual ions from a full macro analysis [83]. These minerals can be dissolved in water in many ways. Industrial waste, other discharge, agricultural waste, and the flow of the water through a rocky region that has a higher salt content are the common reasons for dissolved solids. A certain limit of minerals in the water is actually desirable; however, a much higher concentration of TDS can be harmful to health. According to a panel of professionals with the World Health Organization (WHO), the preferable level of TDS in water is shown in Table 4.3 [84, 85]. Here, the units of TDS are expressed as milligrams per liter (mg/L). However, today, the number of milligrams of solute per kilogram of solution is referred to as parts per million (ppm). Assuming that the density of water is 1.00 g/mL and 1 kg of solution = 1 kg, then 1 mg/L = 1 ppm. Many devices use the ppm unit for measuring TDS.

TABLE 4.3

ACCEPTABILITY WATER BASED ON TDS ACCORDING TO WHO [85]

Level of TDS (milligrams per liter)	**Rating**
Less than 300	Excellent
300–600	Good
600–900	Fair
900–1200	Poor
Above 1200	Unacceptable

4.8.1.2 Electrical Conductivity

Electrical conductivity is the measure of the ability to conduct electricity of an electrolyte solution [86]. It is one of the reliable ways to observe the ionic content of the solution. The value of EC depends on the minerals that dissolved in the aquatic solution. Therefore, EC is directly related to total dissolved solids (TDS) [83]. Higher the mineral content, higher the EC. Increase in ions concentration can enhance electrical conductivity. Therefore, clean water with less ionic contents is supposed to have lower EC. Pure water is actually a good insulator. Electrical conductivity is measured in microsiemens per centimeter (μS/cm). Based on WHO, there is an accessible level for drinking water. This range has been shown in Table 4.4 [84, 87].

TABLE 4.4

ACCEPTABILITY OF WATER BASED ON ELECTRICAL CONDUCTIVITY [87]

Electrical Conductivity (μS/cm)	**Rating**	**Use**
0–800	Good	• Suitable for drinking. • Used in irrigation • Suitable for livestock
800–2,500	Medium	• Can be consumed by humans. • May affect people with kidney problems. • Usable for livestock.
2,500–10,000	Poor	• Not suitable for human consumption. • Can be used for irrigation and cleaning purposes. • Used as drinking water for livestock.
Over 10,000	Unacceptable	• Unacceptable for human consumption. • Not suitable for livestock. • Not usable for irrigation and other household purposes.

4.8.1.3 pH

The pH is a measure of whether a solution is acidic or basic (alkaline). This measure actually determines the concentration of hydrogen ion [H^+] [88] and can be expressed mathematically as pH = –log [H^+]. The pH scale can calculate values from 0 to 14 and is unitless,

where 0 means a highly concentrated strong acid, 14 means a highly concentrated base, and 7 is the neutral pH. Pure water should have a pH of 7.

According to the WHO in 1958, the suggested standard for drinking water was set from 6.5 to 9.2 [84]. In 1984, a new guideline provided for the pH of drinking water and the new range established was 6.5 to 8.5 [89]. This range has been taken as the standard pH range until now. Sometimes the optimum pH range for drinking water is considered to be from 6.5 to 9.5.

4.8.1.4 Turbidity

Turbidity is the measure of haziness or cloudiness of a fluid. It is caused by the large number of particles that are not visible to the naked eye. Turbidity is one of the key parameters of water quality: the less the value of turbidity, the better the quality of the water. Turbidity can be caused by phytoplankton, agricultural waste, sediment, industrial waste, etc. Many different units are used to express the measurement for turbidity: such as Formazine Nephelometric Unit (FNU), Jackson Turbidity Unit (JTU), and Nephelometric Turbidity Unit (NTU). Among these, NTU is considered the most popular. An instrument called a nephelometer with a detector to the side of the light beam was used in this study. Based on the reflected light and color, a turbidity value is provided. Based on the research of WHO, the turbidity of drinking water should not exceed 5 NTU [90]. Deionized and distilled water has a turbidity value of 0.00 to 0.1. However, turbidity values close to 1 NTU are desirable in many cases [91].

4.8.2 Results of Water Treatment

Four sources of water were selected for water treatment:

- Wastewater from a water jet machine from the National Institute of Aviation and Research (NIAR) at Wichita State University.
- Pond Water from 2330 North Oliver Street in Wichita, KS.

- Lake Water from Wichita State University.
- Tap Water from the City of Wichita Water Utility.

All waters were filtered using the water column containing the activated carbon produced earlier. Water quality was evaluated based on four parameters—TDS, EC, pH, and turbidity—before and after filtration.

4.8.2.1 Data from Filtration of Waste Water from Water Jet Machine

Table 4.5 shows data on the quality of wastewater from the water jet machine after the filtration process with different activated carbon-based water columns. Figure 4.43 shows the haziness of water before and after filtration of wastewater from the water jet machine.

TABLE 4.5

WATER QUALITY DATA AFTER FILTRATION OF WASTEWATER FROM WATER JET MACHINE

Source: Waste Water from Water Jet Machine	**Total Dissolved Solids (ppm)**	**Electroconductivity (µS/cm)**	**pH**	**Turbidity (NTU)**
No Treatment	450	900	9.43	146.7
with $ZnCl_2$-activated carbon (Algae)	430	860	7.9	3.1
with $CaCl_2$-activated carbon (Algae)	420	840	8.74	2.1
with $ZnCl_2$-activated carbon (Cloth)	410	820	8.17	1.8
with $CaCl_2$-activated carbon (Cloth)	431	862	8.42	1.8
with $ZnCl_2$-activated carbon (Paper)	430	860	8.21	2.4
with $CaCl_2$-activated carbon (Paper)	420	840	8.38	2.2
with $ZnCl_2$-activated carbon (Date)	419	838	8.49	2.3
with $CaCl_2$-activated carbon (Date)	420	840	8.52	1
with $ZnCl_2$-activated carbon (Olive)	441	882	8.54	1.2
with $CaCl_2$-activated carbon (Olive)	440	880	8.58	1.7

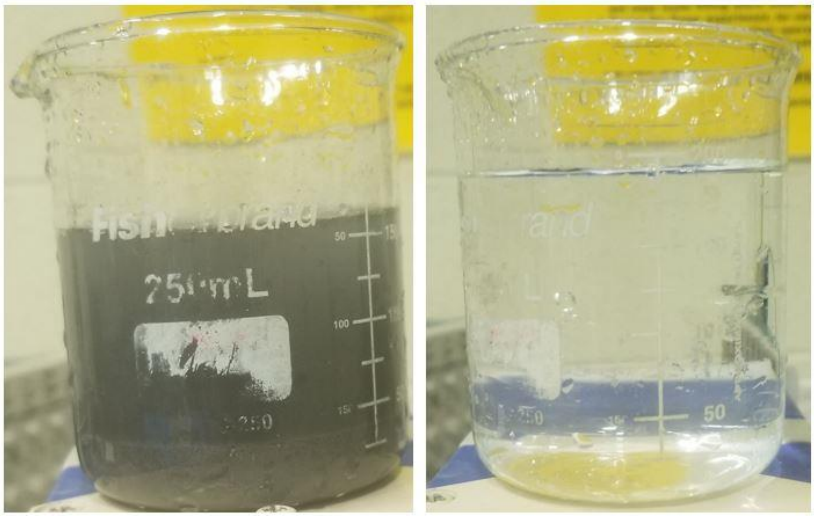

(a) Before Filtration (b) After Filtration

Figure 4.43: Transparency of wastewater from water jet machine: (a) before filtration, and (b) after filtration

The turbidity of wastewater became 17.7 NTU if only filter paper was used to remove the sludge. Least TDS concentration was achieved using the waste cotton cloth-based carbon activated with $ZnCl_2$. The pH and turbidity levels were also in the acceptable reason. The waste paper-based activated carbon did not show good results, as expected. On the other hand, date seed-based carbon activated with $CaCl_2$ showed promising results in turbidity; other parameters, i.e., TDS, EC, and pH were also in the acceptable drinking water range. This may be the result of the interaction properties of the material and the rich amount of carbon content. Olive seed-based activated carbon also showed good results in turbidity and pH, but not good results in TDS and EC.

4.8.2.2 Data from Filtration of Pond Water

Table 4.6 shows pond water quality data from the filtration process with different activated carbon-based water columns. Figure 4.44 shows the haziness of water before and after the filtration of pond water.

TABLE 4.6

WATER QUALITY DATA AFTER FILTRATION OF POND WATER

Source: Pond Water	**Total Dissolved Solids (ppm)**	**Electroconductivity (µS/cm)**	**pH**	**Turbidity (NTU)**
No Treatment	416	832	8.14	16.7
with $ZnCl_2$-activated carbon (Algae)	399	798	8.28	14.3
with $CaCl_2$-activated carbon (Algae)	378	756	8.54	1.3
with $ZnCl_2$-activated carbon (Cloth)	368	736	8.53	1.5
with $CaCl_2$-activated carbon (Cloth)	368	736	8.62	1.3
with $ZnCl_2$-activated carbon (Paper)	409	818	8.47	1.9
with $CaCl_2$-activated carbon (Paper)	410	820	8.52	1.6
with $ZnCl_2$-activated carbon (Date)	389	778	8.49	0.9
with $CaCl_2$-activated carbon (Date)	431	862	8.51	1.3
with $ZnCl_2$-activated carbon (Olive)	399	798	8.45	1.6
with $CaCl_2$-activated carbon (Olive)	368	736	8.44	1.2

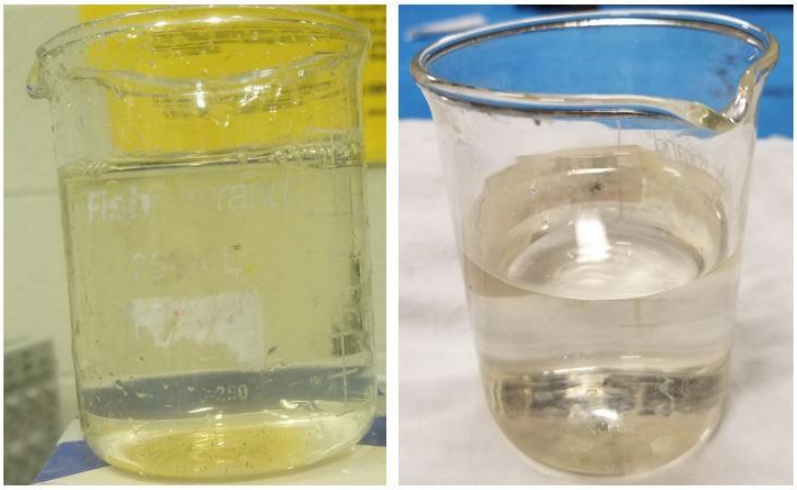

(a) Before Filtration (b) After Filtration

Figure 4.44: Transparency of pond water: (a) before filtration, and (b) after filtration

An unexpected value measuring turbidity was observed on the algae-based carbon activated with $ZnCl_2$, indicating that this data behaved as an outlier. Other than that, all the water

columns provided a reasonable turbidity value. Waste cotton cloth-based activated carbon showed overall better results. Both chemical activations showed TDS of 368 ppm and EC of 736 µS/cm, which were the least respective values. All water columns provided pH values there were suitable for human consumption. Date seed-based carbon activated with $ZnCl_2$ activation provided promising results too. All values reflected that the water was suitable for drinking after filtration. One problem could not be solved by filtration: the color of the yellowish pond water. After filtration, the pond waster was still somewhat yellowish, and its mild odor could not be eliminated.

4.8.2.3 Data from Filtration of Lake Water

Table 4.7 shows data on the quality of lake water from the filtration process with different activated carbon-based water columns. Figure 4.45 shows the haziness of lake water before and after filtration.

TABLE 4.7

WATER QUALITY DATA AFTER FILTRATION OF LAKE WATER

Source: Lake Water	**Total Dissolved Solids (ppm)**	**Electroconductivity (µS/cm)**	**pH**	**Turbidity (NTU)**
No Treatment	197	394	9.2	18.4
with $ZnCl_2$-activated carbon (Algae)	195	390	8.72	6.8
with $CaCl_2$-activated carbon (Algae)	168	338	8.57	1.8
with $ZnCl_2$-activated carbon (Cloth)	189	378	8.59	2.2
with $CaCl_2$-activated carbon (Cloth)	190	380	8.64	1.9
with $ZnCl_2$-activated carbon (Paper)	190	380	8.63	2.1
with $CaCl_2$-activated carbon (Paper)	180	360	8.56	1.7
with $ZnCl_2$-activated carbon (Date)	191	382	8.6	1.7
with $CaCl_2$-activated carbon (Date)	191	382	8.52	1.6
with $ZnCl_2$ activated carbon (Olive)	181	362	8.47	1.6
with $CaCl_2$ activated carbon (Olive)	180	360	8.58	2.1

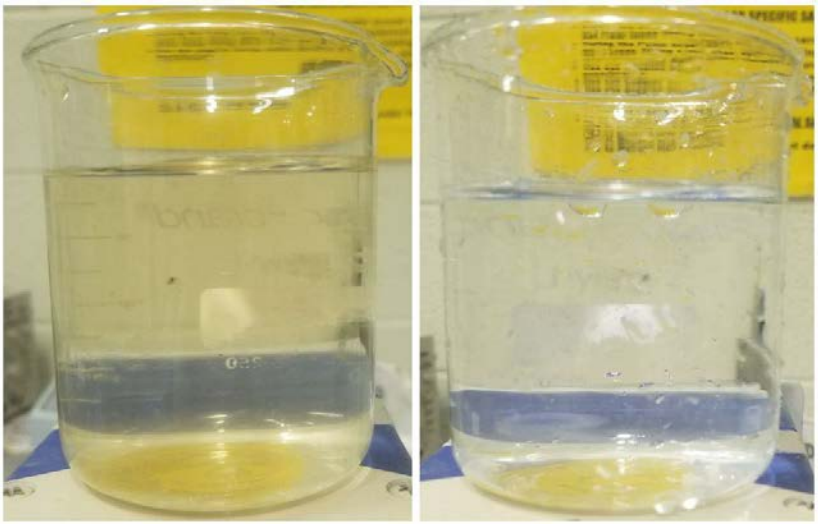

(a) Before Filtration (b) After Filtration

Figure 4.45: Transparency of lake water: (a) before filtration, and (b) after filtration

In this case, except for algae-based carbon activated with $ZnCl_2$, all of the water columns showed suitable water quality for drinking. Moreover, the algae-based carbon activated with $ZnCl_2$ showed the adverse result after filtration. Surprisingly, algae-based carbon activated with $CaCl_2$ provided the best result; the lowest TDS and EC were achieved through this filtration process. Also, waste cotton cloth, waste paper, and olive seed-based activated carbons provided better cleaning of the water. A noticeable change was observed in the lake water filtration. Here, chemical activation by $CaCl_2$ provided better TDS, EC, and turbidity in most cases.

4.8.2.4 Data from Filtration of Tap Water

Table 4.8 shows data on the quality of tap water from the filtration process with different activated carbon-based water columns. By measuring the quality of water supplied by the city of Wichita water utility, it was found that this water is already suitable for human consumption. Our target was to improve that quality by a small margin. In terms of TDS and EC, we were able to reduce them to some content. Waste cotton cloth, waste paper and date seed-based activated carbon

showed better results for any parameters. All of the filtration materials had acceptable pH levels, and turbidity did not exceed more than 1.

TABLE 4.8

WATER QUALITY DATA AFTER FILTRATION OF TAP WATER

Source: Tap water	**Total Dissolved Solids (ppm)**	**Electroconductivity (µS/cm)**	**pH**	**Turbidity (NTU)**
No Treatment	410	820	8.48	0.8
with $ZnCl_2$-activated carbon (Algae)	410	820	8.12	0.8
with $CaCl_2$-activated carbon (Algae)	378	756	8.22	0.9
with $ZnCl_2$-activated carbon (Cloth)	388	776	8.36	0.7
with $CaCl_2$-activated carbon (Cloth)	378	756	8.4	0.8
with $ZnCl_2$-activated carbon (Paper)	410	820	8.49	0.7
with $CaCl_2$-activated carbon (Paper)	388	776	8.49	1
with $ZnCl_2$-activated carbon (Date)	388	776	8.37	0.8
with $CaCl_2$-activated carbon (Date)	389	778	8.46	0.9
with $ZnCl_2$-activated carbon (Olive)	389	778	8.52	0.8
with $CaCl_2$-activated carbon (Olive)	409	818	8.53	0.9

CHAPTER 5

CONCLUSION

In this research study, the effectiveness of activated carbon produced from different materials was investigated in terms of surface area, pore volume, pore radius, and adsorption isotherms. In this study, chemical activation was done using two different chemical agents, i.e., $ZnCl_2$ and $CaCl_2$. Regardless of the material or the activation agent, activated carbon always provided better porosity, adsorption, and surface area than char produced without activation. However, between the two chemical agents ($ZnCl_2$ and $CaCl_2$), which one provided the better porosity, adsorption, and surface area could not be determined because some materials showed better activated carbon with $ZnCl_2$ activation and some with $CaCl_2$ activation. From the BET surface area analysis, it was determined that activated carbon produced from waste paper and waste cotton cloth with $ZnCl_2$ activation provided better values (1496.97 m^2/gm and 1293.02 m^2/gm, respectively). From the BJH pore volume analysis, carbon produced from waste cotton cloth activated with $ZnCl_2$ activation provided better values (0.68654 cm^3/gm). Overall, then, it can be concluded that activated carbon from waste cotton cloth provided the best porosity and adsorption.

A filtration process was designed using that activated carbon. The quality of various sources of water was investigated before and after filtration. Depending on the water source, different activated carbon worked well for different sources. But the activated carbon produced from waste cotton cloth with both $ZnCl_2$ and $CaCl_2$ chemical activation produced a better quality of water after filtration. Surprisingly, the activated carbon from date and olive seeds showed a much better result during filtration. Thus, it can be established that porosity, adsorption, and surface area can be improved by chemical activation and can be used as waste treatment with some further improvement and modifications.

CHAPTER 6

FUTURE WORK

Water is one of the fundamentals of human existence. More parameters need to be considered for determining the quality of drinking water, some of which are listed below:

- Water Hardness
- Total Suspended Solids (TSS)
- Dissolved Oxygen
- Colored Dissolved Organic Matter (CDOM)
- Phosphate Content
- Nitrate Content

If these parameters are evaluated, then a more precise decision can be made about which activated carbon is the best for water filtration. Fourier transform infrared spectroscopy (FTIR) could be performed to obtain the percentage value of the constituents in filtered water.

Recently a very large amount of petroleum and oil has been accidentally spilled, and water mixing with oil is a common problem in many Middle Eastern countries. To separate the two has become a major concern, both environmentally and economically. Because oil has a lower density than water, it normally floats on top of water. The water column filter prototype developed in this research could be used in the future to separate the oil from water.

REFERENCES

LIST OF REFERENCES

[1] Schwarzenbach, R.P., T. Egli, T. Hofstetter, U. Gunten, and B. Wehrli, Global water pollution and human health. *Annual Review of Environment and Resources*, 2010. **35**: pp. 109-136.

[2] World Wildlife Fund, Water scarcity and threats. URL: https://www.worldwildlife.org/threats/water-scarcity [cited August 15, 2018].

[3] Konkel, L., What's in Rio's bay and beaches? *National Geographic News*, 2016. URL: https://news.nationalgeographic.com/2016/08/what-s-in-rio-s-bay-/ [cited August 15, 2018].

[4] Indonesia-Investments, Water pollution in Indonesia causes higher demand for water purifiers. URL: https://www.indonesia-investments.com/business/business-columns/water-pollution-in-indonesia-causes-higher-demand-for-water-purifiers/item5782 [cited August 16, 2018].

[5] Redmon, D., Chapter 13 presentation: Water pollution. Tes Teach. URL: https://www.tes.com/lessons/R19MGnrJWkCz7A/chapter-13-presentation-water-pollution [cited August 17, 2018].

[6] Garg, A., Pollution a major issue. Thoughts Machine. URL: https://anujgarg499.wordpress.com, [cited August 17, 2018].

[7] Ringler C., What's really causing water scarcity in Africa south of the Sahara? International Food Policy Research Institute. URL: http://www.ifpri.org/blog/what%E2%80%99s-really-causing-water-scarcity-africa-south-sahara [cited August 18, 2018].

[8] Jacobsen, E.K., Water filtration. *Journal of Chemical Education*, 2004. **81**(2): p. 224A.

[9] Helbig, W.A., Method for treating liquids with activated carbon. *Google Patents*, 1952.

[10] Derlet, R.W., and T.E. Albertson, Activated charcoal—Past, present and future. *Western Journal of Medicine*, 1986. **145**(4): pp. 493-496.

[11] Jewell, W.J., J. Madras, W. Clarkson, H. Delancy-Pompe, and R. Kabric, Wastewater treatment with plants in nutrient films, 1983, United States Environmental Protection Agency.

[12] Pescod, M. B., Wastewater treatment and use in agriculture. URL: http://www.fao.org/docrep/t0551e/t0551e05.htm [cited August 17, 2018].

[13] United States Geological Survey, A visit to a wastewater-treatment plant: Primary treatment of wastewater, USGS Water-Science School. URL: https://water.usgs.gov/edu/wwvisit.html [cited August 17, 2018].

[14] Mericq, J.-P., S. Laborie, and C. Cabassud, Vacuum membrane distillation for an integrated seawater desalination process. *Desalination and Water Treatment*, 2009. **9**(1-3): pp. 287-296.

[15] Fritzmann, C., J. Lowenberg, T. Wintgens, and T. Melin, State-of-the-art of reverse osmosis desalination. *Desalination*, 2007. **216**(1-3): pp. 1-76.

[16] Aquatech, Largest power plant in philippines uses membrane desalination for purified water. URL: https://www.aquatech.com/project/largest-power-plant-in-philippines-uses-membrane-desalination-for-purified-water [cited August 18, 2018].

[17] Cath, T.Y., Osmotically and thermally driven membrane processes for enhancement of water recovery in desalination processes. *Desalination and Water Treatment*, 2010. **15**(1-3): pp. 279-286.

[18] Wartelle, L.H., and W.E. Marshall, Nutshells as granular activated carbons: Physical, chemical and adsorptive properties. *Journal of Chemical Technology & Biotechnology*, 2001. **76**(5): pp. 451-455.

[19] Amaya, A., N. Medero, N. Tancredi, H. Silva, and C. Deiana, Activated carbon briquettes from biomass materials. *Bioresource Technology*, 2007. **98**(8): pp. 1635-1641.

[20] Johns, M.M., W.E. Marshall, and C.A. Toles, Agricultural by-products as granular activated carbons for adsorbing dissolved metals and organics. *Journal of Chemical Technology & Biotechnology*, 1998. **71**(2): pp. 131-140.

[21] McDougall, G., The physical nature and manufacture of activated carbon. *Journal of the Southern African Institute of Mining and Metallurgy*, 1991. **91**(4): pp. 109-120.

[22] Bansode, R., J. Losso, W. Marshall, R. Rao, and R. Porteir, Adsorption of volatile organic compounds by pecan shell-and almond shell-based granular activated carbons. *Bioresource Technology*, 2003. **90**(2): pp. 175-184.

[23] Cooney, D.O., *Activated Charcoal in Medical Applications*. 1995: CRC Press.

[24] Guo, J., Y. Luo, A. Lua, R. Chi, Y. Chen, X. Bao, and S. Xiang, Adsorption of hydrogen sulphide (H_2S) by activated carbons derived from oil-palm shell. *Carbon*, 2007. **45**(2): pp. 330-336.

[25] Liu, W., R.D. Vidić, and T.D. Brown, Optimization of sulfur impregnation protocol for fixed-bed application of activated carbon-based sorbents for gas-phase mercury removal. *Environmental Science & Technology*, 1998. **32**(4): pp. 531-538.

[26] Zeng, H., F. Jin, and J. Guo, Removal of elemental mercury from coal combustion flue gas by chloride-impregnated activated carbon. *Fuel*, 2004. **83**(1): pp. 143-146.

[27] Zhang, F.-S., J.O. Nriagu, and H. Itoh, Mercury removal from water using activated carbons derived from organic sewage sludge. *Water Research*, 2005. **39**(2-3): pp. 389-395.

[28] Giraldo, L., and J.C. Moreno-Piraján, Synthesis of activated carbon mesoporous from coffee waste and its application in adsorption zinc and mercury ions from aqueous solution. *Journal of Chemistry*, 2012. **9**(2): pp. 938-948.

[29] Acharya, J., J. Sahu, B. Sahoo, C. Mohanty, and B. Meikap, Removal of chromium (VI) from wastewater by activated carbon developed from Tamarind wood activated with zinc chloride. *Chemical Engineering Journal*, 2009. **150**(1): pp. 25-39.

[30] Cho, D.-W., C.-M. Chon, Y. Kim, and H. Song, Adsorption of nitrate and Cr (VI) by cationic polymer-modified granular activated carbon. *Chemical Engineering Journal*, 2011. **175**: pp. 298-305.

[31] Gupta, V., S. K. Srivastava, D. Mohan, and S. Sharma, Design parameters for fixed bed reactors of activated carbon developed from fertilizer waste for the removal of some heavy metal ions. *Waste Management*, 1998. **17**(8): pp. 517-522.

[32] Zanella, O., I. C. Tessaro, and L. A. Feris, Study of $CaCl_2$ as an agent that modifies the surface of activated carbon used in sorption/treatment cycles for nitrate removal. *Brazilian Journal of Chemical Engineering*, 2014. **31**(1): pp. 205-210.

[33] Kadirvelu, K., and C. Namasivayam, Activated carbon from coconut coirpith as metal adsorbent: adsorption of Cd (II) from aqueous solution. *Advances in Environmental Research*, 2003. **7**(2): pp. 471-478.

[34] Gürses, A., C. Dogar, S. Karaca, M. Acikyildiz, and R. Bayrak, Production of granular activated carbon from waste *Rosa canina* sp. seeds and its adsorption characteristics for dye. *Journal of Hazardous Materials*, 2006. **131**(1-3): pp. 254-259.

[35] Batzias, F., and D. Sidiras, Dye adsorption by calcium chloride treated beech sawdust in batch and fixed-bed systems. *Journal of Hazardous Materials*, 2004. **114**(1-3): pp. 167-174.

[36] Tsai, W., C. Y. Chang, M. C. Lin, S. F. Chien, H. F. Sun, M. F. Hsieh, Adsorption of acid dye onto activated carbons prepared from agricultural waste bagasse by $ZnCl_2$ activation. *Chemosphere*, 2001. **45**(1): pp. 51-58.

[37] Rodrigues, L.A., L. A. Ribeiro, G. P. Thim, R. R. Ferreira, M. O. Alvarez-Mendez, and A. Coutinho, Activated carbon derived from macadamia nut shells: An effective adsorbent for phenol removal. *Journal of Porous Materials*, 2013. **20**(4): pp. 619-627.

[38] Ndi Nsami, J., and J. Ketcha Mbadcam, The adsorption efficiency of chemically prepared activated carbon from cola nut shells by on methylene blue. *Journal of Chemistry*, 2013. 7 pp.

[39] Revathi, S., M. B. Shanmuharajan, S. N. Kumar, and R. Vijayalakshmi, Impact of Copper from textile industry effluent and treatment using activated carbon. *International Journal on Applications in Civil and Environmental Engineering*, 2016. **2**(6): pp. 13-14.

[40] Joaquin, A., S.H.A. Al Hadrami, and R. Namdeti, Water analysis using activated carbon from coconut shell. *International Journal of Latest Research in Science and Technology*, 2015. **4**(5): pp. 1-3.

[41] Mozammel, H. M., O. Masahiro, and S. Bhattacharya, Activated charcoal from coconut shell using $ZnCl_2$ activation. *Biomass and Bioenergy*, 2002. **22**(5): pp. 397-400.

[42] Bhatnagar, A., J. Minkyu, C. Yang-Hun, J. Woosik, L. Sang-Hun, and K. Sun-Joon, Removal of nitrate from water by adsorption onto zinc chloride treated activated carbon. *Separation Science and Technology*, 2008. **43**(4): pp. 886-907.

[43] Natalia, M., Y. Sudhakar, and M. Selvakumar, Activated carbon derived from natural sources and electrochemical capacitance of double layer capacitor. *Indian Journal of Chemical Technology*, 2013. **20**: pp. 392-399.

[44] Kocher, J., B. I. Dvorak, and S. Skipton, Drinking water treatment: Activated carbon filtration. Cooperative Extension, Institute of Agriculture and Natural Resources, University of Nebraska-Lincoln., 2003.

[45] Ferrero, F., Dye removal by low cost adsorbents: Hazelnut shells in comparison with wood sawdust. *Journal of Hazardous Materials*, 2007. **142**(1-2): pp. 144-152.

[46] Okoroigwe, E. C., C. M. Saffron, and P. D. Kamdem, Characterization of palm kernel shell for materials reinforcement and water treatment. *Journal of Chemical Engineering and Materials Science*, 2014. **5**(1): pp. 1-6.

[47] Abechi, S., C. E. Gimba, A. Uzairu, and Y. A. Dallatu, Preparation and characterization of activated carbon from palm kernel shell by chemical activation. *Research Journal of Chemical* Sciences, 2013. **3**(1): pp. 54-61.

[48] Wilson, T. O., Factors affecting wood pellet durability. Master's Thesis, Pennsylvania State University, 2010.

[49] Panwar, V., B. Prasad, and K. L. Wasewar, Biomass residue briquetting and characterization. *Journal of Energy Engineering*, 2010. **137**(2): pp. 108-114.

[50] Grover, P., and S. Mishra, Biomass briquetting: Technology and practices. Food and Agriculture Organization of the United Nations, 1996

[51] Nasrin, A. B., M. Choo, W. S. Lim, L. Joseph, S. Michael, M. H. Rohaya, A. A. Astimar, and S. K. Loh, Briquetting of empty fruit bunch fibre and palm shell as a renewable energy fuel. *Journal of Engineering and Applied Sciences*, 2011. **6**: pp. 446-451.

[52] Inomata, K., K. Kanazawa, Y. Urabe, and H. Hosono, Natural gas storage in activated carbon pellets without a binder. *Carbon*, 2002. **40**(1): pp. 87-93.

[53] Hassan, S., L. Kee, and H.H. Al-Kayiem, Experimental study of palm oil mill effluent and oil palm frond waste mixture as an alternative biomass fuel. *Journal of Engineering Science and Technology*, 2013. **8**(6): pp. 703-712.

[54] Wilson, K., H. Yang, C. W. Seo, and W. E. Marshall, Select metal adsorption by activated carbon made from peanut shells. *Bioresource Technology*, 2006. **97**(18): pp. 2266-2270.

[55] Withatanang, K., S. Silapanuntakul, T. Sihabut, and W. Padii, Production of briquette fuel using wastewater sludge and banana peel waste. *Asia-Pacific Journal of Science and Technology*, 2017. **22**(1): pp. 1-7.

[56] Sotannde, O. A., A. Oluyege, and G. Abah, Physical and combustion properties of charcoal briquettes from neem wood residues. *International Agrophysics*, 2010. **24**(2): pp. 189-194.

[57] Suhartini, S., N. Hidayat, and S. Wijaya, Physical properties characterization of fuel briquette made from spent bleaching earth. *Biomass and Bioenergy*, 2011. **35**(10): pp. 4209-4214.

[58] Ward, B. J., T. W. Yacob, and L. D. Montoya, Evaluation of solid fuel char briquettes from human waste. *Environmental Science & Technology*, 2014. **48**(16): pp. 9852-9858.

[59] Arvanitoyannis, I. S., A. Kassaveti, and S. Stefanatos, Current and potential uses of thermally treated olive oil waste. *International Journal of Food Science & Technology*, 2007. **42**(7): pp. 852-867.

[60] Rumpf, H. The strength of granules and agglomerates. In *Agglomeration*. John Wiley, New York, 1962. pp. 379-419.

[61] Manickam, I. N., D. Ravindran, and P. Subramanian, Biomass densification methods and mechanism. *Cogeneration and Distributed Generation Journal*, 2006. **21**(4): pp. 33-45.

[62] Pharma Tips, Granulation & particle-bonding mechanism process, August 31, 2015. URL: http://www.pharmatips.in/Articles/Production/Granulation-Particle-Bonding-Mechanism-Process.aspx [cited August 27, 2018].

[63] Amarasekara, A., F. S. Tanzim, and E. Asmatulu, Briquetting and carbonization of naturally grown algae biomass for low-cost fuel and activated carbon production. *Fuel*, 2017. **208**: pp. 612-617.

[64] Losadhesivos.com, Adhesives—definition of adhesives. URL: https://www.losadhesivos.com/definicion-de-adhesivo.html [cited August 28, 2018].

[65] Bitsize, Structure and bonding. URL: http://www.bbc.co.uk/bitesize/higher/chemistry/energy/bsp/revision/1 [cited August 28, 2018].

[66] Zhao, Y., Z. Ge, H. Lui, and S. Sun, Ability of different microalgae species in synthetic highstrength wastewater treatment and potential lipid production. *Journal of Chemical Technology & Biotechnology*, 2016. **91**(11): pp. 2888-2895.

[67] Gutzeit, G., D. Lorch, A. Weber, M. Engels, and U. Neis, Bioflocculent algal-bacterial biomass improves low-cost wastewater treatment. *Water Science and Technology*, 2005. **52**(12): pp. 9-18.

[68] Ting, H., L. Haifeng, M. Shanshan, Y. Zhang, L. Zhidan, and D. Na, Progress in microalgae cultivation photobioreactors and applications in wastewater treatment: A review. *International Journal of Agricultural and Biological Engineering*, 2017. **10**(1): pp. 1-29.

[69] Shi, J., B. Podola, and M. Melkonian, Removal of nitrogen and phosphorus from wastewater using microalgae immobilized on twin layers: an experimental study. *Journal of Applied Phycology*, 2007. **19**(5): pp. 417-423.

[70] Chan, A., H. Salsali, and E. McBean, Nutrient removal (nitrogen and phosphorous) in secondary effluent from a wastewater treatment plant by microalgae. *Canadian Journal of Civil Engineering*, 2013. **41**(2): pp. 118-124.

[71] Mane, S., A. Vanjara, and M. Sawant, Removal of phenol from wastewater using date seed carbon. J*ournal of the Chinese Chemical Society*, 2005. **52**(6): pp. 1117-1122.

[72] El Nemr, A., A. Khaled, O. Abdelwahab, and A. El-Sikaily, Treatment of wastewater containing toxic chromium using new activated carbon developed from date palm seed. *Journal of Hazardous Materials*, 2008. **152**(1): pp. 263-275.

[73] Islam, M.A., I. A. W. Tan, A. Benhouria, M. Asif, and B. H. Hameed, Mesoporous and adsorptive properties of palm date seed activated carbon prepared via sequential hydrothermal carbonization and sodium hydroxide activation. *Chemical Engineering Journal*, 2015. **270**: pp. 187-195.

[74] Skodras, G., I. Diamantopoulou, A. Zabaniotou, G. Stavropoulos, and G. P. Sakellaropoulos, Enhanced mercury adsorption in activated carbons from biomass materials and waste tires. *Fuel Processing Technology*, 2007. **88**(8): pp. 749-758.

[75] Martinez, M. L., M. M. Torres, C. A. Guzman, and D. M. Maestri, Preparation and characteristics of activated carbon from olive stones and walnut shells. *Industrial Crops and Products*, 2006. **23**(1): pp. 23-28.

[76] Baçaoui, A., A. Yaacoubi, A. Dahbi, C. Bennouna, R. Luu, and F. J. Hodar, Optimization of conditions for the preparation of activated carbons from olive-waste cakes. *Carbon*, 2001. **39**(3): pp. 425-432.

[77] Stavropoulos, G., and A. Zabaniotou, Production and characterization of activated carbons from olive-seed waste residue. *Microporous and Mesoporous Materials*, 2005. **82**(1-2): pp. 79-85.

[78] Hossain, M. Z., M. I. Waly, V. Singh, V. Sequeira, and M. S. Rahman, Chemical composition of date-pits and its potential for developing value-added product—A review. *Polish Journal of Food and Nutrition Sciences*, 2014. **64**(4): pp. 215-226.

[79] MTI Corporation, Quartz tube block.jpg. URL: http://www.mtixtl.com/images/Quartz%20tube%20block.jpg [cited September 10, 2018].

[80] Brunauer, S., P. Emmett, and E. Teller, . *Journal of American Chemical Society*, 1938. **60**: 309–319.

[81] Labani, M. M., R. Rezaee, A. Saeedi, and A. A. Hinai, Evaluation of pore size spectrum of gas shale reservoirs using low pressure nitrogen adsorption, gas expansion and mercury porosimetry: A case study from the Perth and Canning Basins, Western Australia. *Journal of Petroleum Science and Engineering*, 2013. **112**: pp. 7-16.

[82] Wikipedia, Total dissolved solids. URL: https://en.wikipedia.org/w/index.php?title=Total_dissolved_solids&oldid=855290576 [cited September 16, 2018].

[83] Kempster, P. L., H. R. van Vliet, and A. Kühn, The need for guidelines to bridge the gap between ideal drinking-water quality and that quality which is practically achievable and acceptable. *Water SA*, 1997. **23**(2): pp. 163-167.

[84] World Health Organization, Guidelines for drinking-water quality. *WHO Chronicle*, 2011. **38**(4): pp. 104-8.

[85] Safe Drinking Water Foundation, TDS and pH. URL:https://www.safewater.org/fact-sheets-1/2017/1/23/tds-and-ph [cited September 16, 2018].

[86] Wikipedia, Electrical resistivity and conductivity. URL: https://en.wikipedia.org/wiki/Electrical_resistivity_and_conductivity [cited September 18, 2018].

[87] Mary River Catchment Coordinating Committee, Acceptability of water based on electrical conductivity. URL: http://mrccc.org.au [cited September 18, 2018]

[88] Wikipedia, pH. URL: https://en.wikipedia.org/w/index.php?title=PH&oldid=852983829 [cited September 21, 2018].

[89] Kumar, M., and A. Puri, A review of permissible limits of drinking water. *Indian Journal of Occupational and Environmental Medicine*, 2012. **16**(1): pp. 40-44.

[90] Wikipedia, Turbidity. URL: https://en.wikipedia.org/w/index.php?title=Turbidity&oldid=854108199, [cited September 23, 2018].

[91] Ahmed, S., What is the maximum permissible level (MPL) of turbidity in drinking water? *Researchgate*,
URL: https://www.researchgate.net/post/What_is_the_maximum_permissible_level_MPL_of_turbidity_in_drinking_water [cited September 21, 2018].